PL-TR-94-2009

USE OF WIND PROFILER DATA IN SHORT-RANGE FORECASTING

Thomas M. Hamill
Thomas Nehrkorn
Lawrence W. Knowlton

Atmospheric & Environmental Research, Inc
840 Memorial Drive
Cambridge, MA 02139

15 January 1994

Scientific Report No. 2

APPROVED FOR PUBLIC RELEASE; DISTRIBUTION UNLIMITED

PHILLIPS LABORATORY
Directorate of Geophysics
AIR FORCE MATERIEL COMMAND
HANSCOM AIR FORCE BASE, MA 01731-3010

This technical report has been reviewed and is approved for publication.

ARTHUR J. JACKSON
Contract Manager

DONALD A. CHISHOLM
Chief, Atmospheric Prediction Branch
Atmospheric Sciences Division

ROBERT A. McCLATCHEY
Director, Atmospheric Sciences Division

This document has been reviewed by the ESC Public Affairs Office (PA) and is releasable to the National Technical Information Service (NTIS).

Qualified requestors may obtain additional copies from the Defense Technical Information Center. (DTIC). All others should apply to the NTIS.

If your address has changed, if you wish to be removed from the mailing list, or if the addressee is no longer employed by your organization, please notify PL/TSI, 29 Randolph Road, Hanscom AFB, MA 01731-3010. This will assist us in maintaining a current mailing list.

Do not return copies of this report unless contractual obligations or notices on a specific document requires that it be returned.

DISCLAIMER NOTICE

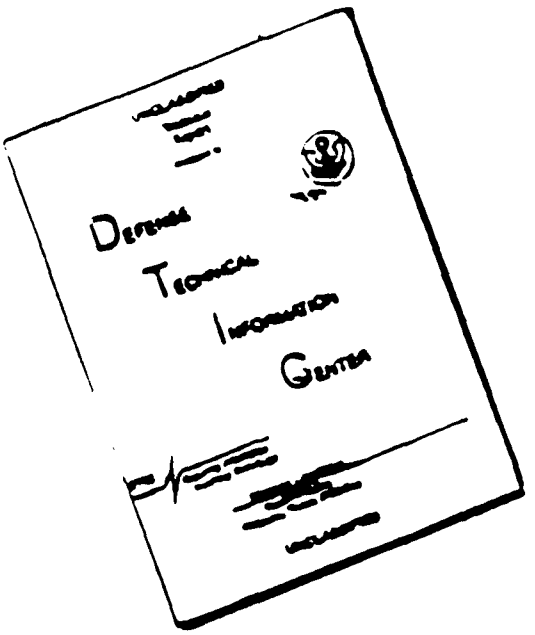

THIS DOCUMENT IS BEST QUALITY AVAILABLE. THE COPY FURNISHED TO DTIC CONTAINED A SIGNIFICANT NUMBER OF PAGES WHICH DO NOT REPRODUCE LEGIBLY.

REPORT DOCUMENTATION PAGE

1 AGENCY USE ONLY (Leave blank)	2 REPORT DATE	3 REPORT TYPE AND DATES COVERED
	January 1994	Scientific No. 2

4 TITLE AND SUBTITLE

Use of Wind Profiler Data in Short-Range Forecasting

5 FUNDING NUMBERS

F19628-92-C-0014
PE 63707F
PR 2684
TA 06
WU LB

6 AUTHOR(S)

Thomas M. Hamill
Thomas Nehrkorn
Lawrence W. Knowlton

7 PERFORMING ORGANIZATION NAME(S) AND ADDRESS(ES)

Atmospheric and Environmental Research, Inc.
840 Memorial Drive
Cambridge, MA 02139

8 PERFORMING ORGANIZATION REPORT NUMBER

9 SPONSORING MONITORING AGENCY NAME(S) AND ADDRESS(ES)

Phillips Laboratory
29 Randolph Road
Hanscom AFB, MA 01731-3010
Contract Monitor: Artie Jackson/GPAP

10 SPONSORING MONITORING AGENCY REPORT NUMBER

PL-TR-94-2009

11 SUPPLEMENTARY NOTES

12a DISTRIBUTION/AVAILABILITY STATEMENT

Approved for public release; distribution unlimited

12b DISTRIBUTION CODE

13 ABSTRACT (Maximum 200 words)

This report describes the results of the second year of a two-year study directed toward improving short-term forecasts and nowcasts through processing of satellite data (year 1) and Doppler profiler data (year 2). Data from the wind profiler demonstration network in the central US were used in a Barnes analysis scheme to produce hourly gridded wind fields and various derived kinematic quantities. The data were displayed in horizontal, vertical, and time-height cross sections. The utility of the profiler data, and profiler derived analyses, for short-term forecasting was demonstrated in a total of eight case studies, covering a wide range of atmospheric conditions. Among the derived quantities, the low-level vertical velocity derived from the horizontal convergence fields was found to be particularly useful for identifying areas of precipitation, while mid-level vorticity and vorticity advection was helpful in identifying quasi-geostrophic forcing mechanisms.

14 SUBJECT TERMS	15 NUMBER OF PAGES
Nowcasting, Wind Profiler, Objective analysis	140
	16 PRICE CODE

17 SECURITY CLASSIFICATION OF REPORT	18 SECURITY CLASSIFICATION OF THIS PAGE	19. SECURITY CLASSIFICATION OF ABSTRACT	20 LIMITATION OF ABSTRACT
Unclassified	Unclassified	Unclassified	SAR

Table of Contents

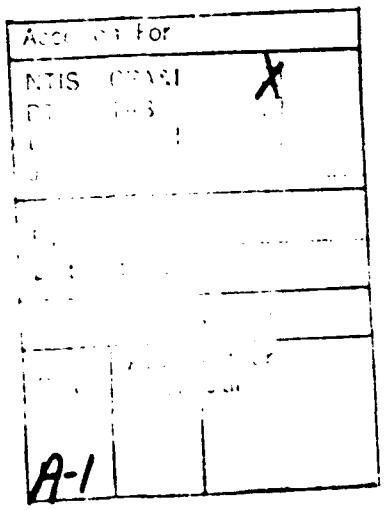

List of Figures

1. Introduction

This report describes the results of the second year of a two-year study directed toward improving short-term forecasts and nowcasts through processing of satellite data (year 1) and Doppler profiler data (year 2). The results of the first year of this study have been reported elsewhere (Hamill and Nehrkorn, 1993a; Hamill and Nehrkorn, 1993b; Nehrkorn et al., 1993). The present report aims to demonstrate the utility of Doppler wind profilers as a weather analysis and forecast tool. This information could then be used to decide whether to include these data in the data stream available at Air Force meteorological workstations such as the Automated Weather Distribution System, or AWDS. The approach taken in this study is to perform a number of retrospective case studies, and to evaluate qualitatively how the additional information provided by the profiler data would have improved nowcasts (0 to 6 hours) and short-term forecasts (3 to 12 hours).

The National Weather Service (NWS) recently deployed a demonstration network of 31 Doppler wind profilers throughout the central U.S. (Figure 1). These profilers, operating at 404.37 MHz, are capable of measuring vertical profiles of the wind from 0.5 to 16.25 km AGL (Chadwick, 1988; van de Kamp, 1988; Weber et al., 1990). The accuracy of hourly wind measurements from the profilers is competitive with radiosondes (Weber and Wuertz, 1990; Weber et al., 1990), and profilers have the distinct advantage of providing information every hour, rather than twice daily, as with U.S. radiosondes.

The usefulness of selected profilers for nowcasting and diagnostic studies is well-documented (Brady and Brewster, 1989; Carlson, 1987; Jewett and Brady, 1989; Naistat, 1993; Neiman and Shapiro, 1989; Walawender, 1993; Zamora et al., 1987). Typically the profiler data is viewed in a time/height cross section, with more recent data to the left and older data to the right (examples of such displays can be found in section 3 of this report). These displays conveniently depict a time series of wind analyses (and often overlays of derived kinematic quantities), allowing the user to trace changes up to the analysis time. An educated forecaster can often make reasonable inferences on the short-term future states of the weather with such displays. Using time/height cross sections, profilers have proved useful for timing of the end of precipitation with trough passage,

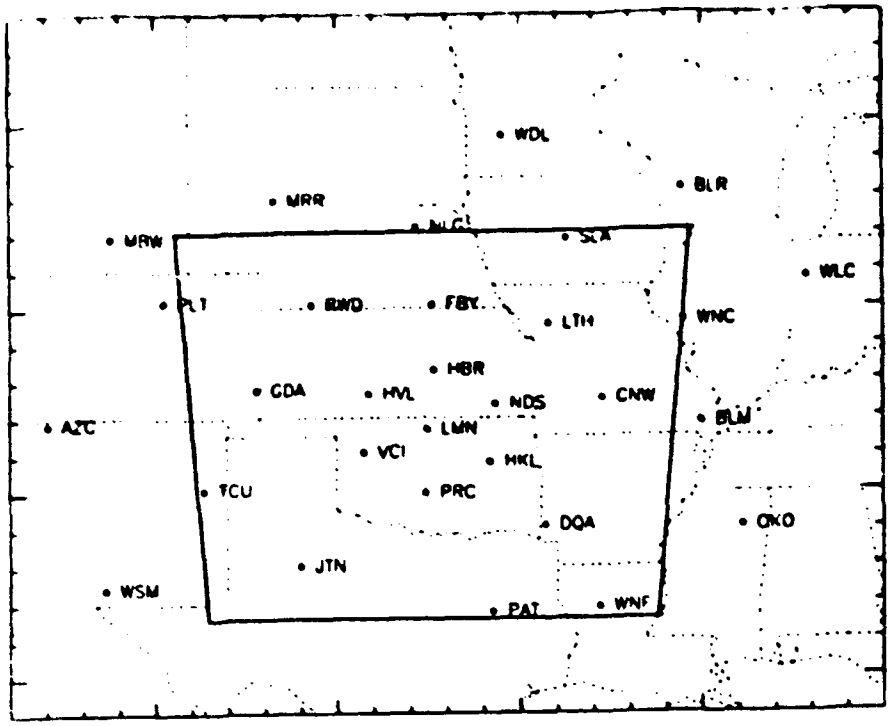

Figure 1: Map of profiler sites and 3-letter identifiers for NOAA's wind profiler demonstration network. Inner box indicates location of analysis domain.

determining the propagation speed of waves, comparing with radiosonde data and model forecasts, detecting fronts, overrunning surfaces, subtle upper-level waves, low-level jets, and upper-level divergence, diagnosing precipitation from derived vertical velocities, and much more.

The usefulness of the network as a whole is less thoroughly explored, primarily since this data has only recently been available. Ralph and Neiman (1993) illustrate profiler network data overlaid on satellite imagery of a mesoscale convective system (MCS) and discuss the utility of divergence diagnosed from a triangle of sites under the MCS. Kuo et al. (1987) and Cram et al. (1991) have explored the retrieval of temperatures and geopotential using multiple profilers. The Mesoscale Analysis and Prediction System (MAPS) run by NOAA/ERL/FSL (Benjamin, 1989; Benjamin et al., 1991; Smith and Benjamin, 1993) now operationally assimilates profiler data and produces new objective analyses every three hours. This analysis is quite robust, since many other data sources such as aircraft and surface observations are also used. However, this data is not

yet widely distributed, and it is only available every three hours though the profiler data is available once an hour.

Since the profiler network has a relatively uniform station spacing and produces reliable observations, it is conducive to hourly, on-site, gridded objective analyses of the wind field (Barnes, 1964). Kinematic quantities such as convergence, integrated vertical velocity, temperature advection, wind speed, vorticity, and vorticity advection can thus be calculated from the hourly analyses and viewed in time/height cross sections, vertical cross sections, or more conveniently, horizontal plots. Meteorologists are used to working with objective analyses and horizontal depictions of weather conditions (e.g., 500 mb heights/vorticity maps). For profilers, such depictions give the forecaster an areal perspective of the weather, allow monitoring of features from hour to hour and easy comparison against other depictions such as forecast model output. Also, conditions upstream can be graphically extrapolated into short-term forecasts. A more conventional time/height cross section would yield fewer clues on the future state of the wind field since only point information is displayed. Still, if time/height cross sections are desired, they can be generated from the objective analyses, even for locations in between profiler sites.

This report documents our effort to explore usage of the wind profiler network data by applying common objective analysis and display methods. The analysis and display software used in this project is described in the next section. Section 3 contains a number of case studies, which illustrate the utility of the profiler data for issuing short-term forecasts. A summary and conclusions are in Section 4, and the references are given in Section 5.

2. Description of Analysis and Display Software

Whereas there is scattered software for the display of single profiler data (e.g. GEMPAK, Penn State, NOAA/FSL), and less software for the analysis and display of dual or triple profilers, there is no software available for the analysis of the demonstration network as a whole. Since the profilers are now a stable, low-error data source, they are naturally amenable to use as a data source in objective analyses. These objective analyses permit the quick calculation and display of a variety of quantities from the resultant gridded data.

2.1. Objective Analysis.

We have designed objective analysis and display software tailored to the profiler demonstration network. For the following case studies, profiler data is analyzed in a constant-height coordinate system using a successive corrections objective analysis. The analysis grid is a Lambert-conformal projection true at 60 and 30 degrees north latitude and centered on 97.5 degrees west longitude and 37 degrees north latitude, with a 25 km grid spacing. The analysis is performed on a 48 x 48 grid to allow use of outlying observations, but only the center 32 x 32 points are displayed (Figure 1). The standard Barnes technique (Barnes, 1964; Barnes, 1973; Koch et al., 1983) is used. Multiple analysis times (e.g., 00Z, 01Z, 02Z, etc.) are typically analyzed in sequence, and in a somewhat nonstandard approach, first guess fields are used. For the first time, the mean wind of all profiler observations at a given level is used as the first guess; for later times, the previous hour's wind analysis is used. Though this makes interpretation and tuning of the Barnes response function more difficult, the resulting analyses are more accurate.

The level of detail present in the analyses is controlled by the choice of parameters for the Barnes scheme, and particularly derived quantities such as vorticity, vorticity advection, divergence, and integrated vertical velocity may be too noisy or overly damped for inappropriate parameter values. The amount of smoothing in the Barnes scheme is controlled by the length scale L_o in the distance weighting function:

$$w_o(r) = \exp\left(\frac{-r^2}{2L_o^2}\right) , \qquad (1)$$

where w_o is the weight given to an observation at a distance r from the analysis grid point. The subscript o indicates the first pass of the analysis; in the second pass, the denominator of the exponent is multiplied by a factor γ, corresponding to a decrease of the length scale. The spectral response of the two passes of the analysis is a known function of the two parameters, L_o and γ (Koch et al., 1983). Koch et al. (1983) argue that for high quality data, the wavelength corresponding to twice the observation spacing (Δs) should be damped by a factor of 2. Using a value of $\gamma = 0.2$, they arrive at a value of $L_o = \Delta s$. For noisier data, they recommend using the same value of L_o, but a larger value of γ. Seaman (1989)

used optimum interpolation theory to arrive at optimal (in the sense of minimizing the squared error) parameter settings, given information about the horizontal correlation length scale of the field to be analyzed (L) and the noise to signal ratio of the data (λ). His results suggest that smaller (larger) values of $L_o / \Delta s$ are optimal for clean (noisy) data; the optimal value of $L_o / \Delta s$ decreases with the normalized station spacing ($\Delta s/L$). For $\Delta s/L = 0.5$, optimal values of $L_o / \Delta s$ range from 0.8 (for $\lambda = 0.1$) to 1.3 (for $\lambda = 0.5$). The value of γ depended mainly on the noise to signal ratio, with larger values for noisier data.

In order to apply the results of Seaman (1989) to our analysis scheme, the statistical properties of the field to be analyzed have to be estimated. Since we make use of a first guess field, the field consists of the residuals from the first guess: for the first analysis time in a sequence, it is simply the deviation from the horizontal average of the winds; for subsequent analysis times, it is the difference between the winds and the previous hour's analysis. Thus, for the first analysis time, the applicable horizontal correlation scale is close to that of the wind field itself, roughly corresponding to L = 600 km (Buell, 1972). At later times, the correlation length scales are likely to be shorter, somewhat similar to what has been documented for short-range numerical weather prediction (NWP) models; numerous studies (Bartello and Mitchell, 1992; Hollett, 1975; Hollingsworth and Lönnberg, 1986; Mitchell, 1990; Thiebaux et al., 1990) suggest values of approximately 200-300 km in that case. The observational error of wind profilers may be estimated from the comparisons with rawinsonde (Weber and Wuertz, 1990; Weber et al., 1990) or Loransonde (Smalley and Morrisey, 1993) data, and compared with the size of the residuals in our analysis. The resulting estimate for the noise to signal ratio (λ) is approximately 0.2, somewhat lower for the first analysis times. Finally, the station spacing Δs in the primary area of interest is approximately 250 km.

Since there is considerable uncertainty in these estimates of L and λ, we experimented with several settings of L_o and γ, estimating the analysis error as the difference between the analysis at randomly chosen observation locations which were withheld from the analysis (as was done in Seaman 1989). From the results of these tests, we finally selected values of L_o = 230 km ($L_o / \Delta s = 0.94$), corresponding to a value of $\lambda = 0.2$, and $\gamma = 0.2$ for the first analysis time, and $\gamma = 0.35$ for subsequent times.

Analysis quality can be enhanced by the careful screening of bad data and judicious vertical averaging. The hourly profiler observations are used only if they have passed all the normal quality control checks such as a vertical shear check and a consensus check (Brewster, 1989). Additionally, a buddy check system is built into the objective analysis so that any observation deviating strongly from the first guess is excluded unless a nearby profiler also observed a similar wind velocity. Since profilers do not record winds precisely at standard MSL elevations, analysis on a constant height surface will by necessity involve the use of multiple profiler observations from surrounding vertical levels. A wind observation at a given height is determined through a weighting of the observations with similar heights. The analysis at height H is a weighted sum of observations at any gate with a height O within 750 m vertical distance from H. The weight W_v given to each of these observations is determined through the equation

$$W_v = \frac{1}{1 + C_v(H - O)^2} \qquad (2)$$

where the coefficient C_v here is $1*10^{-5}m^{-2}$. A plot of the weight versus height difference is shown in Figure 2. The use of this rather than a linear interpolation between two gates yielded more consistent analyses from one vertical level to the next than simple interpolation, especially for sites where some wind observations were missing or deleted in the QC process.

Our objective analysis software allows the user to choose individual height levels for analysis (e.g., 1500 m), or to prespecify a fixed set of 20 analysis levels at either high or low resolution. In high resolution, the analysis is performed every 250 m from 1000 m to 5750 m; in low resolution, the analysis is performed every 750 m from 1500 m to 15750 m.

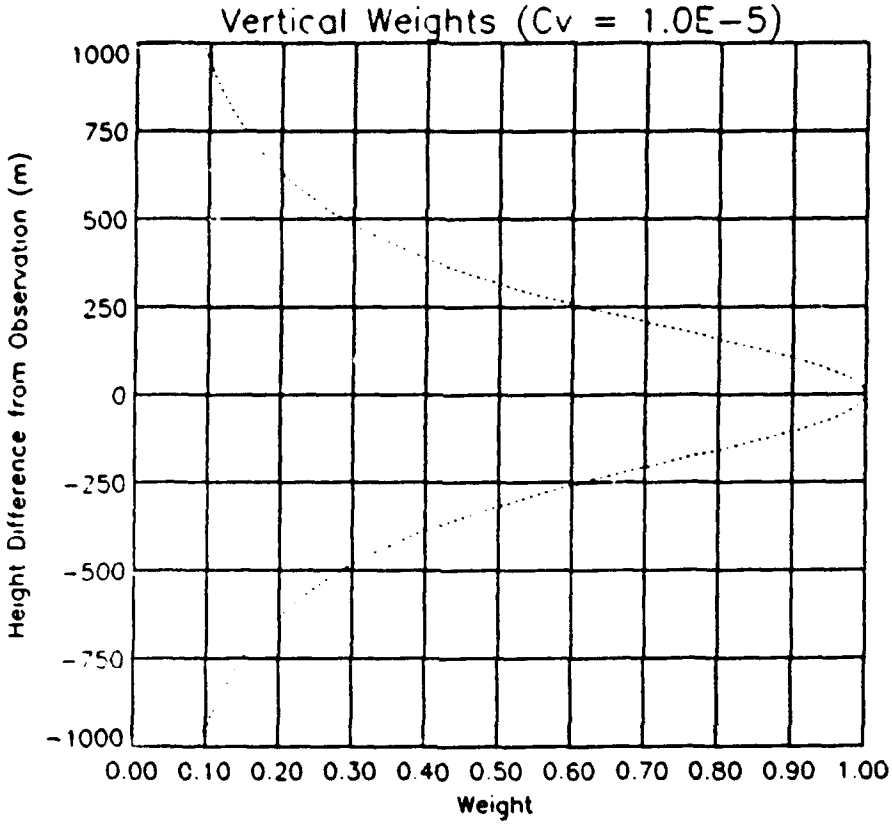

Figure 2: Plot of the weight vs. height difference as given in Equation 2.

2.2. Derived Quantities Calculation.

Once the objective analysis has been completed, a variety of derived quantities can be calculated from the gridded winds. Among these are:

a. **Storm-relative winds**. Assuming that the overall motion of the storm inside the domain is proportional to the average wind speed from all levels and all times, the user can reset winds back and forth from the objectively analyzed value to a "storm relative" value, where this mean wind is subtracted from the analyzed value.

b. **Perturbation winds**. For each point in the analysis domain, a time average over all the selected analysis times can be determined. By subtracting this value from the value at a gridpoint, the perturbation from the presumed mean flow can be determined. This will often enhance the user's ability to detect subtle features embedded within a strong flow.

c. **Absolute vorticity.**

d. **Convergence.**

e. **Analyzed vertical velocities.** The profiler network archives not only the U and V wind components, but also a W component. This is also objectively analyzed and available for display. However, its value as a diagnostic is limited; in areas of precipitation, for example, the reported vertical velocity will usually reflect the fall velocity of the precipitation, not the motion of the ambient air.

f. **Vertical velocities from divergence equation**. As with numerical forecast models, the gridded horizontal wind velocities can be used to determine a compatible vertical velocity through the divergence equation. We assume vertical velocities are zero at the lowest analysis level, and then determine vertical motion through upward integration of the net divergence.

g. **Vorticity advection**.

h. **Geostrophic temperature advection**. Assuming the winds are geostrophic, the wind shear in a layer between two analysis levels can be used to detect temperature advection (Neiman and Shapiro, 1989), which could potentially be useful for determining whether an area is stabilizing or destabilizing.

2.3. Methods of Displaying the Data.

We have also designed a software package for the convenient display of the profiler analyses and derived products. The analyses can be displayed in one of three ways:

a. **Time / height cross section.** For a user-specified location, which can be either an analysis grid point, or an intermediate point to which data are interpolated, profiler data are displayed in a coordinate system with height as the ordinate, and time as the abscissa.

b. **Vertical cross section.** The user specifies two endpoints, and the software will either loop through a time series of cross sections, or display them one at a time.

c. **Horizontal cross section**. The user selects a height level for display, and again, the software will either loop through a time series of cross sections, or display them one at a time.

2.4. Other Display Software.

Also available to us are assorted other software display packages. Each of these packages was used for some part of the profiler project; data was often available from one data stream for our older case studies, and a different data stream for newer cases. Often a given display capability (e.g., plotting surface observations) was available from many of the software packages used, but we could not standardize because of these different data streams. The software available to us is described below:

a. **Existing AIMS software**. We use the AIMS (Gustafson et al., 1991; Gustafson et al., 1987) computer system for the display of:

1. Raw surface observations
2. Numerical guidance such as FOUS and MOS (Klein and Glahn, 1974)
3. Gridded manually digitized radar output (MDR)
4. Skew-T's.

b. **New AIMS software**: We have also specially designed some additional software for this project:

b.1. **GOES data display**. Using the data visualization language PV-WAVE, we can conveniently loop GOES satellite data, either in its native projection or remapped to the profiler domain.

b.2. **Raw Profiler data**. These observations can be displayed in horizontal cross section at any MSL height for a single time or looped. Profiler winds at a particular height are obtained as a weighted vertical average of nearby observation levels, as in the objective analysis. The display domain here is an expanded version of the domain used in the objective analysis. These displays are useful for checking the accuracy of the objective analysis, particularly in cases where data coverage is sparse, or where the profiler data contains outliers and the buddy check procedure may be invoked.

b.3. **Precipitation data**. Using NMC's river forecast database of rainfall observations, the 12Z- to 12Z daily rainfall observations for thousands of sites can be displayed, permitting the determination of areas of significant precipitation more accurately.

c **GEMPAK** . This display package, running on a Sun workstation, was used primarily for the display of conventional data, such as surface observations, upper-air observations, and Skew-T's. The software also can display forecast model output (NGM data) and profiler data in time/height cross-sections.

d. **WXP**. The WXP package developed by Purdue University was used to plot observations and analyses, as well as NGM forecasts. This package was used for NMC forecast and analysis data available to us through another project at AER, for parts of 1992 and 1993.

3. Case Studies

In the following, a total of 8 case studies are presented. For each case, a particular forecast problem is identified, and the accuracy of the forecast guidance (other than profiler data) available to forecasters is assessed. The role of profiler data in improving on the forecast guidance is demonstrated qualitatively. In many of the cases, comparisons between NGM forecasted and observed precipitation are used as one indicator of the quality of the NGM forecast. These comparisons must be interpreted with care, because NGM forecasts represent 80 km grid box averages, while observed amounts at individual sites can vary strongly on that scale, particularly in convective situations. In addition, NGM precipitation forecasts are affected by the spin-up of the model during the first 6-12 hours. For these reasons, precipitation forecast errors are only used to show timing or placement errors, or in conjunction with forecast errors of other fields.

3.1. March 9, 1992: Texas/Oklahoma Convective Rain Event

Between 06 and 12 UTC 9 March 1992, 1-2" of convective rainfall fell across northeast Texas and southeast Oklahoma. The 00 UTC NGM forecast failed to forecast the significant rainfall. The forecast period and area of interest in this case is 06 to 12 UTC 9 March over eastern Texas and Oklahoma. Short-term forecasts with observations and forecast guidance available at 03 UTC, and

nowcasts with data available at 06 UTC, are considered and compared to the verifying observations and analyses between 06 and 12 UTC. Profiler data at 03 UTC allow early identification of NGM forecast errors in this case, and subsequent profiler data illustrate key aspects of the circulation.

3.1.1. Standard Meteorological Data Available Before the Storm.

The flow at the surface is characterized by a strong low moving east from southeast Colorado. At 03 UTC 9 March (Figure 3) the center of the low is located in western Kansas, with snow, rain, and thunderstorms to the north and west. Extending south from the center of the low, a sharp dry line is moving through western Oklahoma and central Texas with a moist, southerly flow from the Gulf of Mexico ahead of it. A thunderstorm is reported at McAlester, OK (MLC) at 03 UTC, Wichita Falls, TX (SPS) at 00 and 03 UTC, and at Abilene, TX (ABI) at 03 UTC (see Figure 3 for station locations). The convection associated with this dry line can be seen to move east and intensify in the manually digitized radar summaries. At 03 UTC 9 March (Figure 4), a line of intense convection (echoes with levels 5 and 6) stretches from southwest Texas to central Oklahoma.

The 00 UTC 9 March upper air maps are shown in Figures 5 and 6. At 850 mb (Figure 5) there is moist southerly flow over northeast Texas and eastern Oklahoma; at 700 mb and 500 mb (Figure 6), dry air is moving in from the southwest, leading to an environment conducive to convection. Also visible at 500 mb is a jet streak approaching from the southwest, which is also present at 300 mb (not shown).

The 00 UTC 9 March NGM forecast guidance for the 6h precipitation ending at 12 UTC 9 March (Figure 7) shows a large area of .2" to .8" accumulation associated with the frontal precipitation in northern Colorado, Kansas, and points to the north and east, but only relatively light precipitation (.1"-.3") in eastern Texas and Oklahoma. The reason for this forecast is apparent in the 700 mb vertical velocity forecasts valid at 06 UTC (Figure 8) and 12 UTC (Figure 9), which show most of central and western Texas under large scale sinking motion, and only weak upward motion in Oklahoma at 06 UTC, being replaced by sinking motion by 12 UTC over all but the easternmost part of the state. The 500

mb forecast maps indicate negative vorticity advection (contributing to sinking motion) over Texas at 06 UTC, and both Texas and Oklahoma at 12 UTC (Figure 10). Warm advection at 850 mb (not shown) accounts for the area of weak upward motion, and light precipitation, in eastern Texas and Oklahoma in the NGM forecast. The warm and moist low level flow also accounts for the predicted destabilization apparent in the forecast maps of the lifted index (Figures 11 and 12). A band of negative lifted indices, which exists in Oklahoma and eastern Texas at 00 UTC, moves east through the forecast period, indicating instability and a favorable environment for convection. A forecaster presented with this information would have to balance the observation of the approaching dry line convection, and the somewhat favorable lifted index forecast, against the vertical velocity and precipitation forecast from the NGM, which suggest that convective precipitation would be suppressed to some degree. A reasonable forecast in this situation would be for a chance of thunderstorms for northeast Texas and southeast Oklahoma, but most likely not a widespread area of large accumulations.

3.1.2. Information Available During and After the Storm.

The 06 UTC (Figure 13), 09 UTC (Figure 14), and 12 UTC (Figure 15) 9 March surface maps show the line of convection in central Oklahoma and central Texas continuing to move east. A heavy thunderstorm is reported at Dallas, TX (DFW) at 08 UTC with moderate rain showers there at 07 UTC and 11 UTC. The corresponding manually digitized radar summaries (Figures 16 - 18) show continued convection extending from central Texas to the northeast. The thunderstorm line continues to move east through Oklahoma, and the area of convection expands in northeast Texas between 08 and 10 UTC. Twenty-four hour precipitation accumulations (Figure 19) in excess of .5" are widespread across northeast Texas and southeast Oklahoma, with several sites reporting 1"-2".

The verifying upper air analysis for 12 UTC 9 March at 500 mb (Figure 20) shows northeast Texas under the right entrance region of the jet streak with positive vorticity advection (PVA) centered over DFW. This PVA is possibly responsible for the moderate rain shower at DFW at 11 UTC. The NGM failed to

forecast the PVA (viz. Figure 10), and thus underforecast the large scale ascent and resulting precipitation.

3.1.3. Utility of the Profiler Data.

The profiler data in this case provide early indications of the NGM underforecasts of the large scale ascent. The 03 UTC 9 March profiler derived 3000 m winds and vertical velocity (Figure 21) show an expansive area of upward motion of > 10 cm/s over north central Texas, which corresponds well to the position of the thunderstorm line in Figures 3 and 4. A vertical cross section to the northwest of DFW (not shown) indicates that this vertical velocity extends over a deep layer. Comparison of Figure 21 with the NGM forecast valid 3 hours later suggests that the NGM forecast implies an unreasonably fast weakening and movement to the east of this area of ascent. Since these analyses would be available around the same time as the 00 UTC NGM guidance, a forecaster could use this deviation from the NGM to make a more confident forecast of showers and thunderstorms downstream of this upward motion. The 06 UTC profiler derived 3000 m winds and vertical velocity in Figure 22 confirms this deviation and the time-height cross section of winds and vertical velocity over DFW in Figure 23 continues this trend through 12 UTC. The upward motion increases significantly above 3000 m after 10 UTC as the right entrance region of the 500 mb jet streak moves over DFW. The heavy thunderstorm at DFW occurs during a local upward motion maximum between 07 and 08 UTC followed by a second surge in upward motion preceding a brief moderate rain shower at 11 UTC (however, there is no rain reported at 03 UTC, the time of another maximum of upward motion). Plots of NGM forecast and profiler derived low (850 mb) and upper (300 mb) level convergence valid at 06 UTC (not shown) generally confirm the conclusions from the 700 mb vertical velocity plots: the NGM forecasted low level divergence and upper level convergence, whereas the profiler analyses show low level convergence and upper level divergence over northeast Texas and southeast Oklahoma.

The vertical velocity displayed in Figure 23 can be compared to differential vorticity advection and temperature advection, in an attempt at identifying the quasi-geostrophic dynamic forcing mechanisms. Figure 24 shows the vorticity advection in the same display as vertical velocity in Figure 23. Interestingly,

differential NVA is apparent over DFW between 00 and 10 UTC, which contributes to sinking motion. However, winds are veering with height at 3000 m and below, indicating warm advection. Plots of explicitly calculated temperature advection (not shown) generally confirm this conclusion, although they tend to be somewhat noisy. The differential NVA is weakened by 10 UTC, and replaced by PVA at 12 UTC; this is accompanied by an increase in the large scale ascent at 3000 m and above, possibly contributing to the moderate rain shower at DFW at 11 UTC. As was discussed earlier, the NGM failed to forecast this PVA.

In summary, the profiler analyses at 03 UTC and 06 UTC allow the forecaster to monitor deviations from the NGM and, in this case, increase the likelihood of convection and heavier than forecasted rainfall for northeast Texas and southeast Oklahoma for the period 06 UTC to 12 UTC. Comparison of profiler derived quantities with independent observations indicate a good correspondence between analyzed 3000 m vertical velocity and observed convection in this case. Analysis of dynamic forcing terms show low level warm advection to be the primary driving force for the large scale ascent and destabilization, with positive vorticity advection becoming a factor at the end of the forecast period.

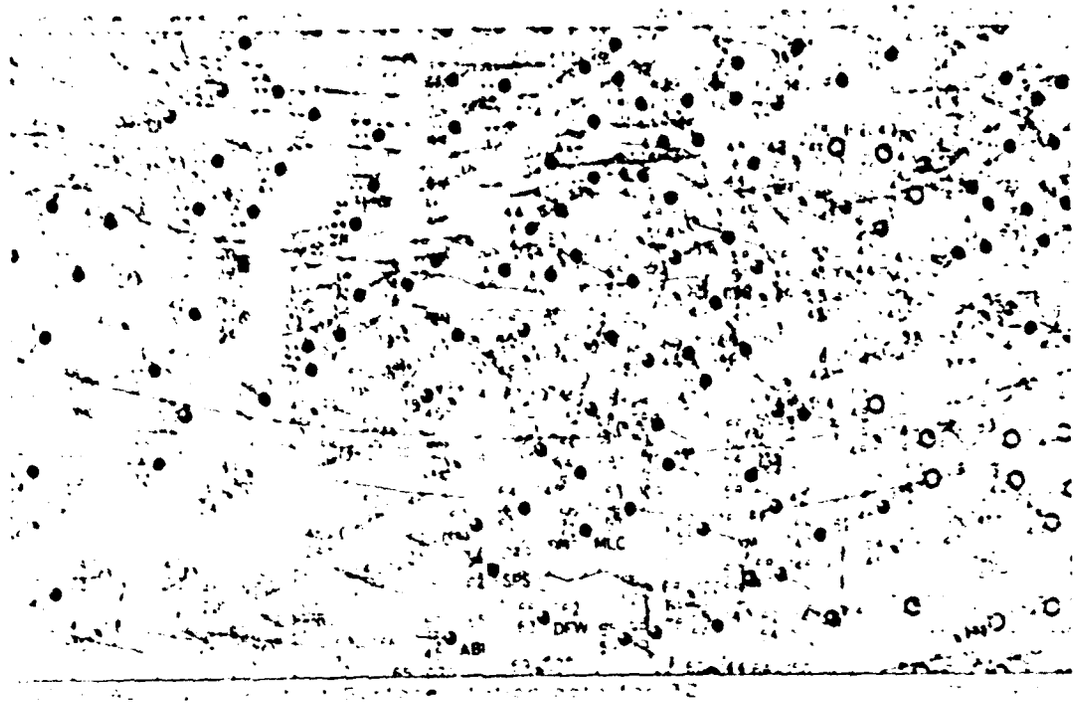

Figure 3: Surface weather map and sea-level pressure analysis (contours labeled in mb) for 03 UTC 9 March 1992. Wind symbols follow standard meteorological practice: 10 kts (5 kts) for each full (half) barb, 50 kt for each pennant

Figure 4: Manually digitized radar (MDR) summary for 03 UTC 9 March 1992

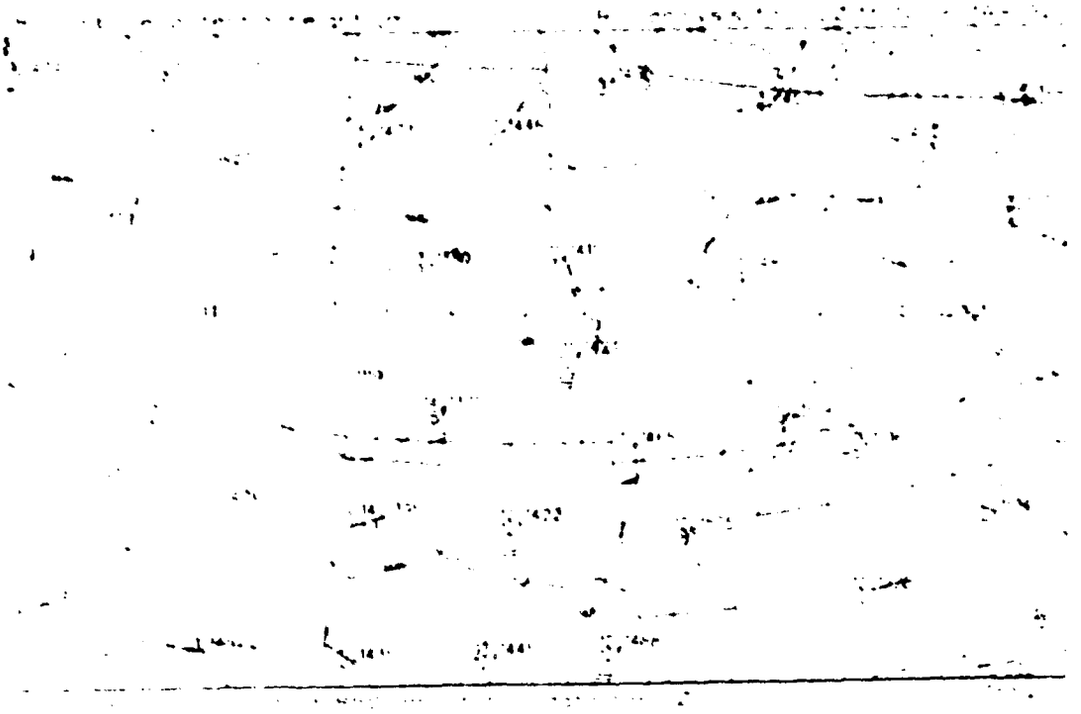

Figure 5: 850 mb weather map and height analysis (contours labeled in dm) for 00 UTC 9 March 1992.

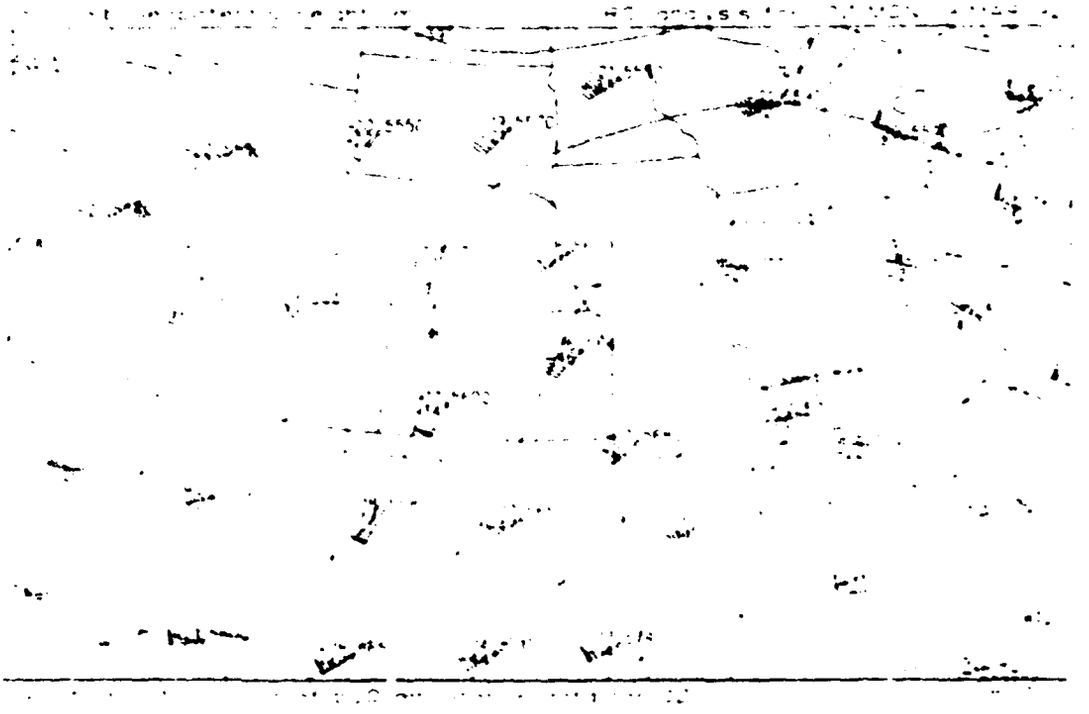

Figure 6: 500 mb weather map and height analysis for 00 UTC 9 March 1992.

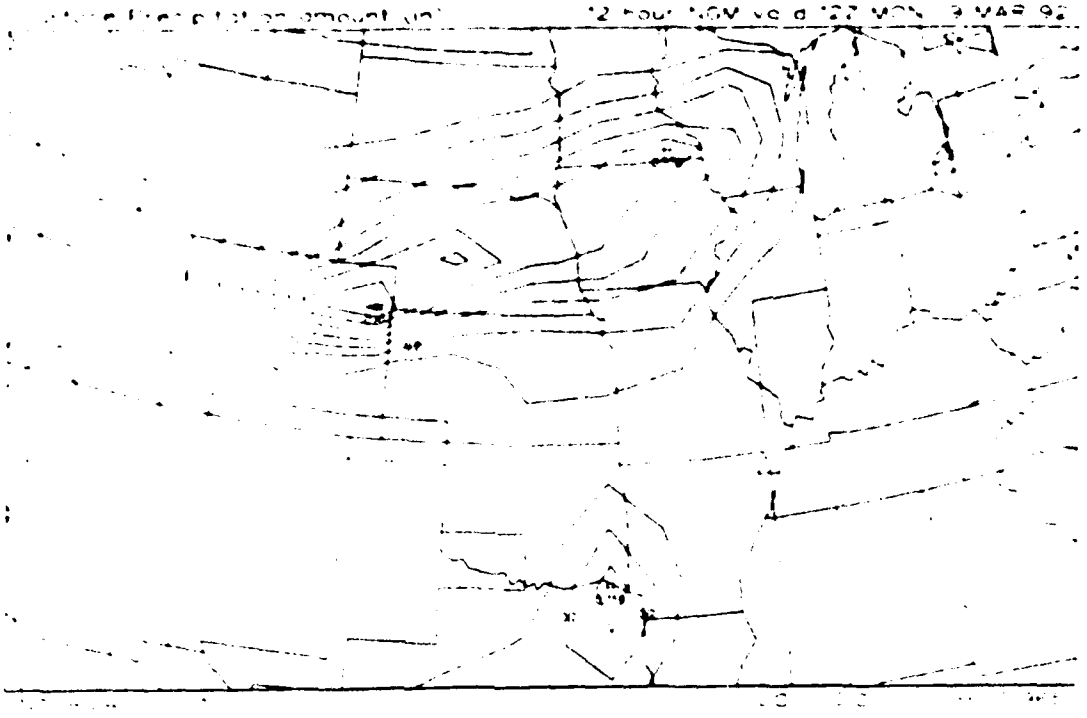

Figure 7: NGM 00 UTC 9 March 1992 forecast of 6-hour accumulated precipitation (in), valid 12 UTC 9 March 1992.

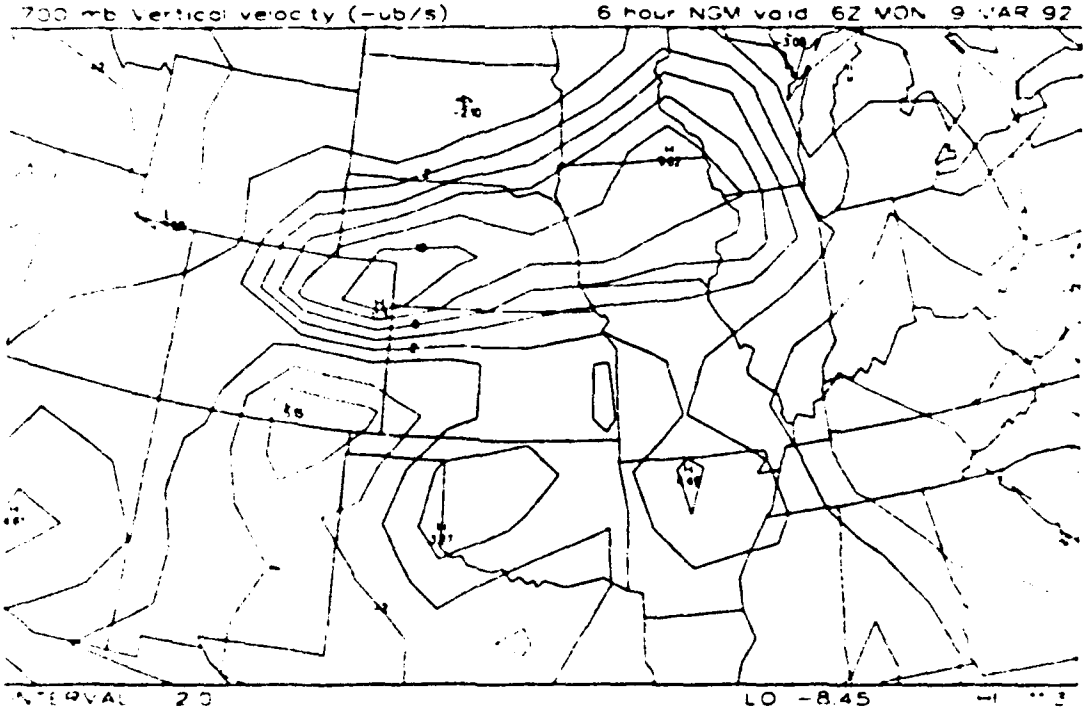

Figure 8: NGM 00 UTC 9 March 1992 forecast of 700 mb vertical velocity (μb/s, or cm/s), valid 06 UTC 9 March 1992.

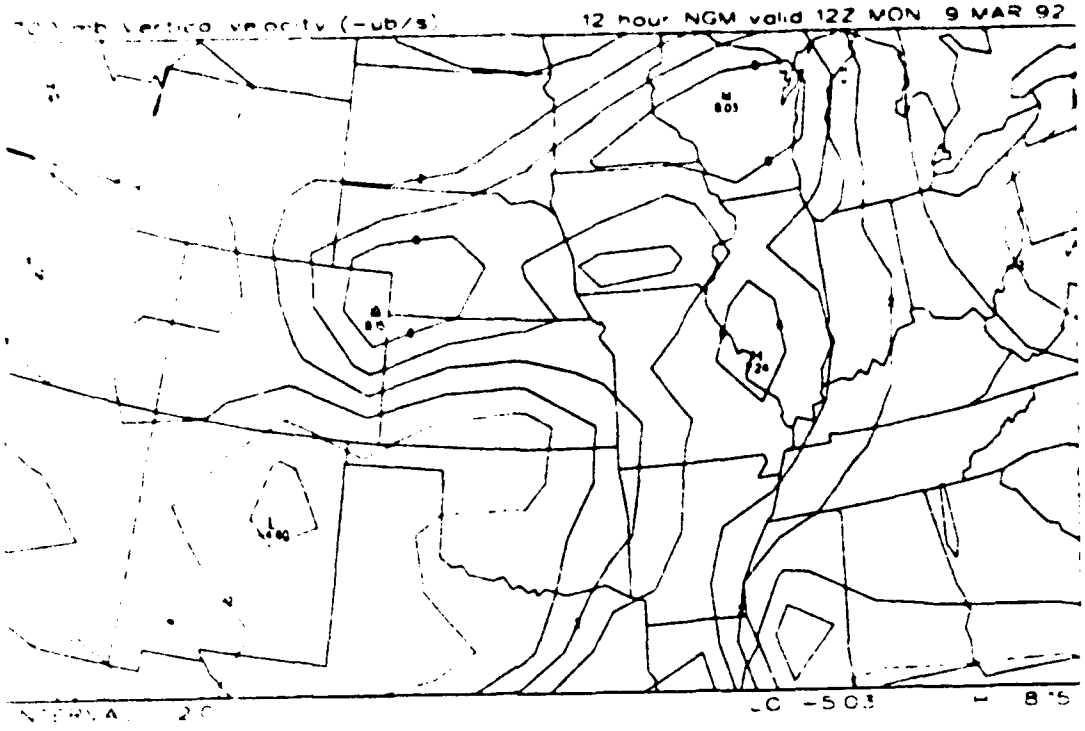

Figure 9: NGM 00 UTC 9 March 1992 forecast of 700 mb vertical velocity (μb/s, or cm/s), valid 12 UTC 9 March 1992.

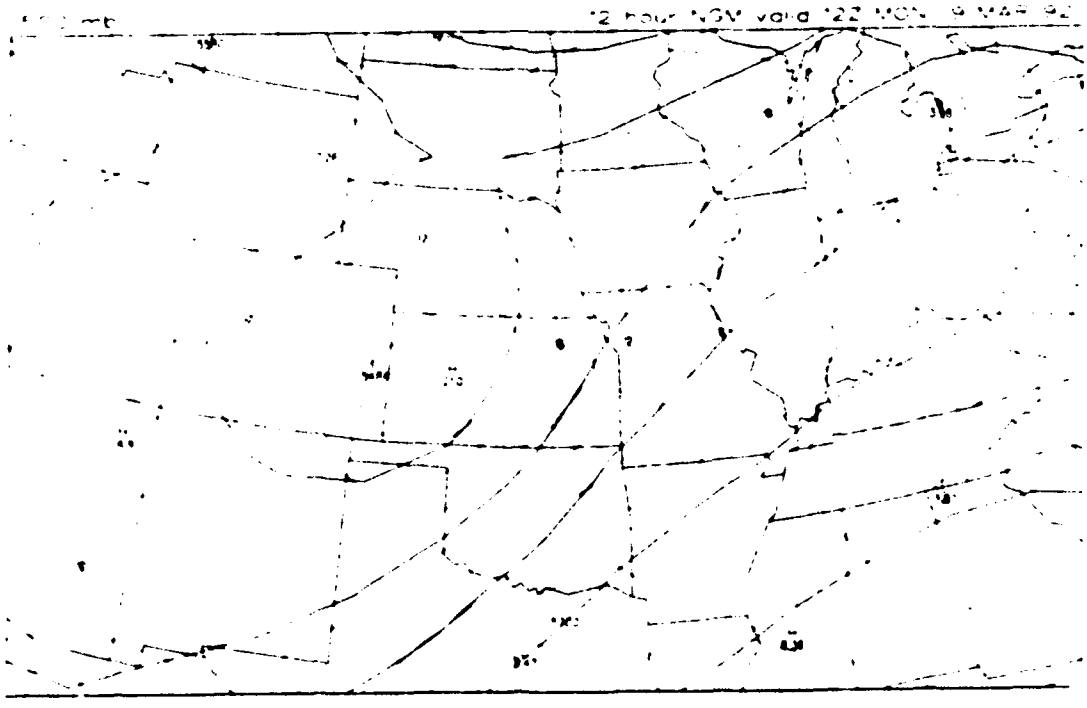

Figure 10: NGM 00 UTC 9 March 1992 forecast of 500 mb height (solid lines) and absolute vorticity ($10^{-5}s^{-1}$, dashed lines), valid 12 UTC 9 March 1992.

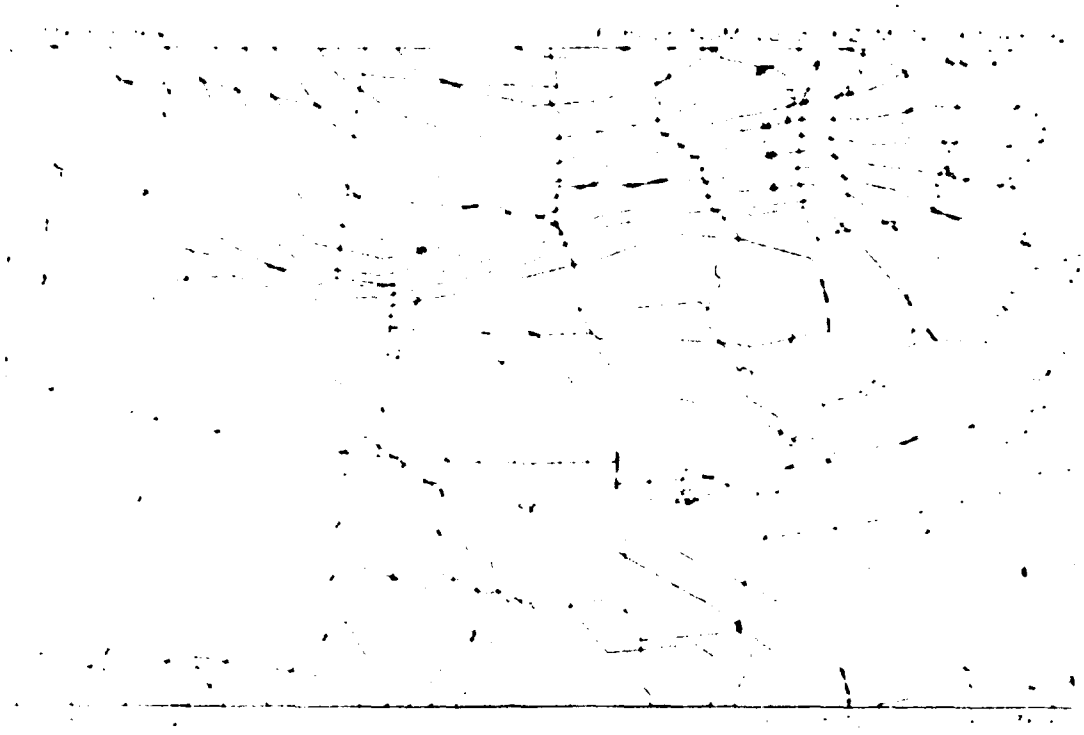

Figure 11: NGM 00 UTC 9 March 1992 forecast of surface lifted index, valid 06 UTC 9 March 1992.

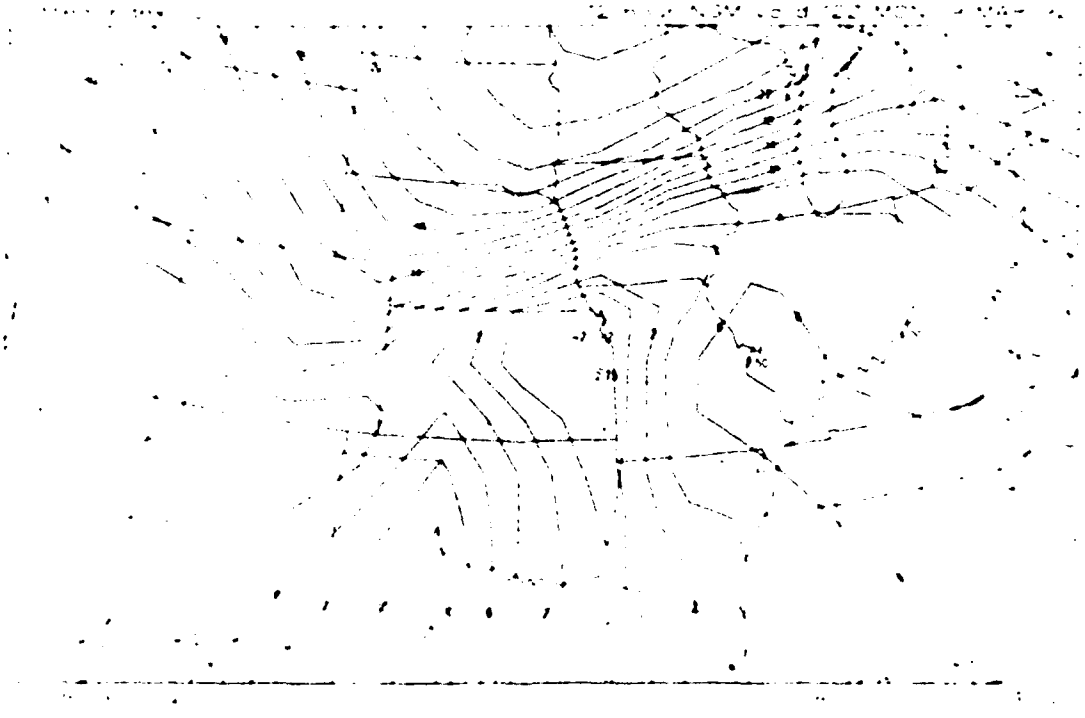

Figure 12: NGM 00 UTC 9 March 1992 forecast of surface lifted index, valid 12 UTC 9 March 1992.

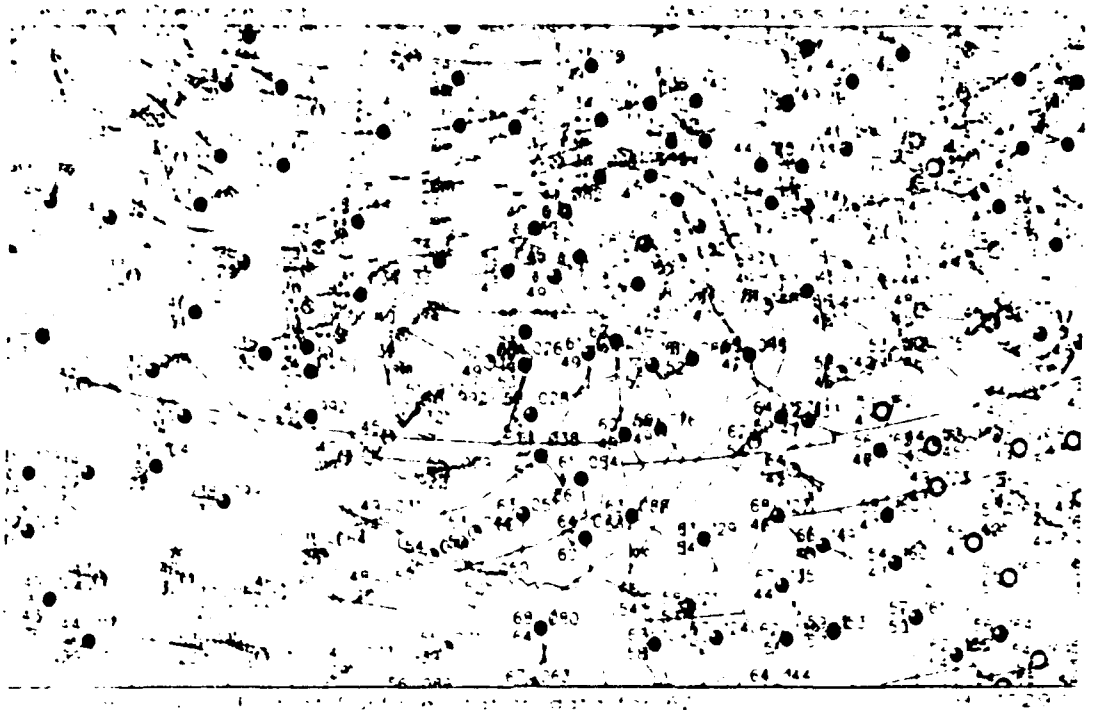

Figure 13: Surface weather map and sea-level pressure analysis for 06 UTC 9 March 1992.

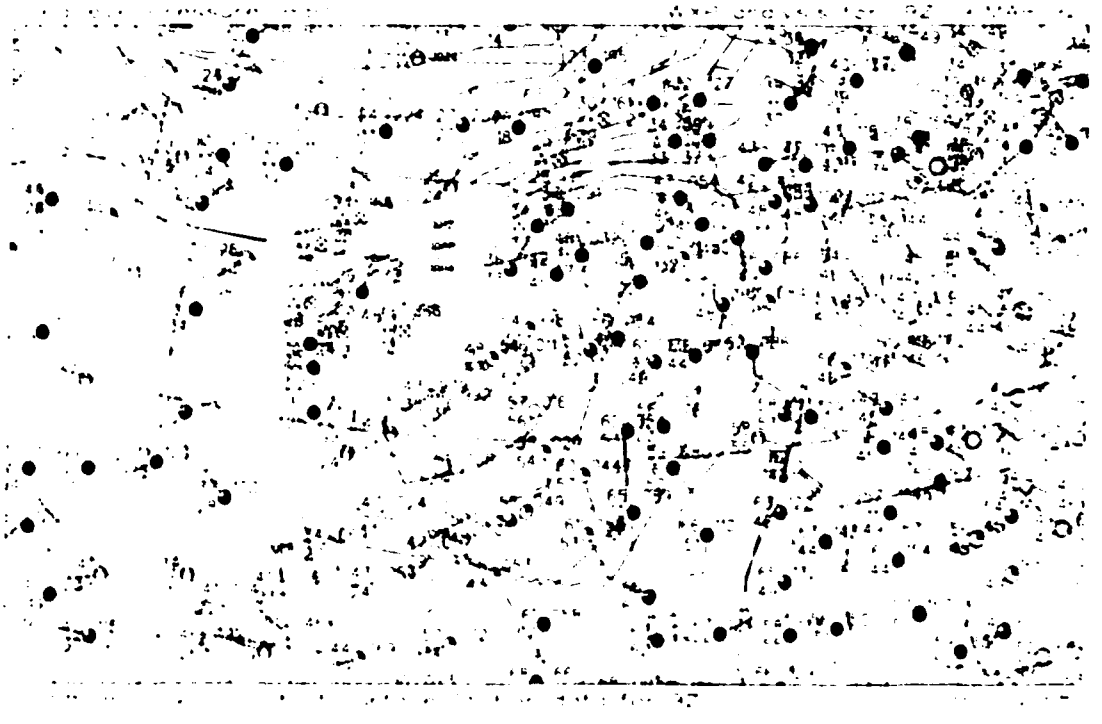

Figure 14: Surface weather map and sea-level pressure analysis for 09 UTC 9 March 1992.

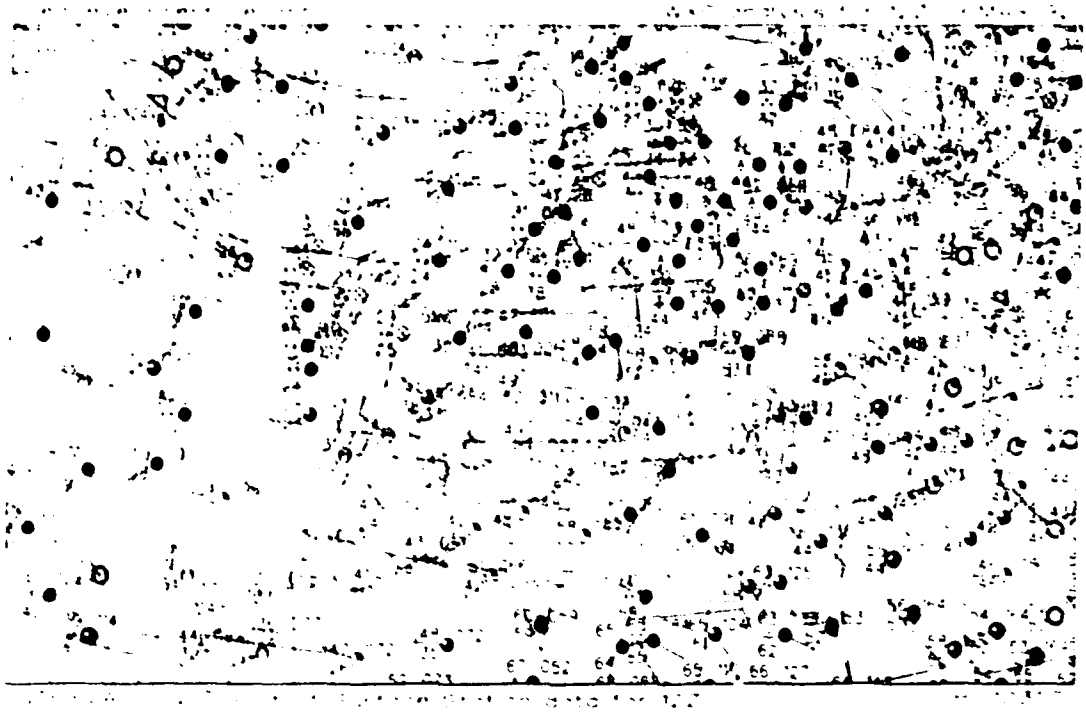

Figure 15: Surface weather map and sea-level pressure analysis for 12 UTC 9 March 1992.

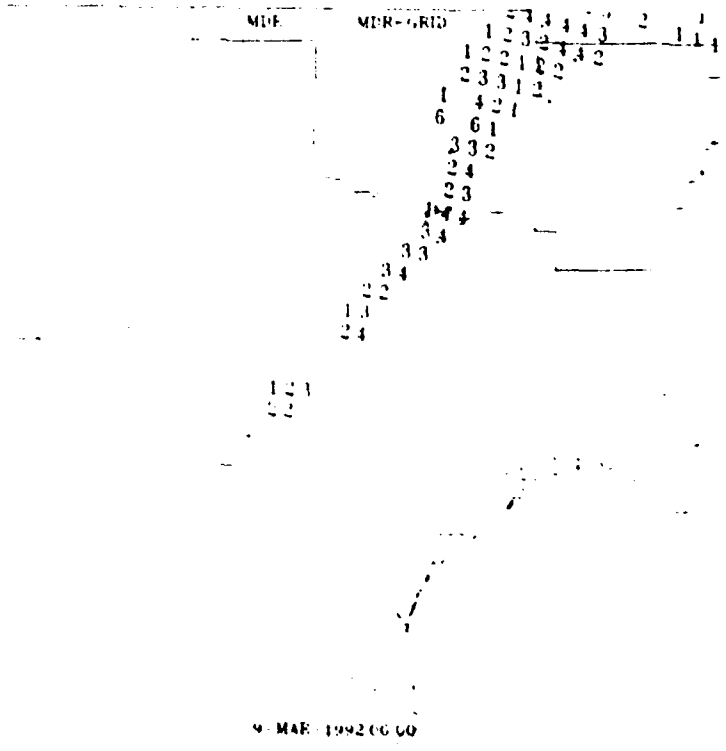

Figure 16: MDR summary for 06 UTC 9 March 1992.

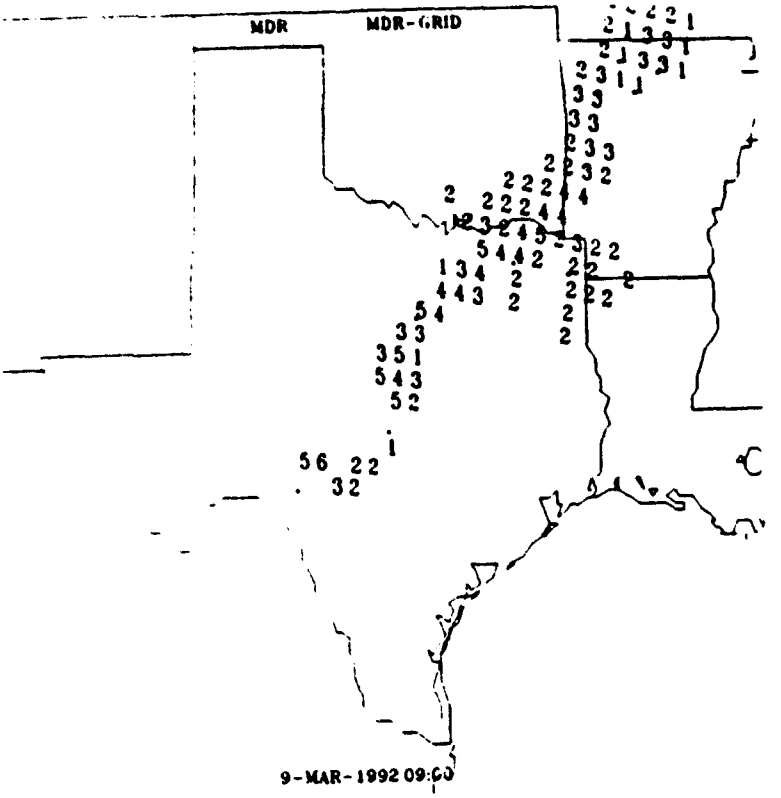

Figure 17: MDR summary for 09 UTC 9 March 1992.

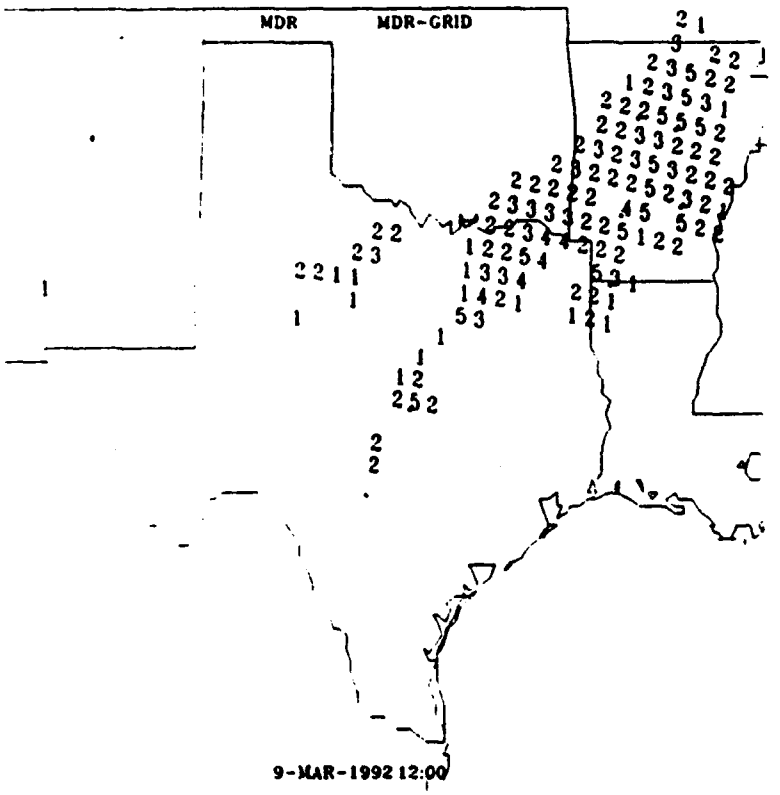

Figure 18: MDR summary for 12 UTC 9 March 1992.

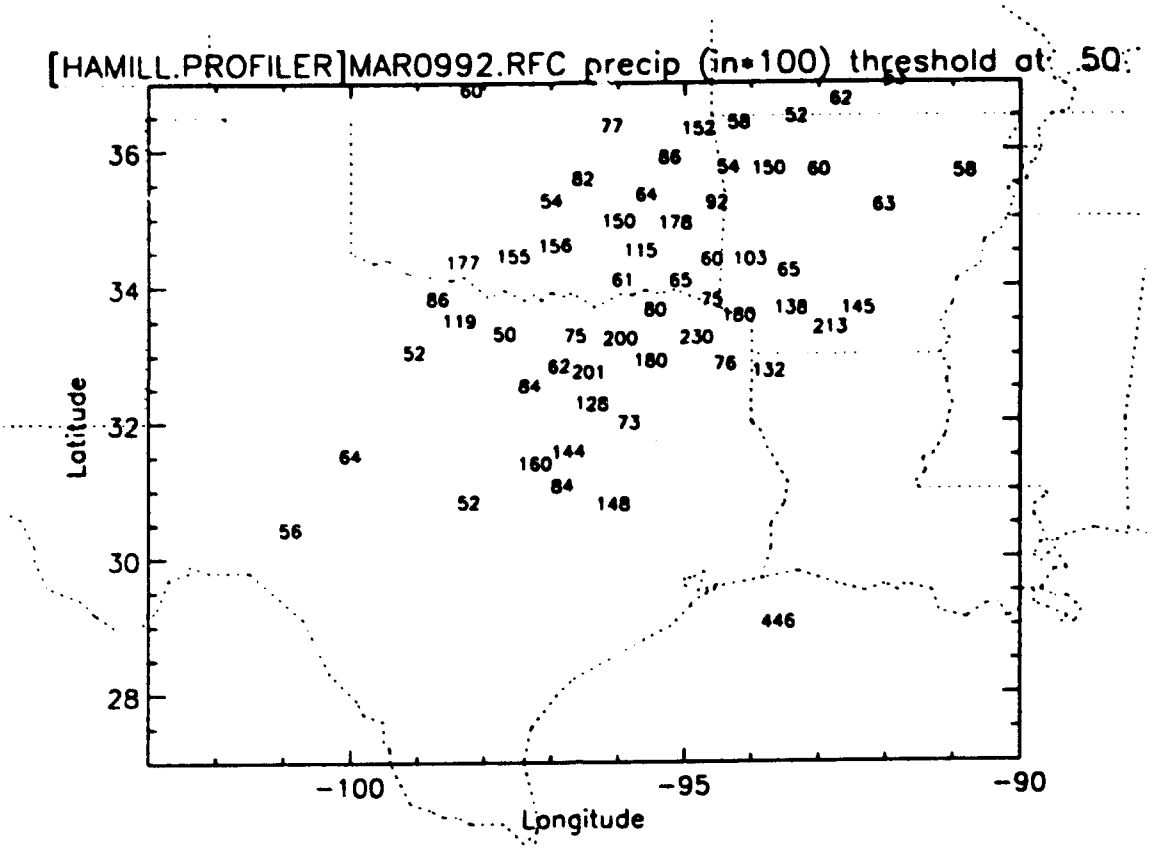

Figure 19: Map of 24-hr precipitation ending at 12 UTC 9 March 1992. Only values in excess of .5 in are plotted.

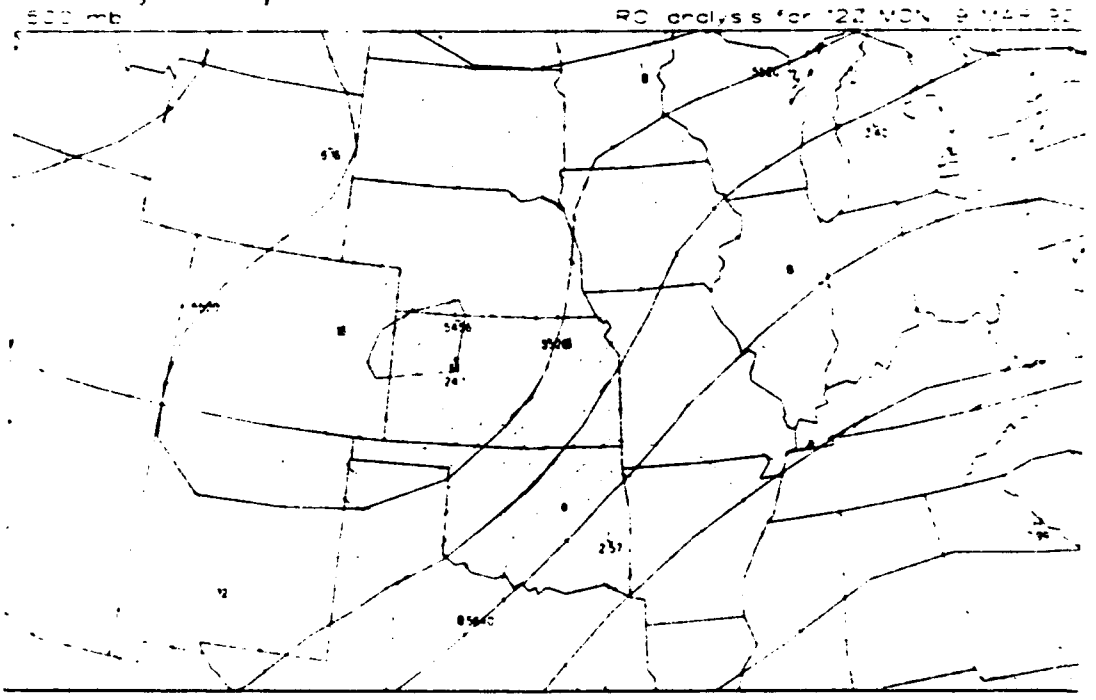

Figure 20: 500 mb analysis of height (solid lines) and absolute vorticity (dashed lines) for 12 UTC 9 March 1992.

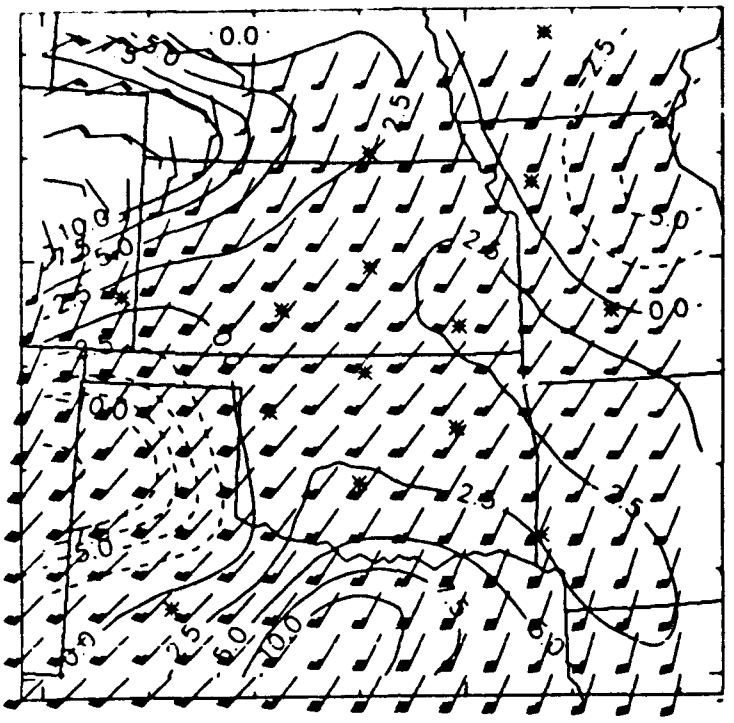

Figure 21: Profiler-derived analysis of winds and integrated vertical velocity (cm/s) at 3000 m for 03 UTC 9 March 1992.

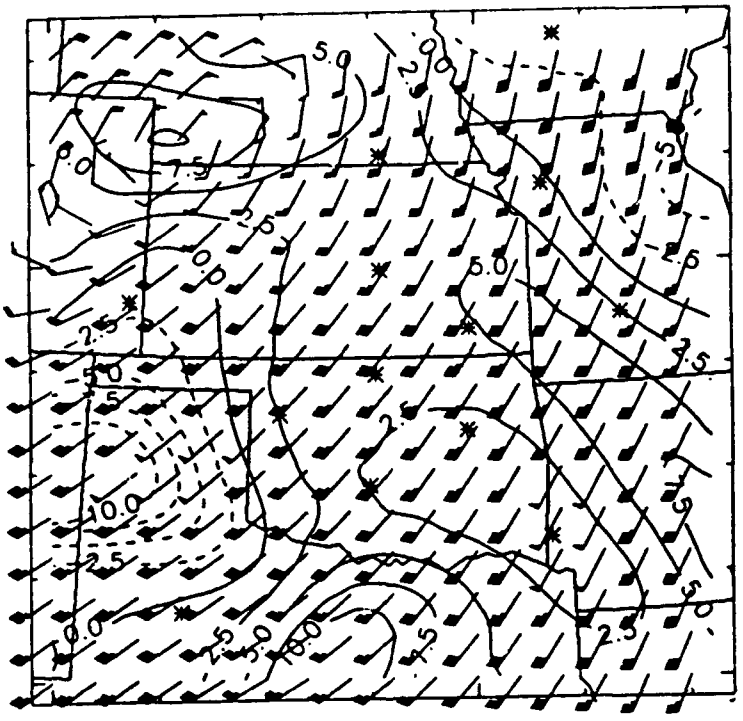

Figure 22: Profiler-derived analysis of winds and integrated vertical velocity (cm/s) at 3000 m for 06 UTC 9 March 1992.

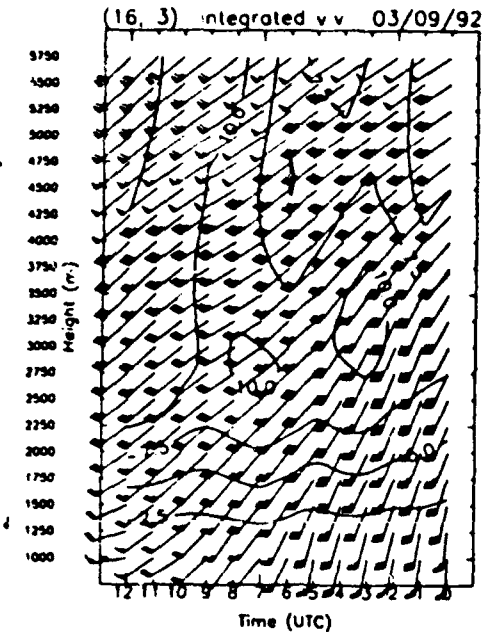

Figure 23: Time-height cross section of profiler-derived winds and integrated vertical velocity (cm/s) for DFW for 00-12 UTC 9 March 1992.

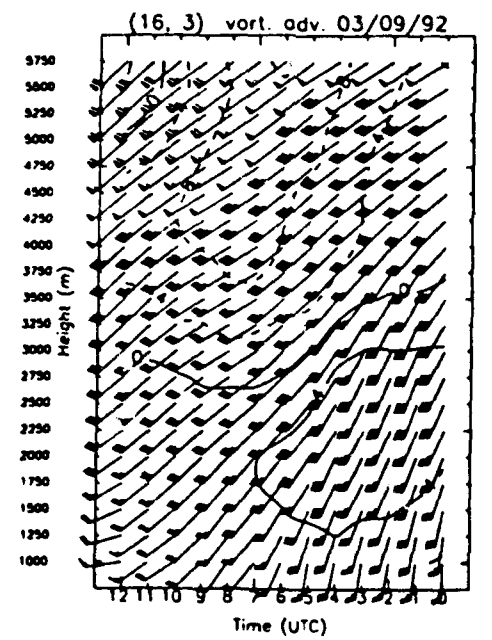

Figure 24: Time-height cross section of profiler-derived winds and vorticity advection ($10^{-9}s^{-2}$) for DFW for 00-12 UTC 9 March 1992.

3.2. July 26, 1992: Missouri mesoscale convective complex

A mesoscale convective complex (MCC) deposited 1-3" of rain in northwest Missouri between 00 and 12 UTC 26 July 1992, with 1" falling between 06 and 12 UTC. The NGM drastically underforecast the amount of rainfall between 06 and 12 UTC. A convective outbreak also resulted in 1"-3" of rain in Kansas between 00 and 12 UTC, with the NGM making a good precipitation forecast between 06 and 12 UTC. The forecast problem of interest in this case is the period between 06 and 12 UTC, for Kansas and Missouri. We consider nowcasts made with data available up to 06 UTC.

3.2.2. Standard Meteorological Data Available Before the Storm.

The 03 and 06 UTC surface maps shown in Figures 25 and 26 show a stationary front through central Kansas and northwest Missouri with a weak low along the central Oklahoma-Kansas border. Winds are from the northwest to the north of this front, and moist southerly winds with dewpoints in the low to mid 70's are overrunning this front from the south and helping to produce thunderstorms to the north. The 03 UTC manually digitized radar summary (Figure 27) shows echoes extending from eastern Colorado through Kansas to northwest Missouri. Level 5 echoes exist in northwest Missouri and level 6 echoes exist in western Kansas. By 06 UTC (Figure 28), convection had largely ceased in eastern Colorado, and weakened over extreme western Kansas. Infrared satellite imagery was only available to us at 00 UTC (Figure 29); it shows an oval cloud mass over the Missouri-Iowa border that is suggestive of an MCC. Convective clouds are also evident over southeast Colorado and western Kansas.

The 00 UTC upper air maps show moist southwesterly flow at 850 mb (Figure 30) over Kansas, Oklahoma, and Missouri, with northerly flow to the north. A weak trough is over the Colorado-Kansas border at 700 mb (Figure 31) and 500 mb (not shown), causing the area of convection there visible in Figure 29. Low level convergence is apparent in Figure 30 over Kansas and northwest Missouri, contributing to upward motion. Upper level (200 mb, not shown) divergence is occurring over that same area.

The 00 UTC NGM forecast guidance for 6 hour precipitation accumulations ending at 12 UTC (Figure 32) shows heavy precipitation (up to 1.02") over

western Kansas, but only light precipitation (0.2" and less) over eastern Kansas and western Missouri. The 700 mb vertical velocity forec- ' .J at 06 UTC (Figure 33) shows upward motion in eastern Colorado ' 'ansas in association with the mid-level trough, and sinking moti stern Kansas and Missouri. Over the next 6 hours, the maximum vertic . :ity is predicted to move east to central Kansas, with weak ascent replacing descent over Missouri by 12 UTC (Figure 34). Forecasts of 850 mb and 200 mb convergence for 06 UTC (not shown) reflect this pattern: low level convergence and upper level divergence is predicted for Kansas, while the opposite is true for northwest Missouri. The forecast for the Kansas region is relatively straightforward in this case: both the NGM forecast guidance, and the observations of ongoing convective activity available at 06 UTC indicate the likelihood of significant convective rainfall for the next 6 hours. For northwest Missouri, the situation is more complicated: while the NGM guidance suggests little or no precipitation over this region, observations of convective activity over the previous 6 hours are in obvious contradiction to the forecast guidance. An experienced forecaster would thus likely overrule the NGM guidance to some degree, although he or she might expect the convection to decrease in response to the predicted unfavorable dynamic forcing.

3.2.2. Information Available During and After the Storm.

The surface front remains nearly stationary from northern Missouri through southeast Kansas after 06 UTC, as does a weak low along the eastern Oklahoma-Kansas border. Both features are visible in Figure 35, the 09 UTC surface map. Overrunning continues to produce thunderstorms north of this front in Kansas and northwest Missouri, including a heavy thunderstorm at Kansas City (MCI - see Figure 34 for station location) at 08 UTC. The 06-09 UTC manually digitized radar summaries show decreasing convective activity in western Kansas, but continued convection, including level 5 echoes, in central and eastern Kansas, and northwest Missouri. The two areas of thunderstorms in northwest Missouri and Kansas have merged into one MCC by 09 UTC (Figure 36). The hourly observations from Kansas City show thunderstorms between 05 UTC and 09 UTC, with a heavy thunderstorm at 08 UTC. MCI received 1.06" of rain between 06 and 12 UTC, whereas the NGM only forecasted .15". Figure 37 shows several sites near MCI with large (1.5" - 3.3") 24-hour accumulations.

3.2.3. Utility of the Profiler Data.

Plots of the profiler derived 3000 m horizontal winds and vertical velocities at 03 UTC (not shown) and 06 UTC (Figure 38) show weak sinking motion developing over western Kansas, and upward motion intensifying to over 10 cm/s over northwest Missouri. However, the data coverage of the eastern part of the domain is insufficient to resolve small-scale features of the flow field. Comparison with the radar summary at that time (Figure 28) shows a good correspondence between analyzed upward motion and convective activity over northeast Kansas and northwest Missouri, but in western Kansas widespread level 2 and 3 echoes, and scattered level 4 and 5 echoes, exist in an area characterized by generally downward large scale motion at 3000 m. While it is possible that the profiler derived winds may have been influenced by echoes from rainfall or low level thunderstorm outflow (although the effect of this is probably quite small, since profiler winds are only measured above 0.5 km AGL), a more likely explanation is that this precipitation is not linked to low-level ascent, as is the case with dissipating convection. In any case, the profiler vertical velocity field clearly is in direct contradiction to the NGM forecast for this period (Figure 33) - the signs of predicted and analyzed vertical velocity are reversed over Kansas and Missouri. A forecaster supplied with this additional information would thus be more confident in overriding the NGM forecast guidance in the forecast for northwest Missouri, and call for significant convective activity. Convection in eastern Kansas would be expected to diminish in response to the large scale descent, in accordance with the verifying observations (viz. Figure 36).

Plots of profiler derived 1500 m (not shown) and 12,750 m (Figure 39) horizontal wind and convergence analyses at 06 UTC show the strongest low level convergence is occurring over northwest Missouri beneath upper level divergence and very little convergence is occurring over western Kansas beneath strong upper level thunderstorm outflow. Although the analyzed upper level divergence may seem extreme, it is clearly supported by the available profiler observations (Figure 40). The time series of profiler derived winds and convergence above MCI between 00 UTC and 12 UTC (Figure 41) shows low-level convergence and upper level divergence throughout the entire time period,

with the strongest low level convergence occurring just before the heavy thunderstorm at 08 UTC.

In summary, profiler derived analyses of vertical velocity leading up to the forecast period (06 UTC - 12 UTC) show large deviations from the NGM guidance over eastern Kansas and northwest Missouri, indicating diminishing convection over eastern Kansas, and increasing convection over northwest Missouri. Although an experienced forecaster could have concluded that the NGM was underforecasting precipitation in Missouri from the radar and surface observation leading up to 06 UTC, the profiler data would have served to explain the observed discrepancy in terms of the underlying large scale forcing, and resulted in a more precise and confident forecast.

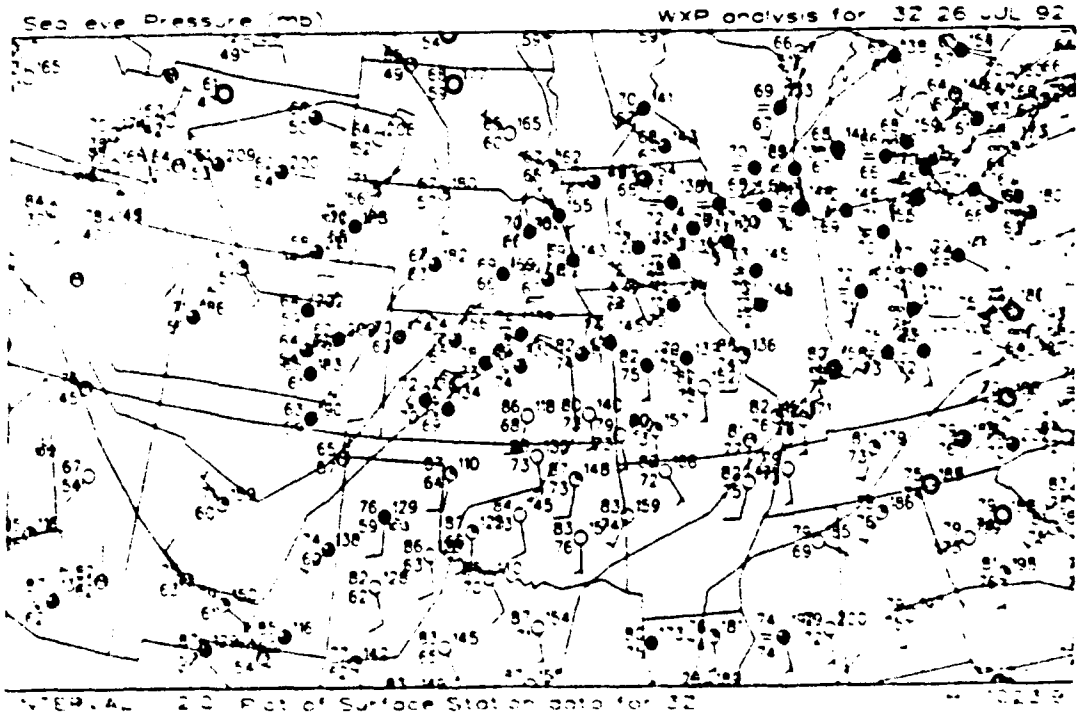

Figure 25: Surface weather map and sea-level pressure analysis for 03 UTC 26 July 1992.

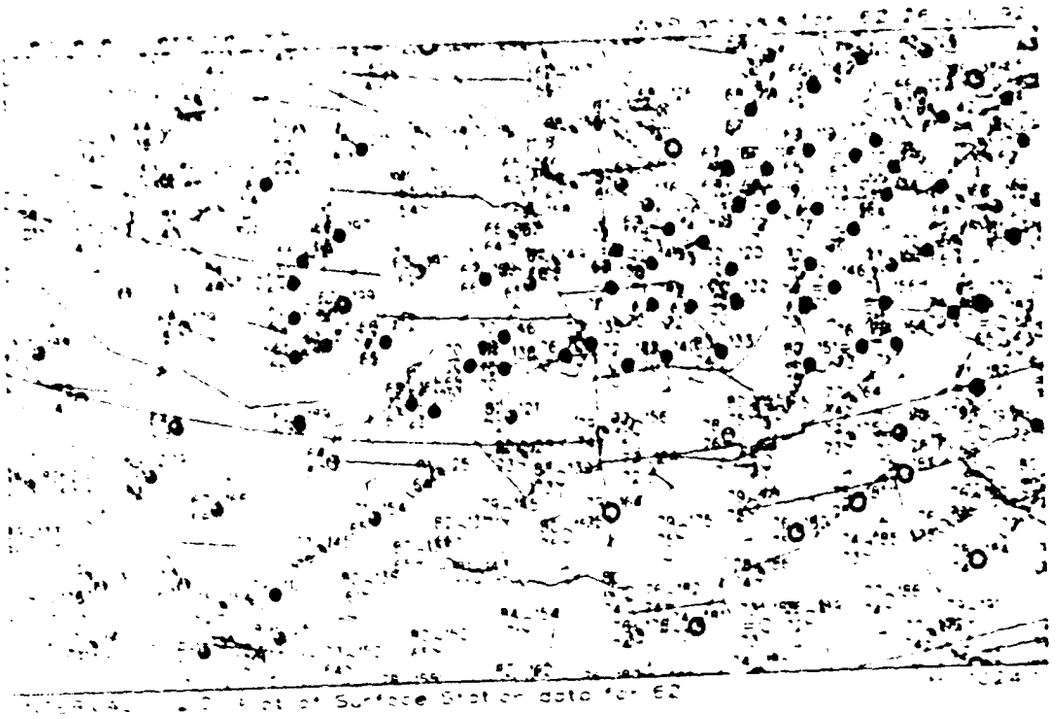

Figure 26: Surface weather map and sea-level pressure analysis for 06 UTC 26 July 1992.

Figure 27: MDR summary for 03 UTC 26 July 1992.

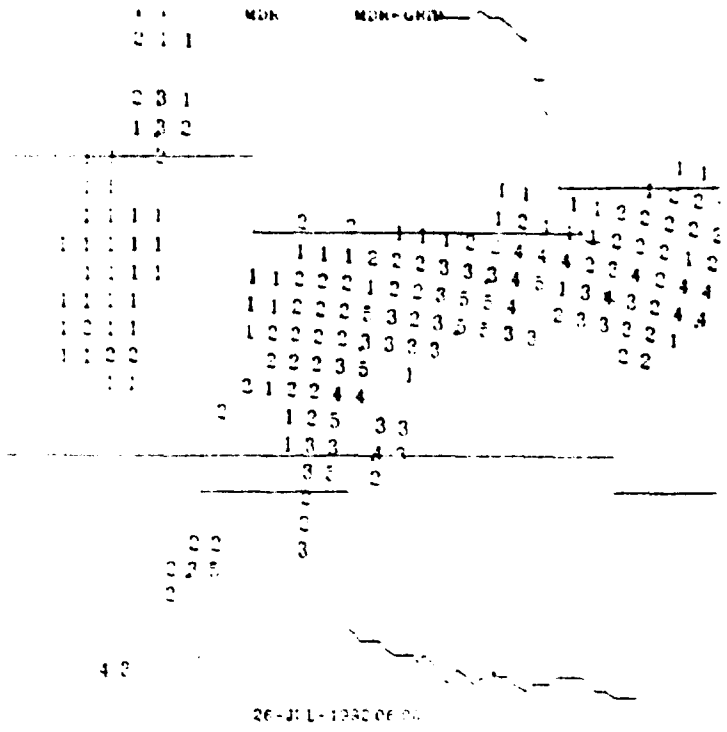

Figure 28: MDR summary for 06 UTC 26 July 1992.

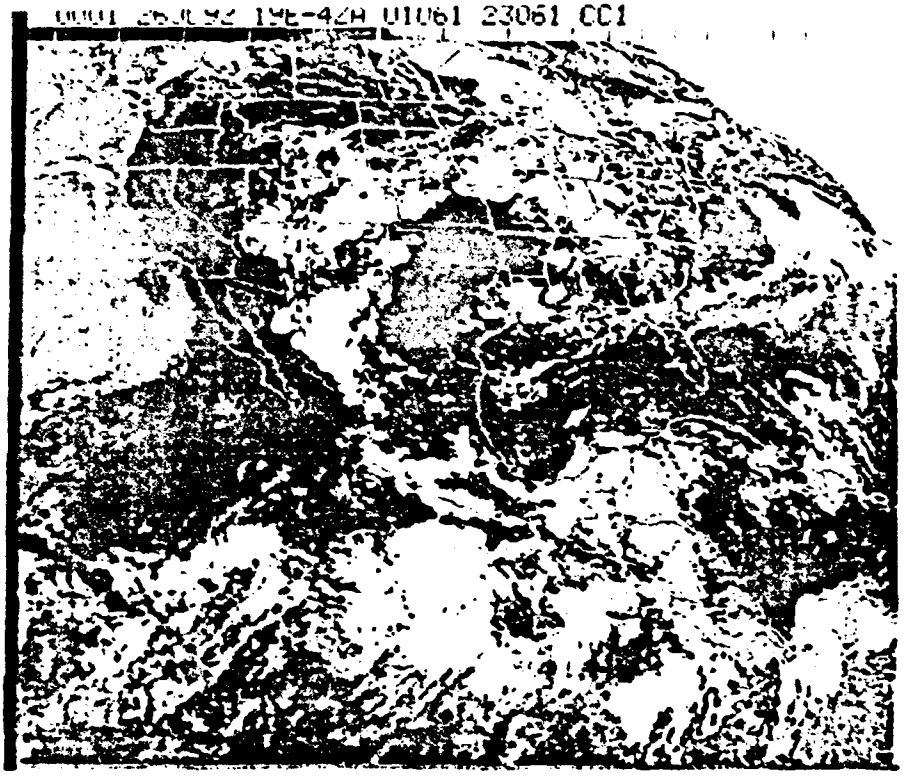

Figure 29: Infrared satellite image for 00 UTC 26 July 1992.

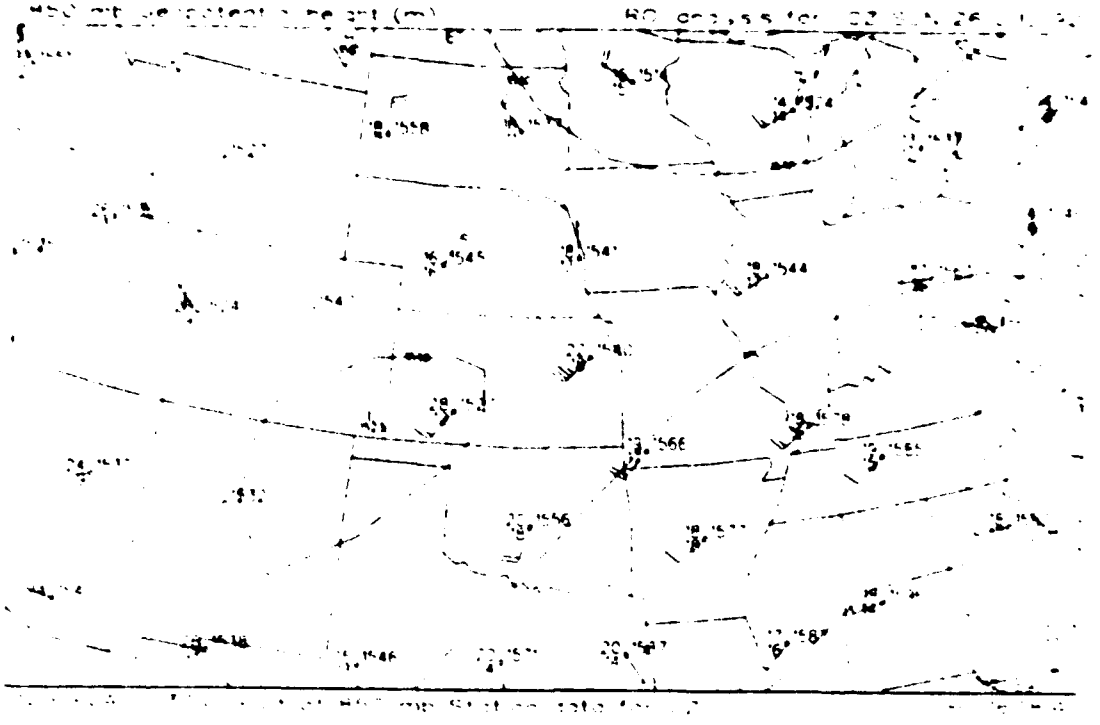

Figure 30: 850 mb weather map and height analysis for 00 UTC 26 July 1992.

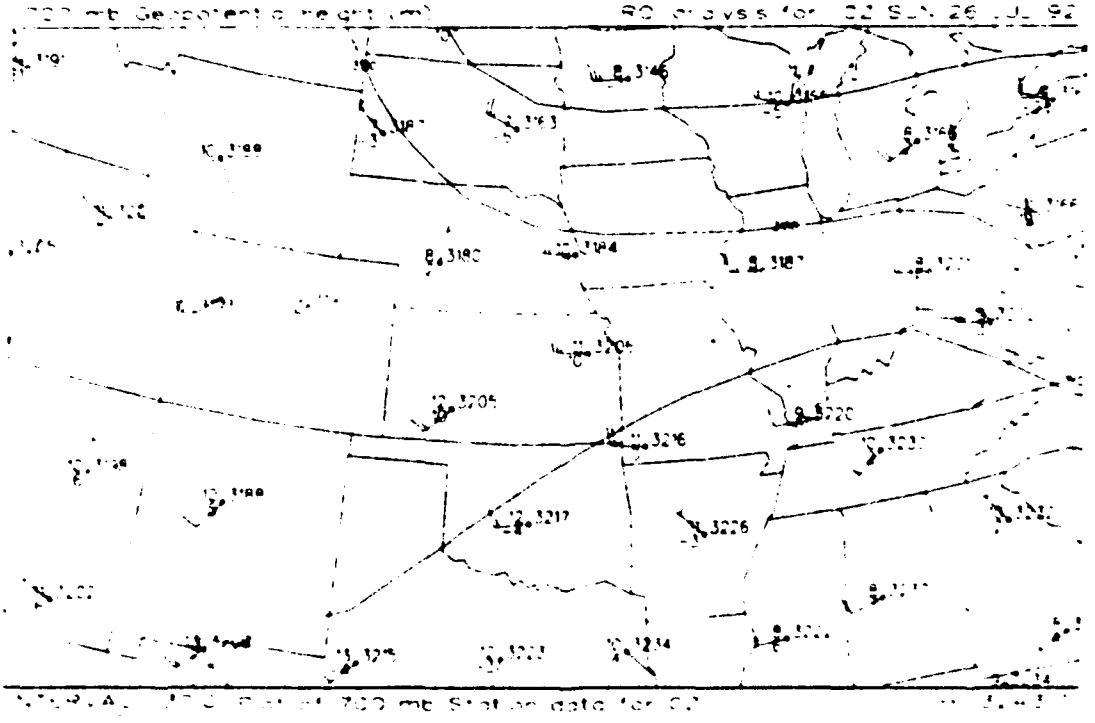

Figure 31: 700 mb weather map and height analysis for 00 UTC 26 July 1992.

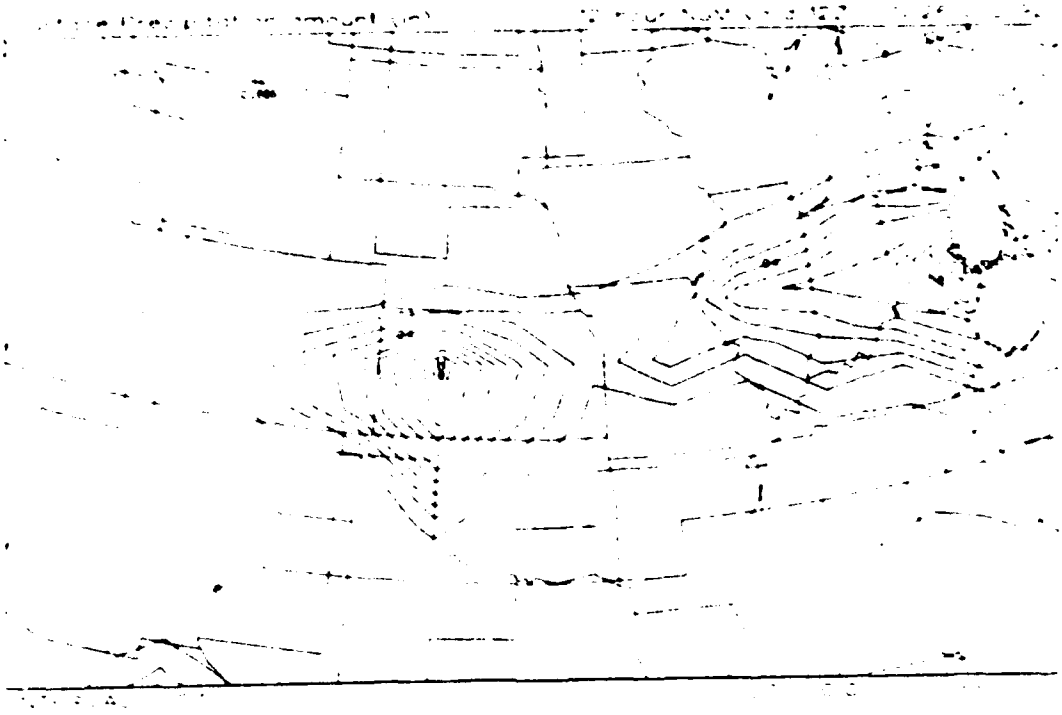

Figure 32: NGM 00 UTC 26 July 1992 forecast of 6-hour accumulated precipitation, valid 12 UTC 26 July 1992.

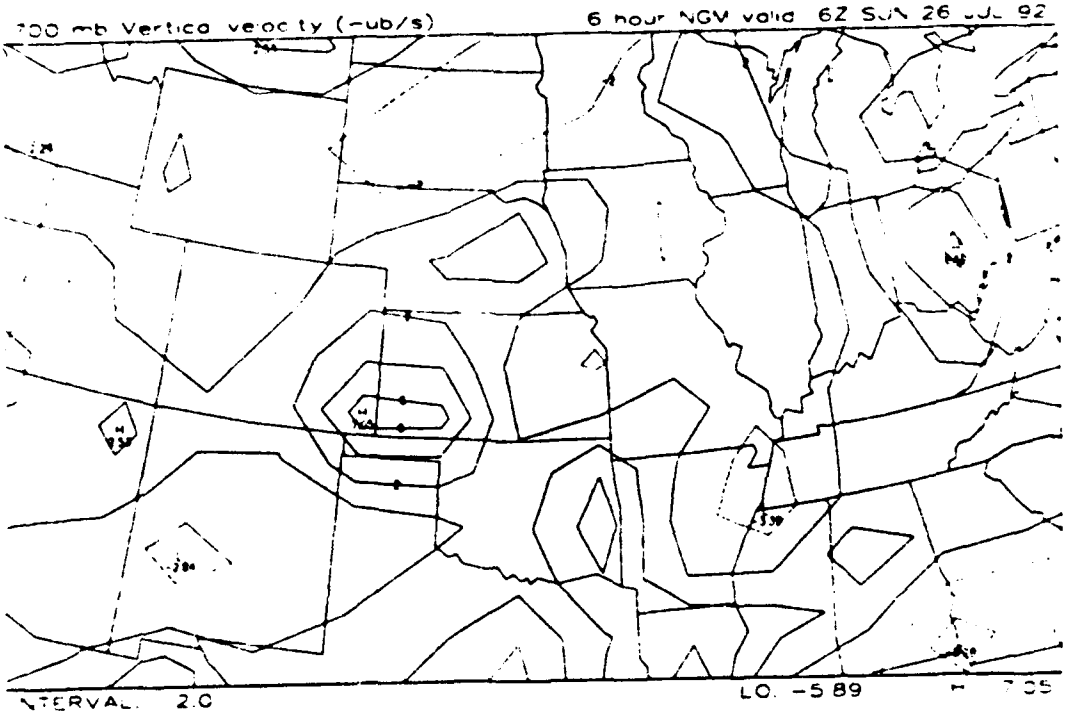

Figure 33: NGM 00 UTC 26 July 1992 forecast of 700 mb vertical velocity (μb/s, or cm/s), valid 06 UTC 26 July 1992.

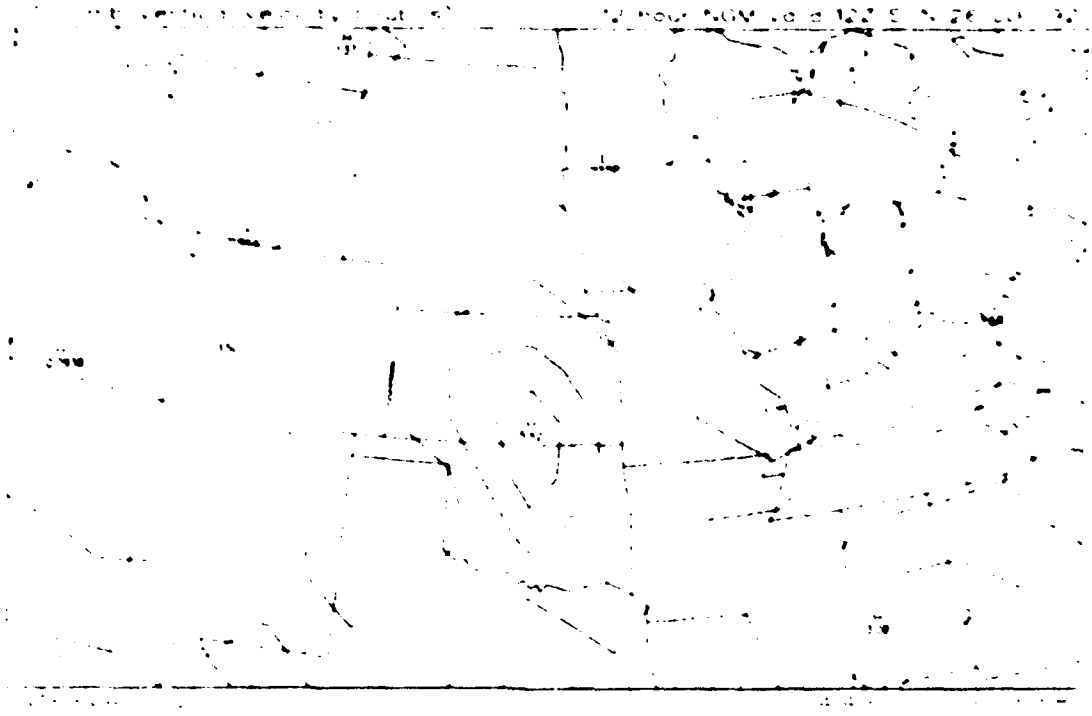

Figure 34: NGM 00 UTC 26 July 1992 forecast of 700 mb vertical velocity (μb/s, or cm/s), valid 12 UTC 26 July 1992

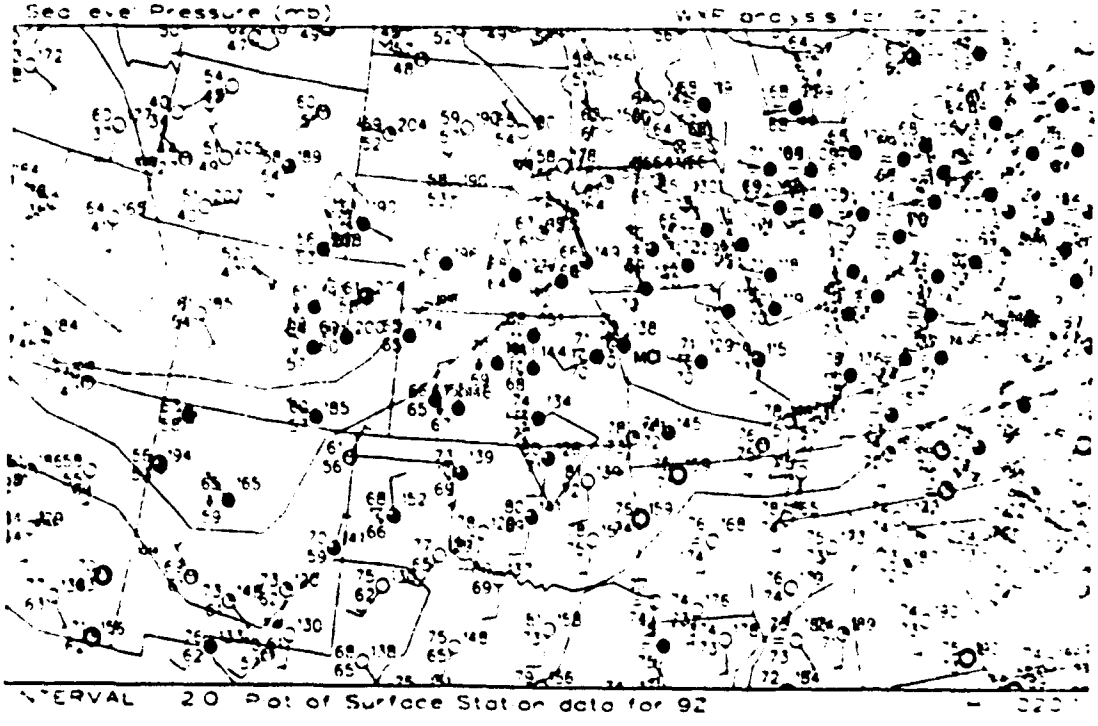

Figure 35: Surface weather map and sea-level pressure analysis for 09 UTC 26 July 1992.

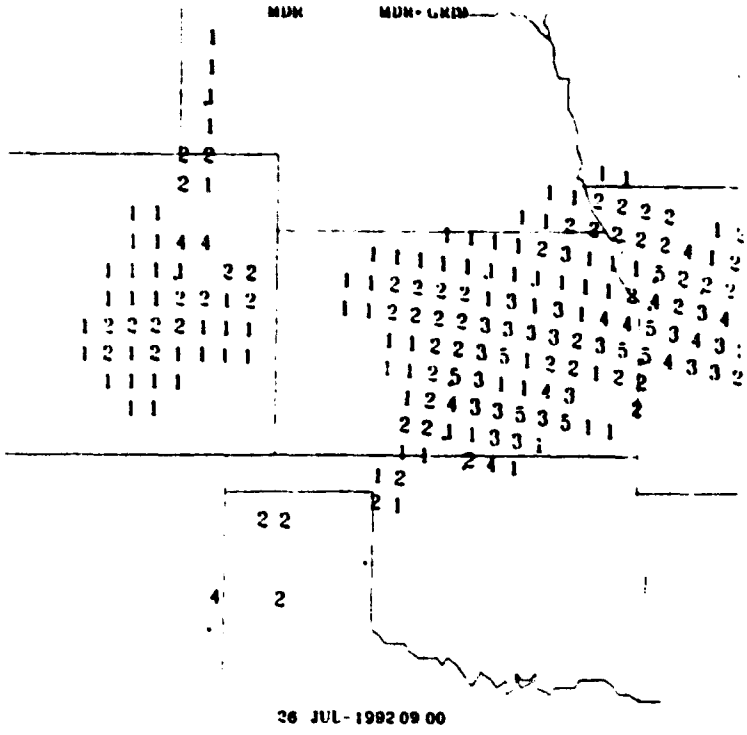

Figure 36: MDR summary for 09 UTC 26 July 1992.

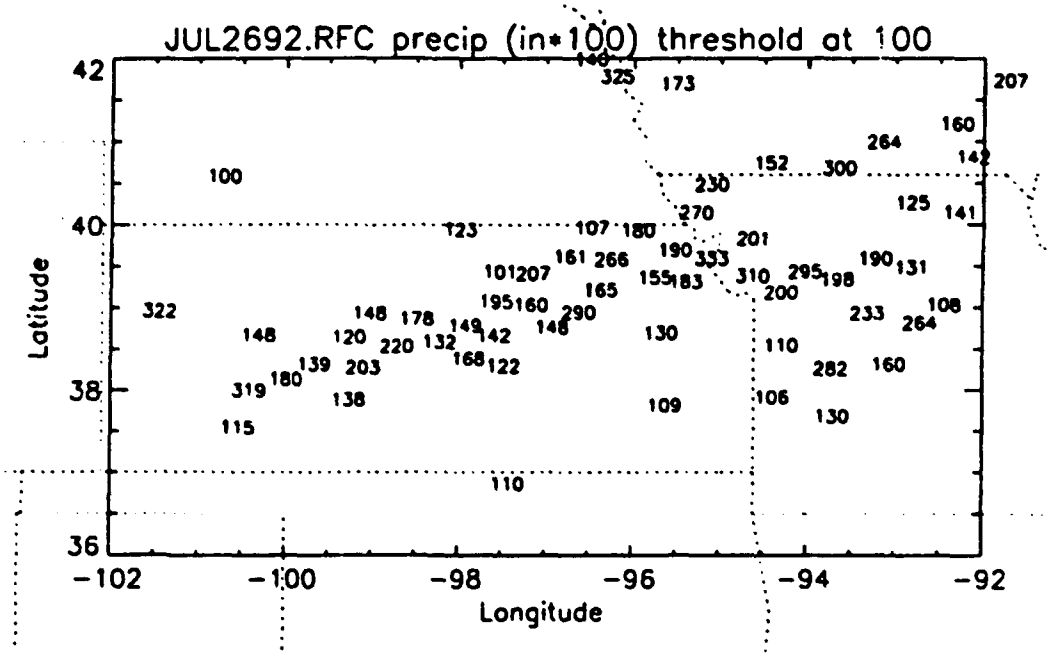

Figure 37: Map of 24-hr precipitation ending at 12 UTC 26 July 1992. Only values in excess of 1.0 in are plotted.

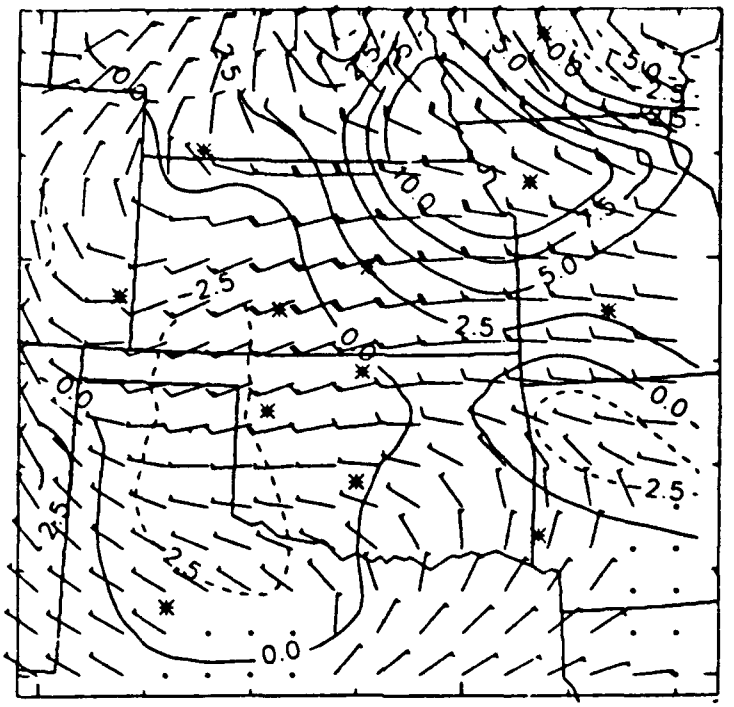

Figure 38: Profiler-derived analysis of winds and vertical velocity (cm/s) at 3000 m for 06 UTC 26 July 1992.

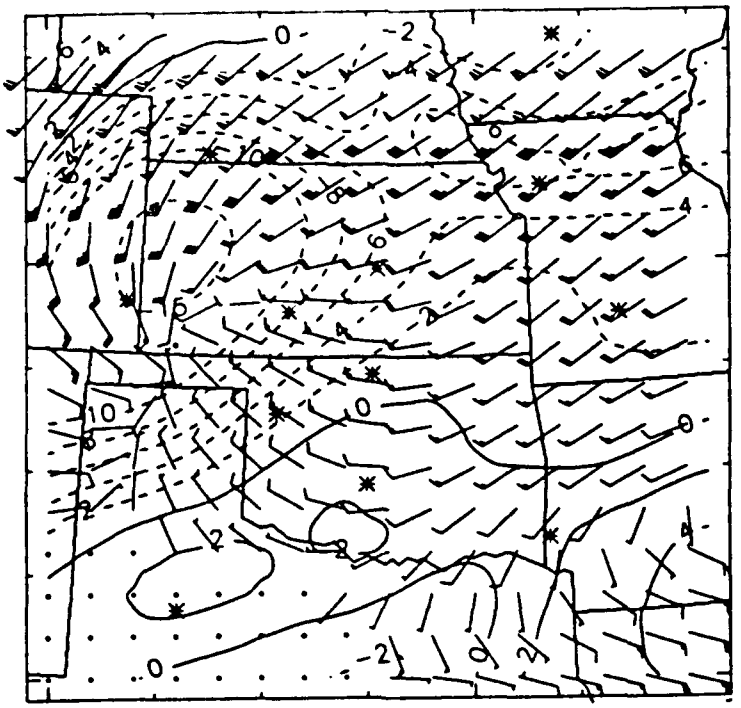

Figure 39: Profiler-derived analysis of winds and horizontal convergence (in $10^{-5}s^{-1}$) at 12750 m for 06 UTC 26 July 1992.

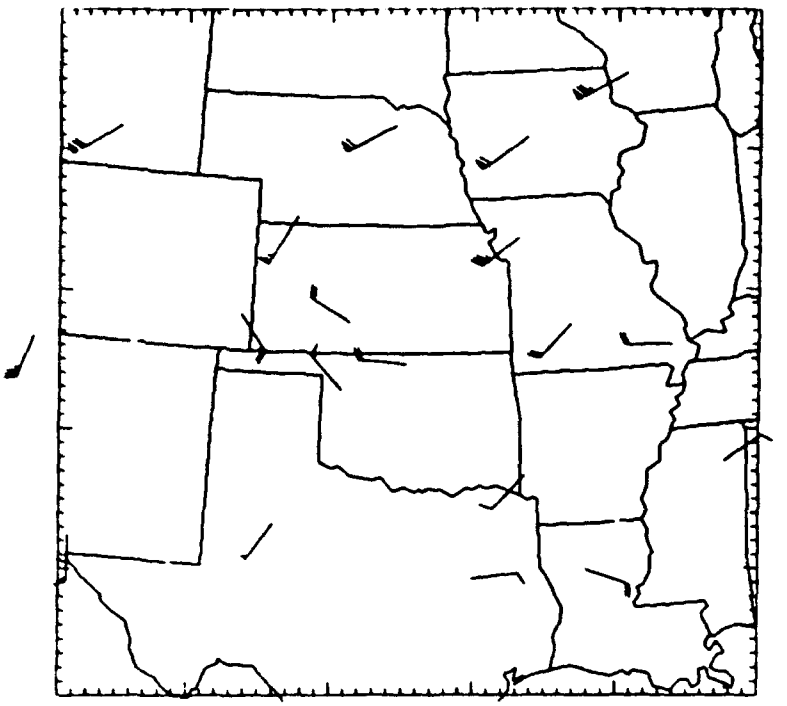

Figure 40: Profiler data used in the analysis shown in Figure 39.

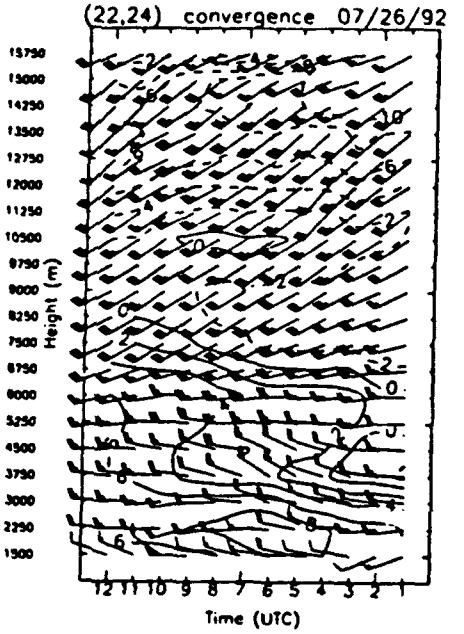

Figure 41: Time-height cross section of profiler-derived winds and horizontal convergence (in $10^{-5}s^{-1}$) for MCI for 00-12 UTC 26 July 1992.

3.3. August 4, 1992: Oklahoma mesoscale convective complex

Between 00 and 12 UTC 4 August 1992, a mesoscale convective complex (MCC) produced up to 5" of rain in north central Oklahoma. The 00 UTC NGM correctly forecasted the location of the maximum precipitation between 06 and 12 UTC, but drastically underforecast the amount. We examine the utility of profiler data for forecasts for the period 06 UTC to 12 UTC, issued at 03 UTC (short-term forecast) and 06 UTC (nowcast).

3.3.1. Standard Meteorological Data Available Before the Storm.

The 03 UTC surface map in Figure 42 shows a cold front through central Oklahoma, which is moving slowly to the south. Moist air from the Gulf of Mexico is overrunning this front and producing clouds to the north. Scattered showers and thunderstorms are occurring in eastern Colorado and western Kansas. The 03 UTC manually digitized radar summary (Figure 43) shows strong thunderstorms (level 6 echoes) in southeast Colorado and western Kansas, and a level 5 echo at the Kansas/Oklahoma border. Figure 44 shows the 0330 UTC infrared satellite image. Skies are mostly clear in Oklahoma while convective clouds are evident in western Kansas and eastern Colorado.

The 00 UTC upper air maps show a moist southerly flow at 850 mb (Figure 45) and a dry northwesterly flow at 700 mb (Figure 46), producing potential instability over Oklahoma. The rawinsonde report from Amarillo, TX (AMA) indicates a jet streak over the Texas panhandle at 200 mb (not shown), which places Oklahoma in the left exit region of the jet, a region where upper level divergence induces upward motion and potential instability can be realized. The Norman, OK (OUN) sounding at 00 UTC indicates fairly light winds throughout the troposphere, and a moist layer (16 g/kg) under a capping inversion and dry layer at 800 mb, with a lifted index of approximately -5° - all conditions favorable for significant convective precipitation, provided the capping inversion can be penetrated.

The 00 UTC NGM forecast guidance for 6 hour precipitation accumulations ending at 12 UTC (Figure 47) indicate maximum precipitation of slightly over .5" centered over north central Oklahoma. The 700 mb vertical velocity forecasts valid at 06 UTC (Figure 48) and 12 UTC (Figure 49) show the maximum vertical

velocity increasing from 5 cm/s to over 7.5 cm/s as it moves east from the Oklahoma panhandle to north central Oklahoma. The 500 mb forecast maps for those times (not shown) show a weak 500 mb short wave trough and associated vorticity maximum approaching north central Oklahoma from the northwest.

Surface maps and radar summaries between 03 UTC and 06 UTC (Figures 50 and 51) show further southward movement of the approaching cold front, decreasing convective activity in eastern Colorado, and increasing convection in southern Kansas and northern Oklahoma. Level 5 and 6 echoes indicate the presence of heavy thunderstorms in southwestern Kansas and northern Oklahoma. A short-term forecast issued with data and guidance available at 03 UTC would most likely follow the NGM guidance: a strong likelihood of convection in north central Oklahoma, with little reason to expect a large deviation from the forecasted precipitation amounts, aside from locally heavy storms. At 06 UTC, the large number of strong echoes at the Kansas/Oklahoma border would cause a forecaster to revise the predicted precipitation amount upward.

3.3.2. Information Available During and After the Storm.

After 06 UTC, the cold front continues to move slowly to the south through central Oklahoma with overrunning moist air from the south continuing to feed thunderstorms to the north (see the surface map at 10 UTC in Figure 52). Thunderstorms are increasing with time over northern Oklahoma with heavy thunderstorms occurring over Tulsa (TUL) at 10 UTC and Oklahoma City (OKC) at 11 UTC (see Figure 52 for station locations). The manually digitized radar summaries (see Figure 53 for 10 UTC) show the thunderstorms in southern Kansas and northern Oklahoma developing the characteristic oval shape of an MCC and moving slowly to the east. The heaviest thunderstorms associated with level 6 echoes occur in north central Oklahoma between 06 and 08 UTC. The 1030 UTC infrared satellite image in Figure 54 shows the oval shape in the MCC cloud mass over Oklahoma. The 24-hr accumulations shown in Figure 55 are in excess of 3" in several locations in north-central Oklahoma and south-central Kansas, with one report of 5.2", in a wide-spread area of amounts over 1".

3.3.3. Utility of the Profiler Data.

Figures 56 and 57 show the 03 and 06 UTC profiler derived 3000 m horizontal winds and vertical velocities. At 03 UTC, weak upward motion is analyzed over central and eastern Oklahoma, with sinking motion over the then active area of convection in eastern Colorado and Kansas. However, because of missing winds in the Texas panhandle and over New Mexico, the analyzed convergence and vertical velocity to the east of the inner network are unreliable for this case. At 06 UTC, analyzed vertical velocities are roughly twice the predicted (2 cm/s vs. 4-5 cm/s, viz. Figure 43) over north central Oklahoma. This discrepancy indicates the potential for greater than forecasted precipitation, but by itself would not support deviating by 3"-5" from the forecast guidance. Likewise, the low level (850 mb) convergence at 06 UTC is approximately twice what the NGM predicted for that time (not shown). Since this convergence is occurring in a very moist air mass (surface dewpoints in the 70s), this convergence is related to precipitation amounts both because of the forcing of thunderstorms through large-scale ascent, and because of the supply of low-level moisture it represents.

The time-height cross section of profiler derived horizontal winds and convergence over Enid, OK (END) in Figure 58 shows the maximum low level convergence (and, consequently, upward motion) occurring during the heaviest thunderstorm activity around 08 UTC. The cross section also reveals passage of an upper level jet streak, and upper level divergence maximum, at and after 08 UTC.

In summary, neither the conventional observations nor the profiler analyses available at 03 UTC would cause a forecaster to significantly increase the NGM forecasted precipitation amount for north central Oklahoma. By 06 UTC, radar information indicated intense convection starting in Oklahoma, and profiler derived analyses of low level convergence and upward motion indicated an underforecast by a factor of approximately two. The profiler data thus amplify and confirm the indications from the radar data, and motivate a forecaster to predict more rain than the NGM did. It is doubtful, however, that even with this additional information the extreme accumulations of 3"-5" would have been predicted in this case.

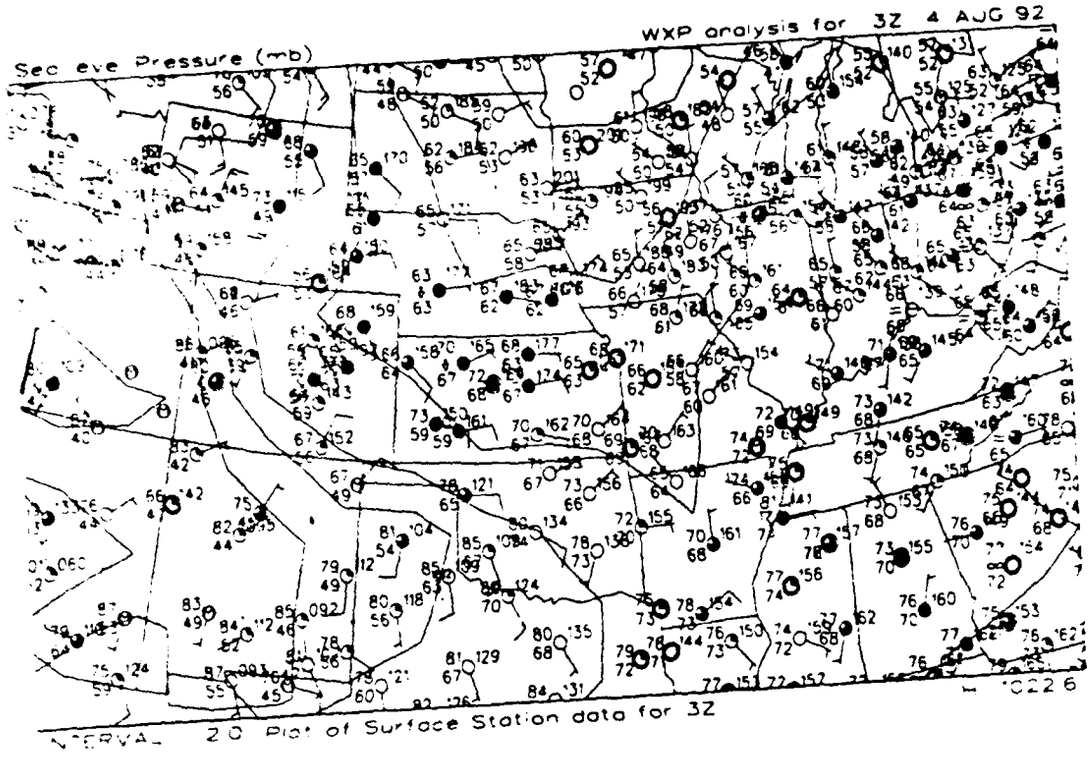

Figure 42: Surface weather map and sea-level pressure analysis for 03 UTC 4 August 1992.

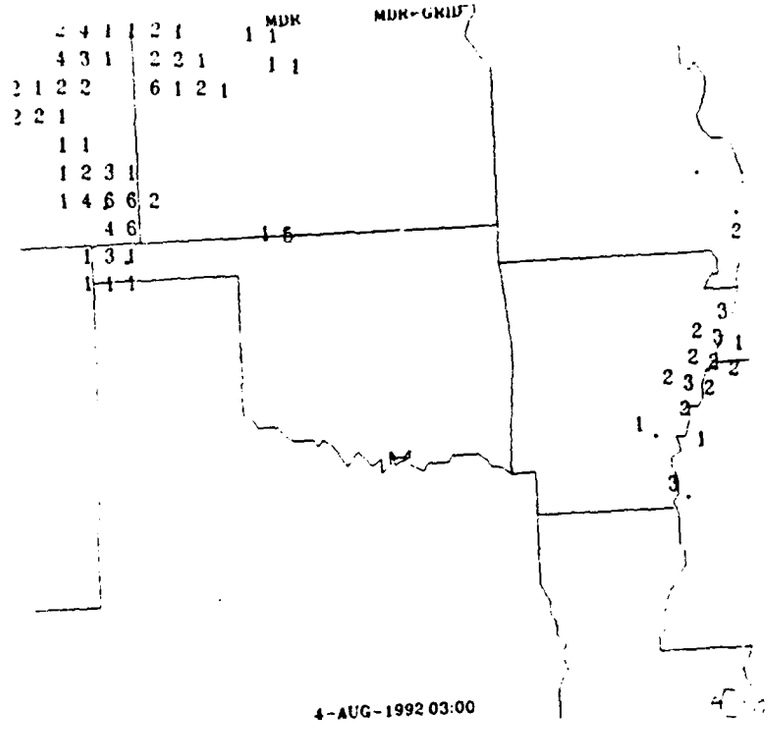

Figure 43: MDR summary for 03 UTC 4 August 1992.

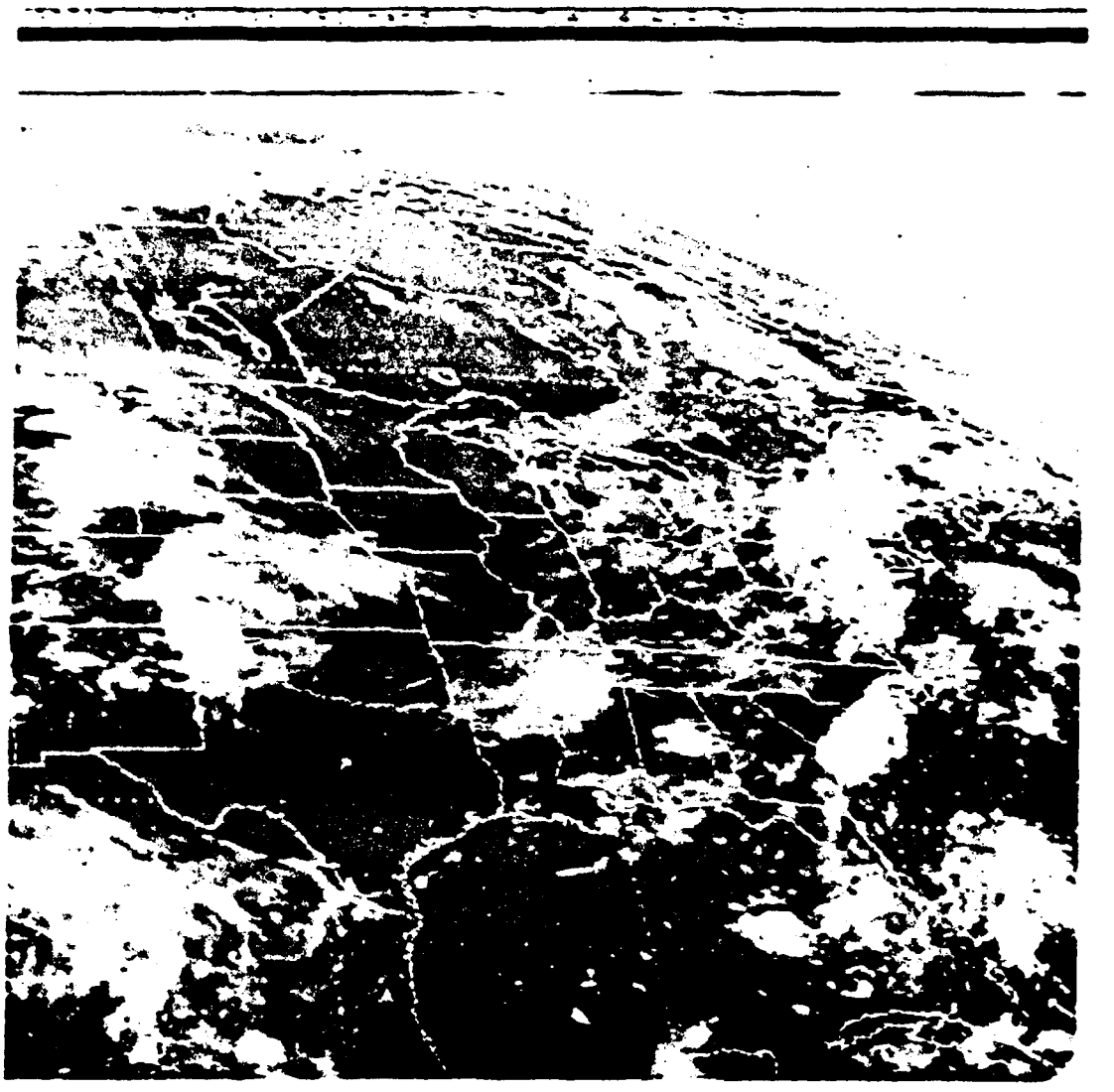

Figure 44: Infrared satellite image for 0330 UTC 4 August 1992.

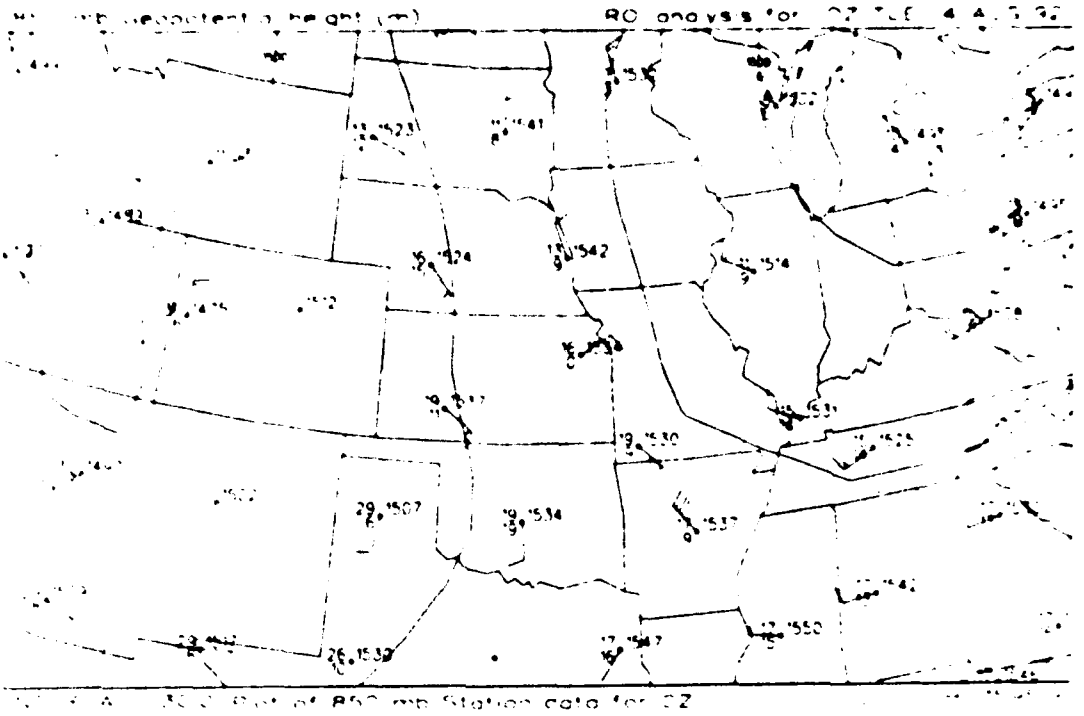

Figure 45: 850 mb weather map and height analysis for 00 UTC 4 August 1992.

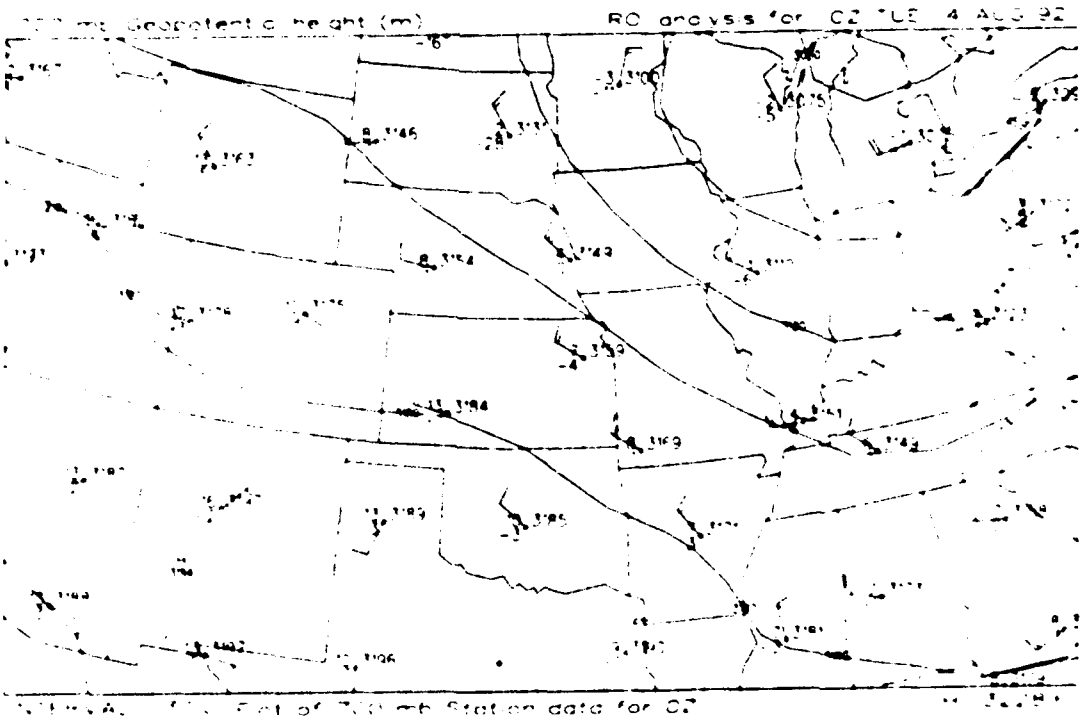

Figure 46: 700 mb weather map and height analysis for 00 UTC 4 August 1992.

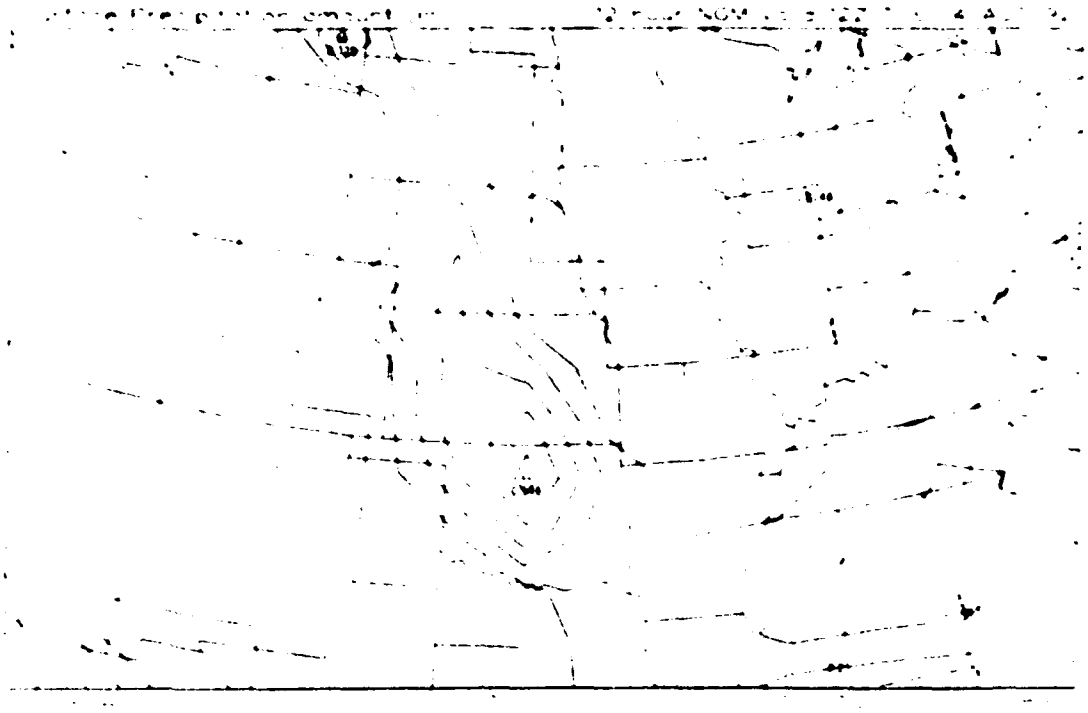

Figure 47: NGM 00 UTC 4 August 1992 forecast of 6-hour accumulated precipitation, valid 12 UTC 4 August 1992.

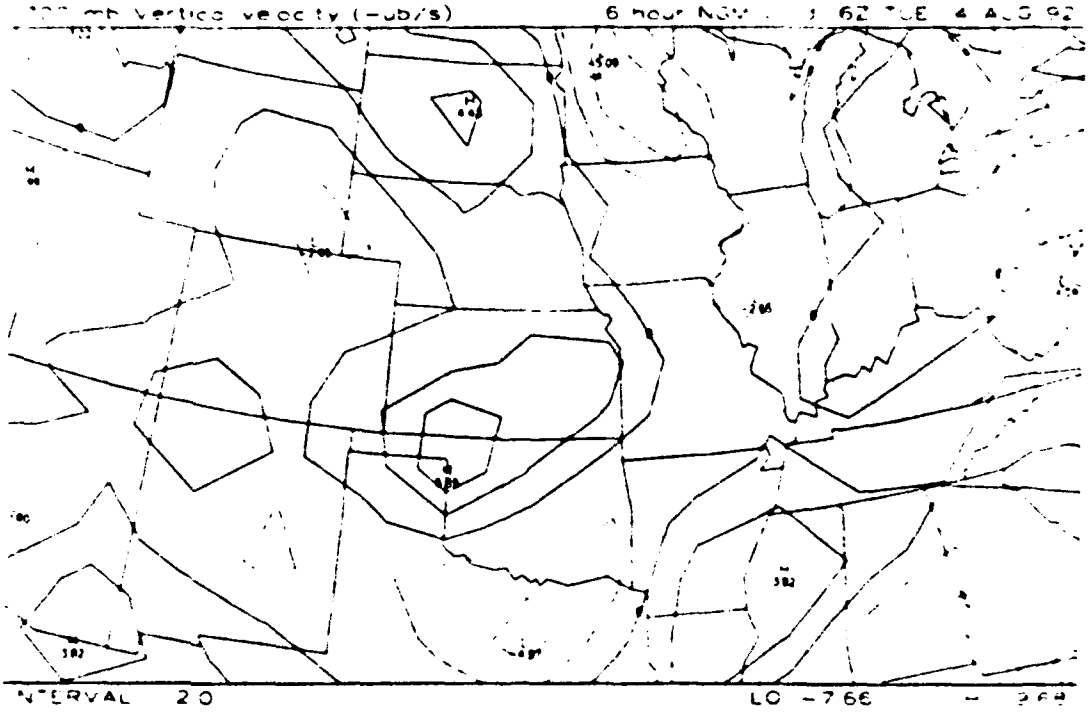

Figure 48: NGM 00 UTC 4 August 1992 forecast of 700 mb vertical velocity (μb/s, or cm/s), valid 06 UTC 4 August 1992.

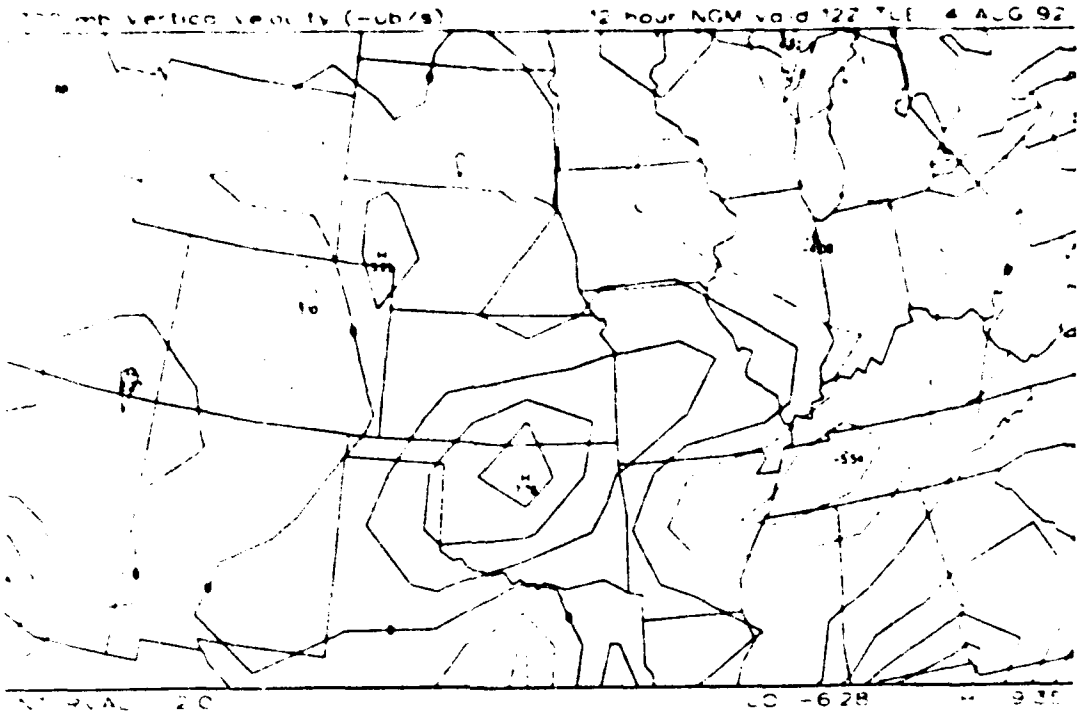

Figure 49: NGM 00 UTC 4 August 1992 forecast of 700 mb vertical velocity (μb/s, or cm/s), valid 12 UTC 4 August 1992.

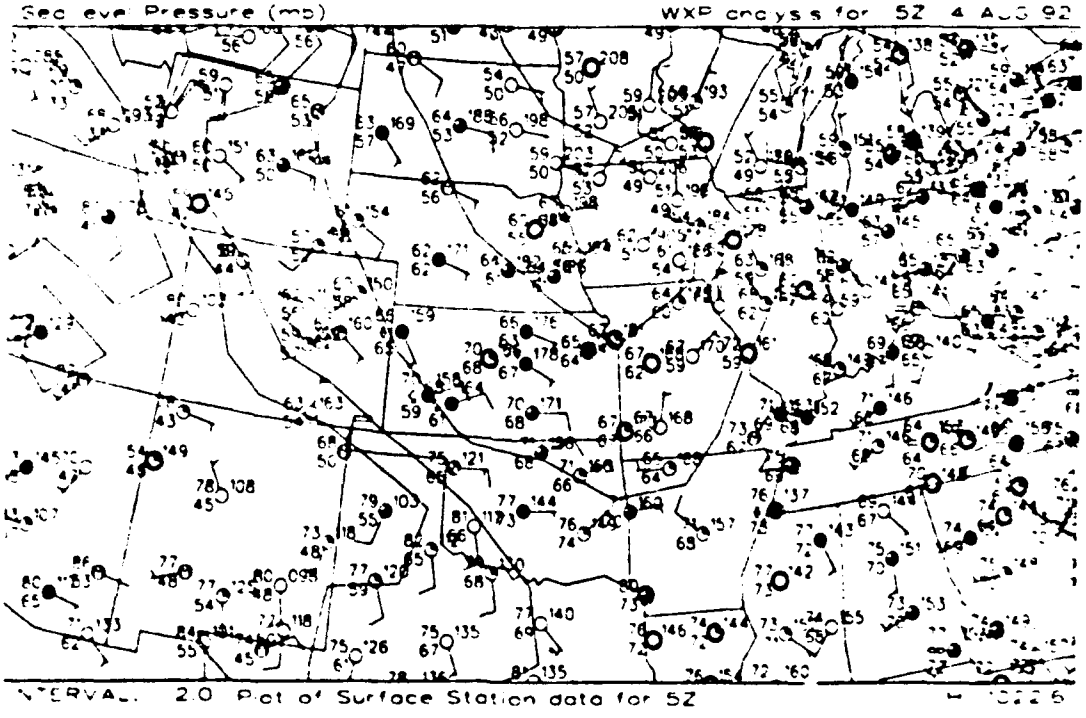

Figure 50: Surface weather map and sea-level pressure analysis for 05 UTC 4 August 1992.

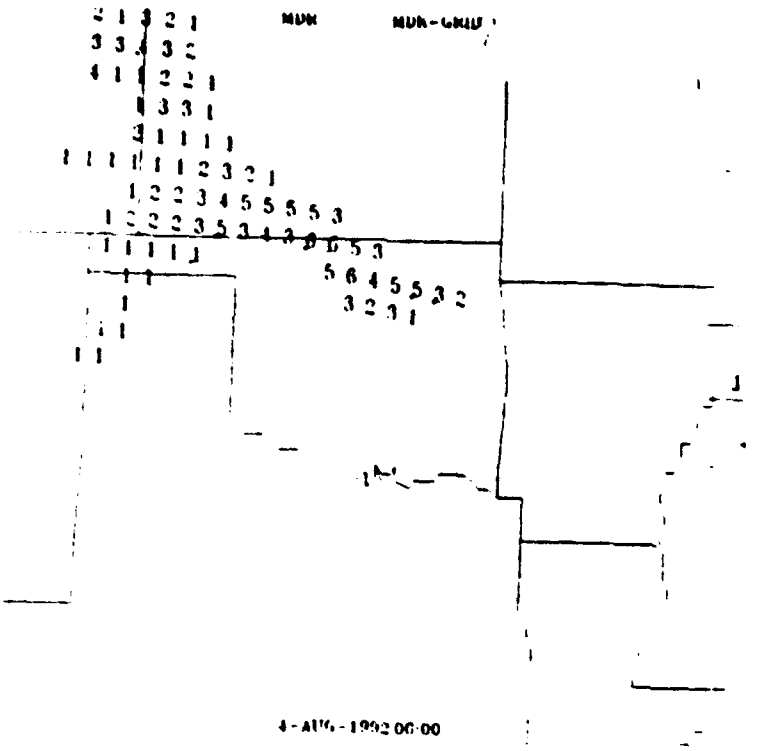

Figure 51: MDR summary for 06 UTC 4 August 1992.

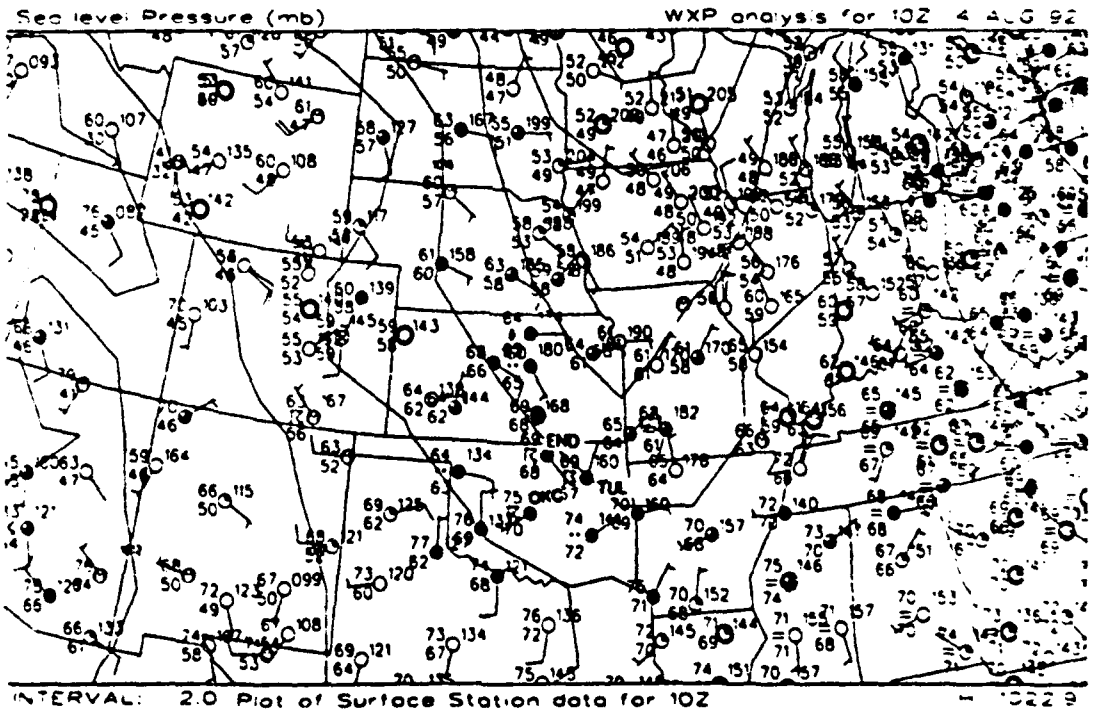

Figure 52: Surface weather map and sea-level pressure analysis for 10 UTC 4 August 1992.

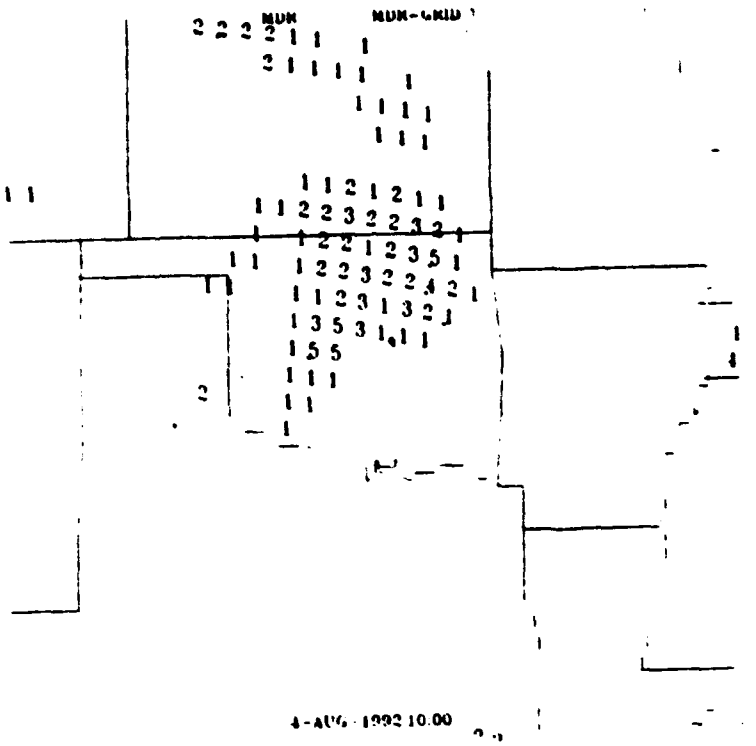

Figure 53: MDR summary for 10 UTC 4 August 1992.

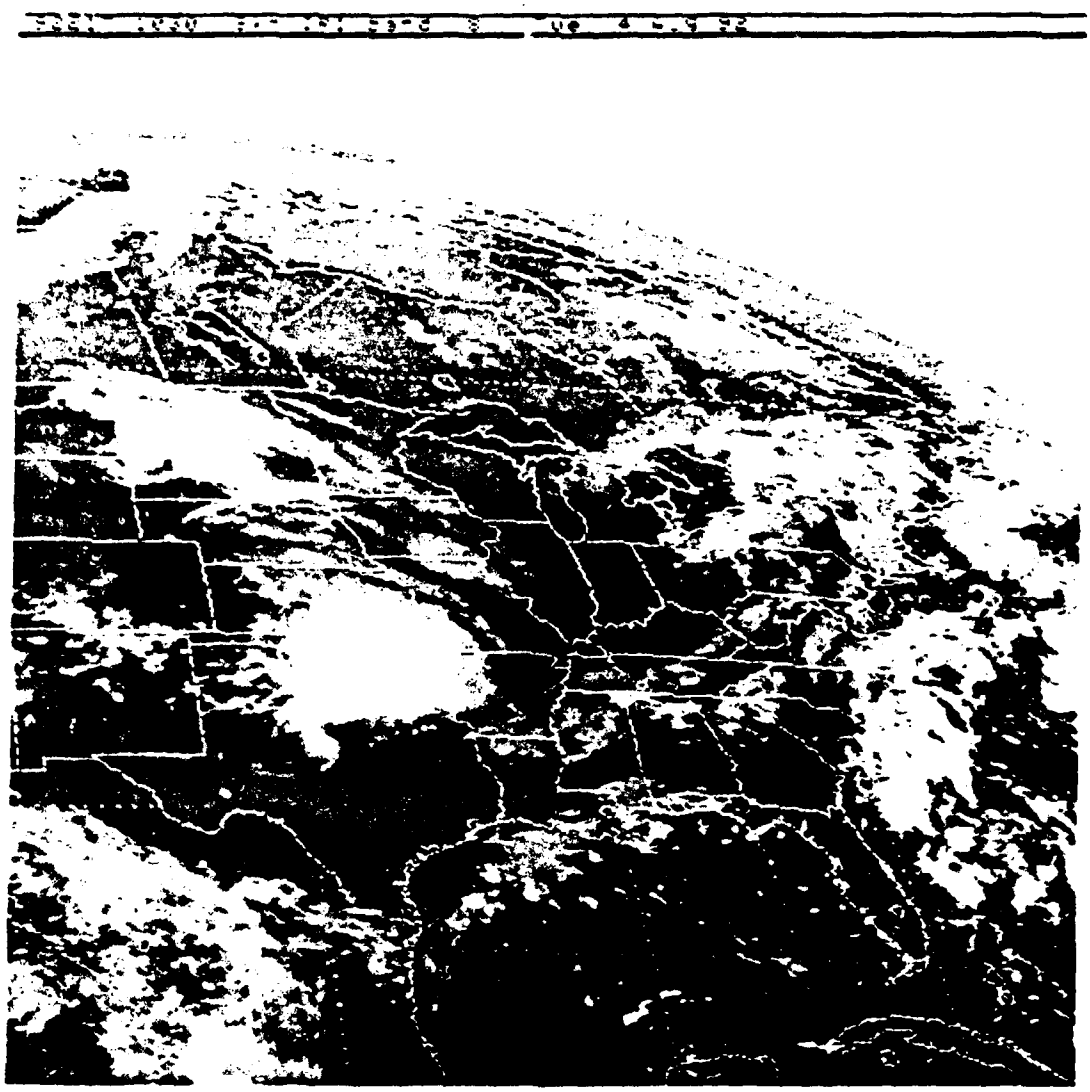

Figure 54: Infrared satellite image for 1030 UTC 4 August 1992.

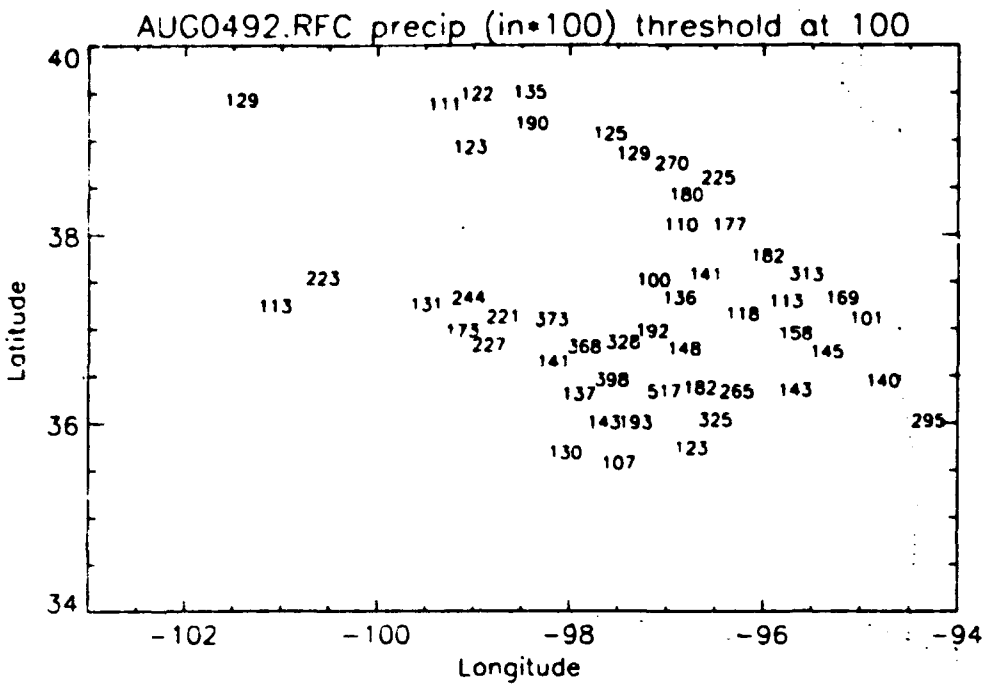

Figure 55: Map of 24-hr precipitation ending at 12 UTC 4 August 1992. Only values in excess of 1.0 in are plotted.

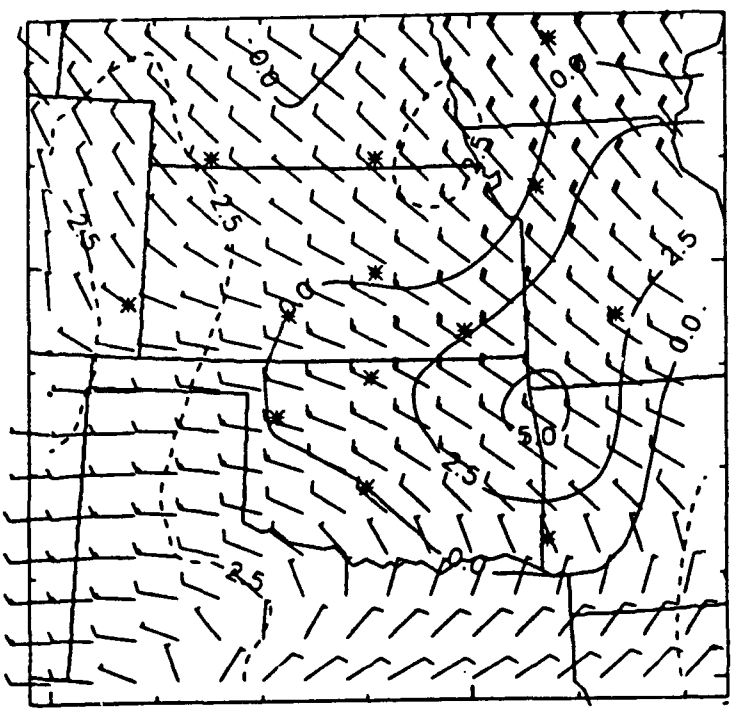

Figure 56: Profiler-derived analysis of winds and integrated vertical velocity (cm/s) at 3000 m for 03 UTC 4 August 1992.

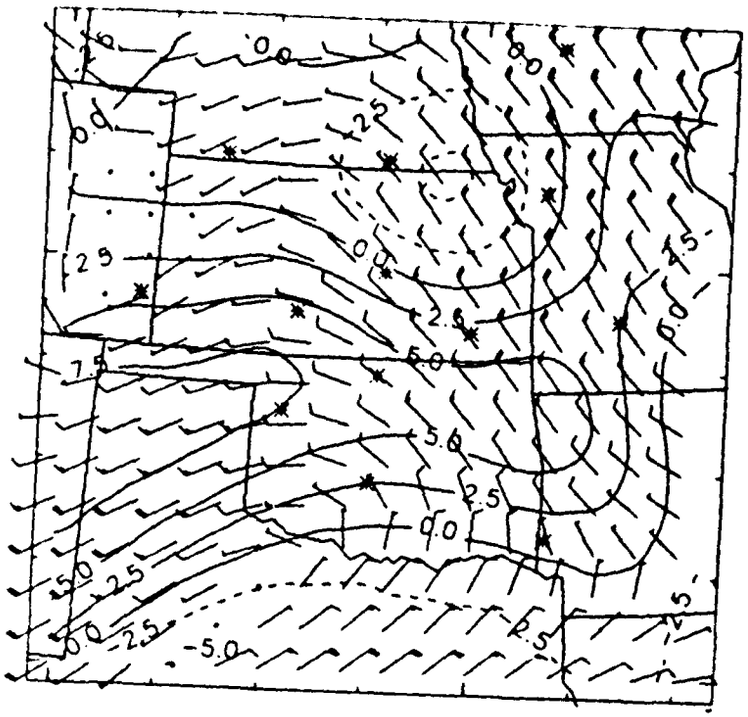

Figure 57: Profiler-derived analysis of winds and integrated vertical velocity (cm/s) at 3000 m for 06 UTC 4 August 1992.

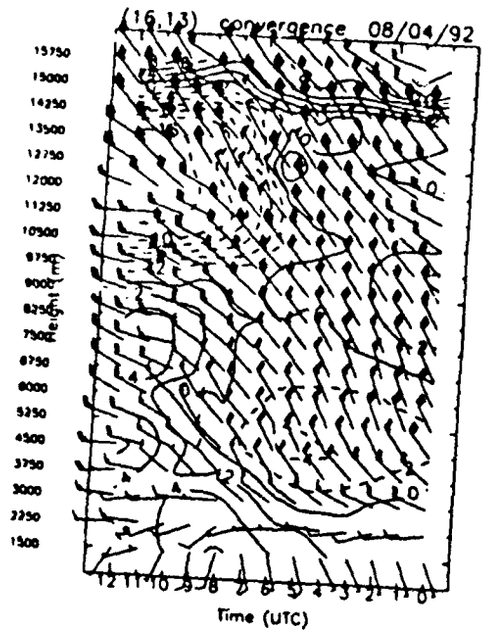

Figure 58: Time-height cross section of profiler-derived winds and horizontal convergence (in $10^{-5}s^{-1}$) for END for 00-12 UTC 4 August 1992.

3.4. October 7, 1992: Kansas frontal rain event

Between 18 UTC 7 October 1992 and 12 UTC 8 October 1992 2"-4" of rain fell on north central Kansas in association with an intensifying low pressure system. The NGM forecast guidance for this area called for 1"-2" of rain between 12 UTC 7 October and 00 UTC 8 October, but with a timing error: it predicted roughly equal amounts for the 6-hour periods ending at 18 UTC and 00 UTC, whereas no rain was observed before 18 UTC, and more rain than predicted was observed between 18 UTC and 00 UTC. The reasons for this forecast error are examined in the following, and the role of profiler data in its early identification are demonstrated.

3.4.1. Standard Meteorological Data Available Before the Storm.

The surface maps at 12 UTC (Figure 59) and 18 UTC (Figure 60) show a low pressure center moving from the Texas panhandle to south central Kansas along a strong baroclinic zone. Overrunning air from the south is leading to moderate rain and thunderstorms to the north of the low in northwest Kansas. The 13 UTC (Figure 61) and 18 UTC (Figure 62) manually digitized radar summaries show a weakening area of rainfall in western Kansas. The rainfall is making slow progress into eastern Kansas.

The 12 UTC upper air maps show a closed circulation at 850 mb (Figure 66), and a trough tilting westward with height at 700 mb, 500 mb (Figure 67), and 300 mb. The winds at 700 to 300 mb are strongest behind the trough, indicating the potential for further deepening. Significant upper level diffluence is occurring over eastern Kansas ahead of this digging trough, contributing to upward motion. A possible low level nocturnal jet exists over the Texas panhandle, but the air is relatively dry. However, Gulf of Mexico air should eventually be tapped as the trough moves east.

The 12 UTC NGM 6 hour precipitation forecasts valid 18 and 00 UTC, respectively, are shown in Figures 65 - 66. The NGM forecasts .5-1" of rain for north central Kansas between 12-18 UTC and 18-00 UTC. Precipitation maxima move northeastward, with the largest precipitation confined to the northeast corner of Kansas for the period ending at 00 UTC. This trend is also reflected in the NGM 6 and 12 hour forecasts of 700 mb vertical velocity, valid at 18 UTC

(Figure 67) and 00 UTC (Figure 68), which show the maximum upward motion persisting over north central Kansas between 12 and 00 UTC, whereas weak ascent in western Kansas is being replaced by descent by 00 UTC. The corresponding 500 mb forecasts of height and absolute vorticity are shown in Figures 69 and 70. At 850 mb (not shown), warm (cold) advection is forecasted to occur in eastern (western) Kansas at 18 UTC, being replaced by cold advection over the entire state by 00 UTC.

3.4.2. Information Available During and After the Storm.

The verifying surface maps for the period between 18 UTC and 00 UTC show a continued northeast movement of the low, with rain occurring over much of eastern and north central Kansas by 23 UTC (Figure 71). The most intense rainfall evident in the manually digitized radar summaries occurs in eastern Oklahoma and southeast Kansas, though level 4 echoes are evident in central and northeast Kansas by 23 UTC (Figure 72). Salina, KS (SLN - see Figure 71 for station location) reported no rainfall before 18 UTC (compared to an NGM forecast of .9"), followed by light rain giving way to thunderstorms by 21 UTC; 2.01" fell between 18 and 00 UTC, compared to an NGM forecast of .7". Thus, the NGM overforecast the precipitation at Salina before 18 UTC, and underforecasted between 18 UTC and 00 UTC.

The verifying 00 UTC 500 mb analysis of height and vorticity (Figure 73) shows stronger than forecasted PVA over north central Kansas, which is consistent with the heavier than forecasted rainfall in this area between 18 and 00 UTC.

3.4.3. Utility of the Profiler Data.

The 18 UTC profiler derived 3000 m horizontal winds and vertical velocities shown in Figure 74 indicates that the maximum upward motion is over central Kansas/Nebraska, to the northwest of the NGM forecast position (Figure 67). This is consistent with the radar summaries. A number of profiler sites were unavailable for this analysis, but the area of low-level convergence and resulting upward motion over central Kansas is well supported by the available observations (Figure 75). The 18 UTC 5500 m horizontal winds and absolute vorticity (Figure 76) shows the maximum PVA, the primary forcing mechanism

for the upward motion in this case, to the west of the NGM forecast position (Figure 69). Another interesting feature in Figure 76 is the jet streak over the Texas panhandle and southwest Oklahoma. The northeastward progression of this jet streak can be seen in the hourly sequence of 5500 m analyses of wind speed shown in Figures 77-79. The corresponding plot of profiler observations at 20 UTC (Figure 80) clearly shows this jet streak in the inner network over central Oklahoma; comparison with the analysis shows the smoothing effect of the analysis over that area. The southward extension of the jet streak into Texas must be regarded with caution, since no profiler observations were available over that area at that time.

In summary, the NGM was too fast in moving the upward motion and associated rainfall into eastern Kansas, resulting in an overprediction for north central Kansas for the period ending at 18 UTC, and an underprediction for the following 6 hours. The 00 UTC verifying 500 mb maps show that this is related to the placement of the maximum positive vorticity advection. Both these forecast errors are clearly evident in the profiler derived analyses at 18 UTC, allowing forecasters to issue a corrected nowcast at that time. The profiler analyses at earlier times (not shown) would possibly allow a earlier detection of this trend, but this is hard to assess without side-by-side comparisons of forecasts and analyses.

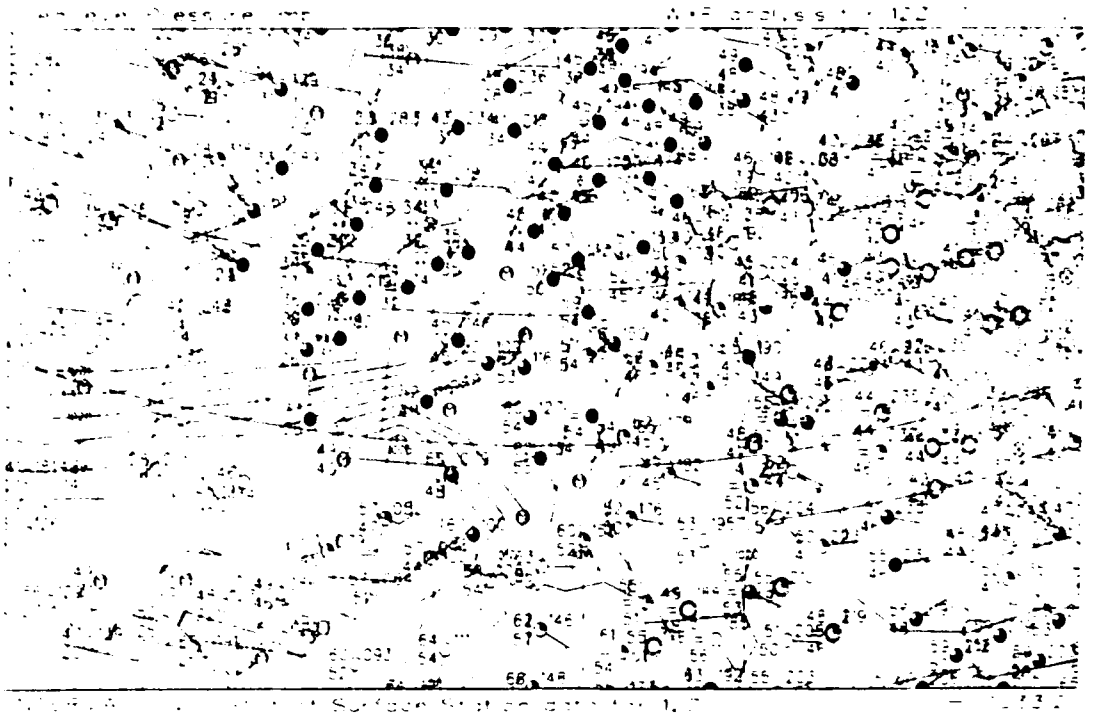

Figure 59: Surface weather map and sea-level pressure analysis for 12 UTC 7 October 1992.

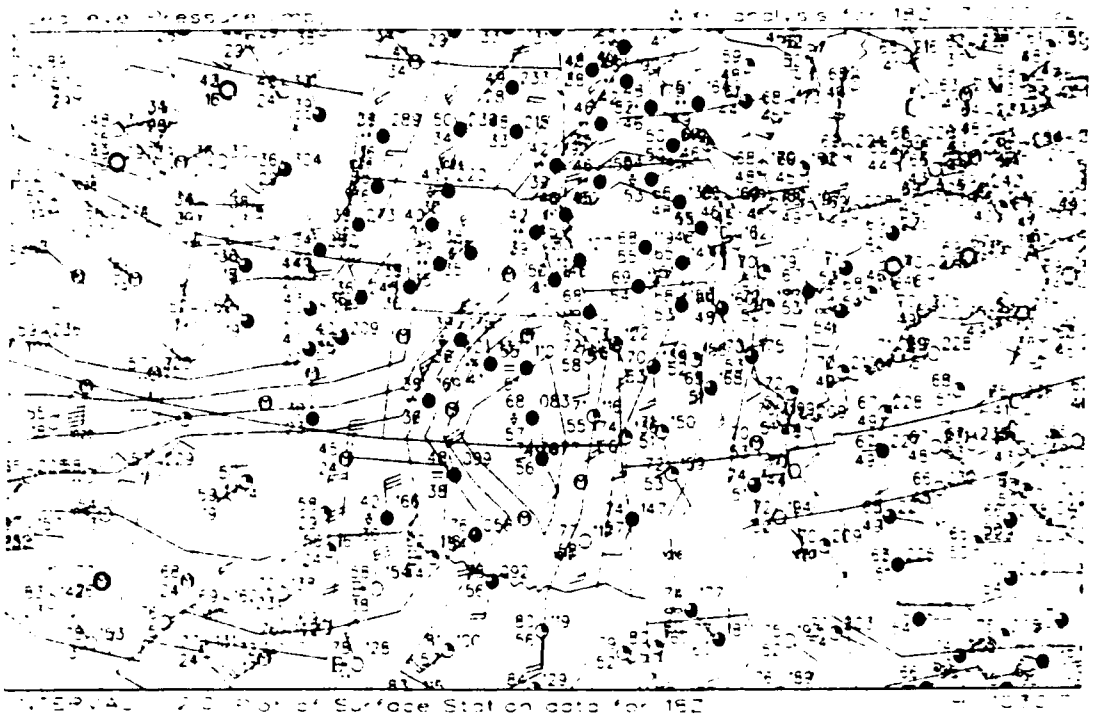

Figure 60: Surface weather map and sea-level pressure analysis for 18 UTC 7 October 1992.

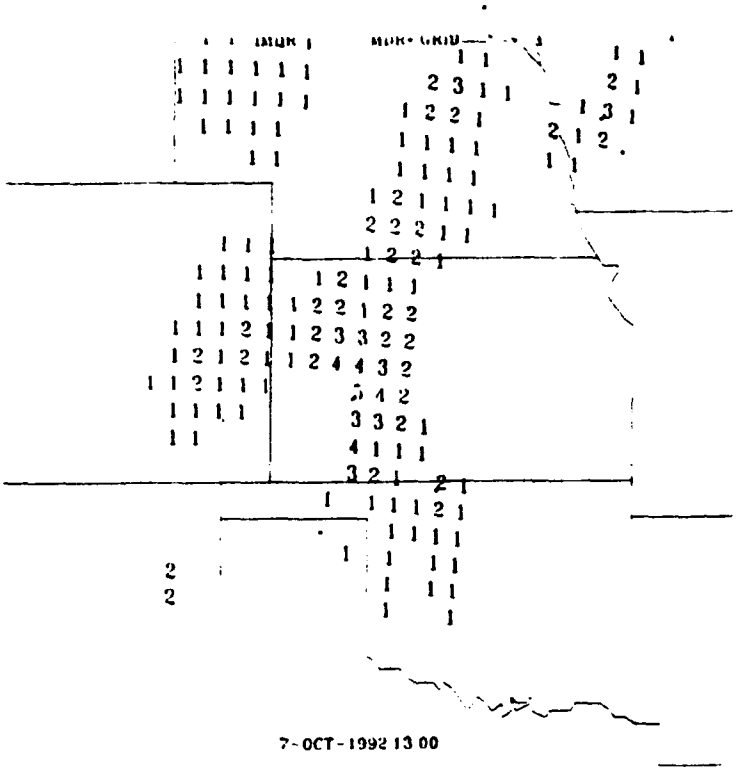

Figure 61: MDR summary for 13 UTC 7 October 1992.

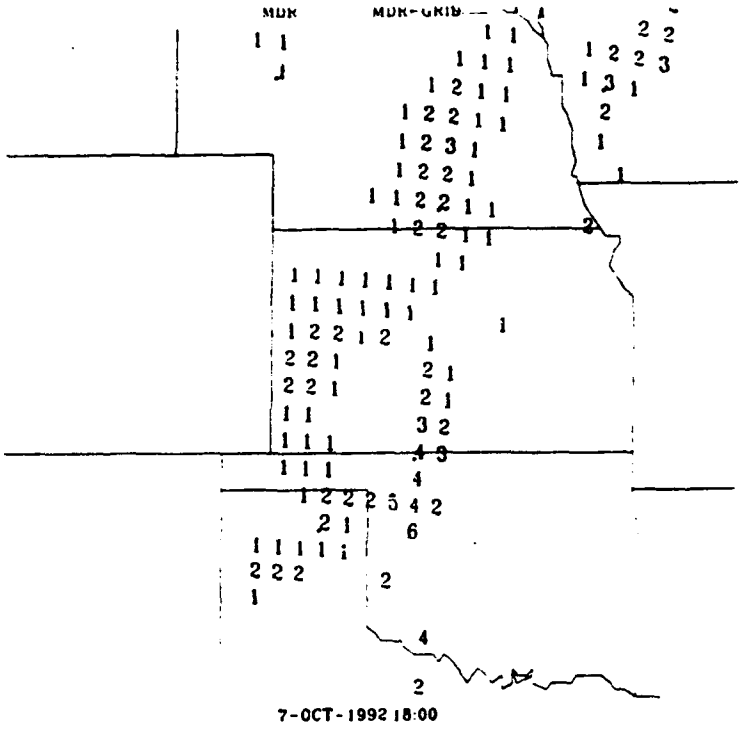

Figure 62: MDR summary for 18 UTC 7 October 1992.

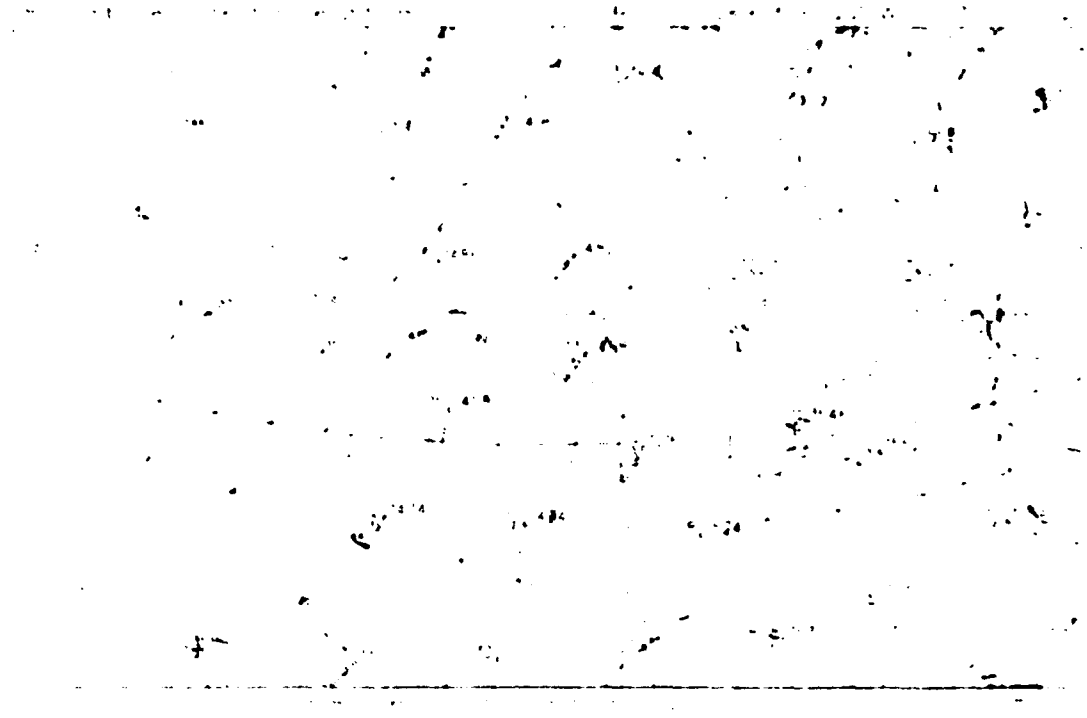

Figure 63: 850 mb weather map and height analysis for 12 UTC 7 October 1992.

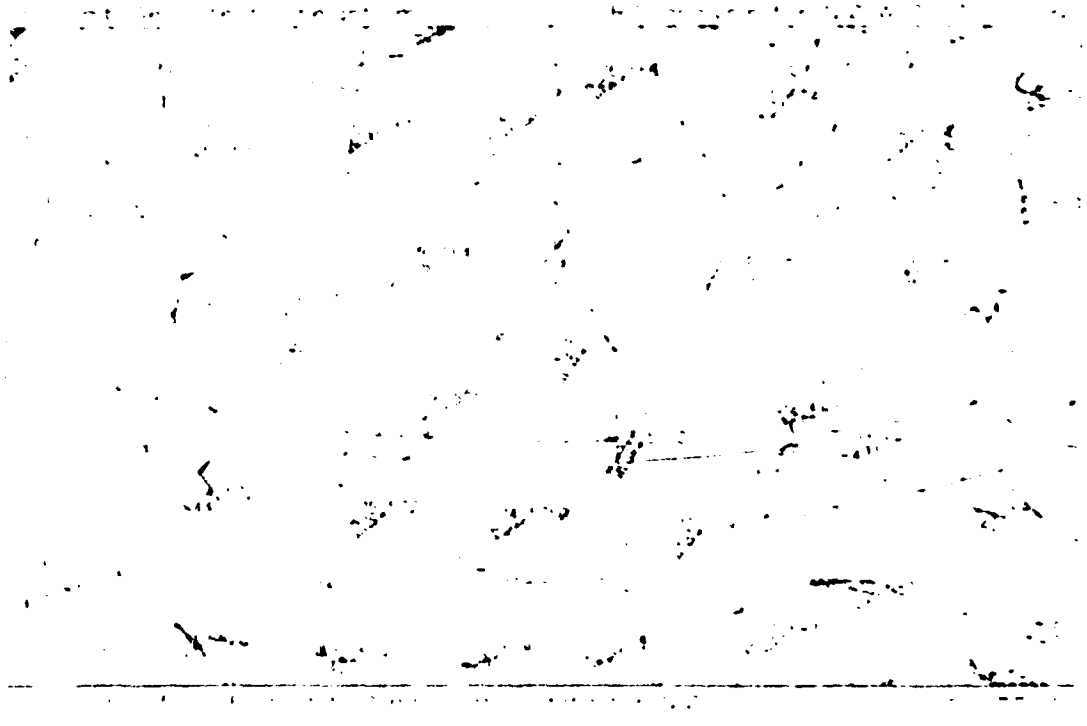

Figure 64: 500 mb weather map and height analysis for 12 UTC 7 October 1992.

Figure 65: NGM 12 UTC 7 October 1992 forecast of 6-hour accumulated precipitation, valid 18 UTC 7 October 1992.

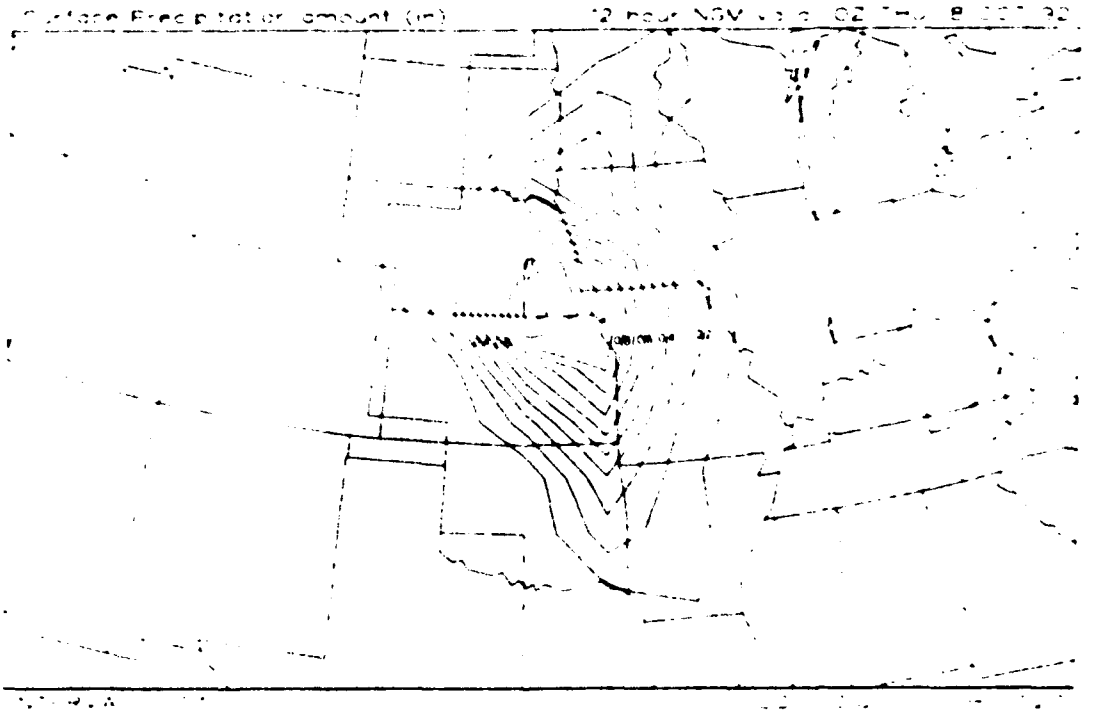

Figure 66: NGM 12 UTC 7 October 1992 forecast of 6-hour accumulated precipitation, valid 00 UTC 8 October 1992.

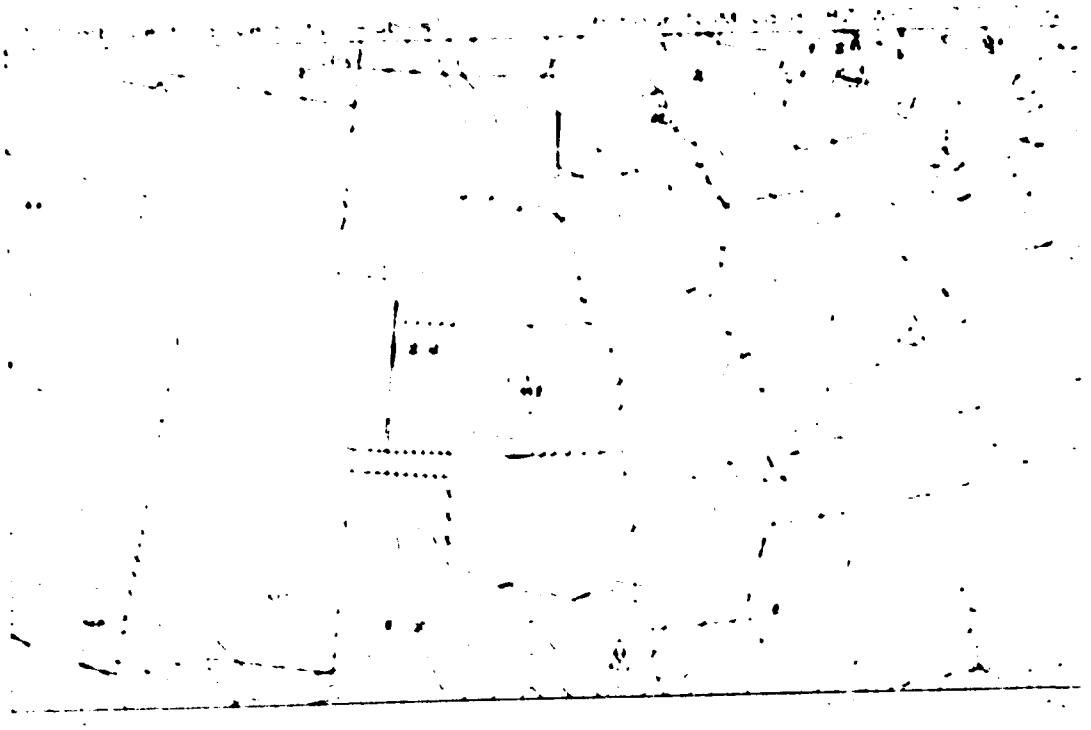

Figure 67: NGM 12 UTC 7 October 1992 forecast of 700 mb vertical velocity (10^{-1}μb/s, or mm/s), valid 18 UTC 7 October 1992.

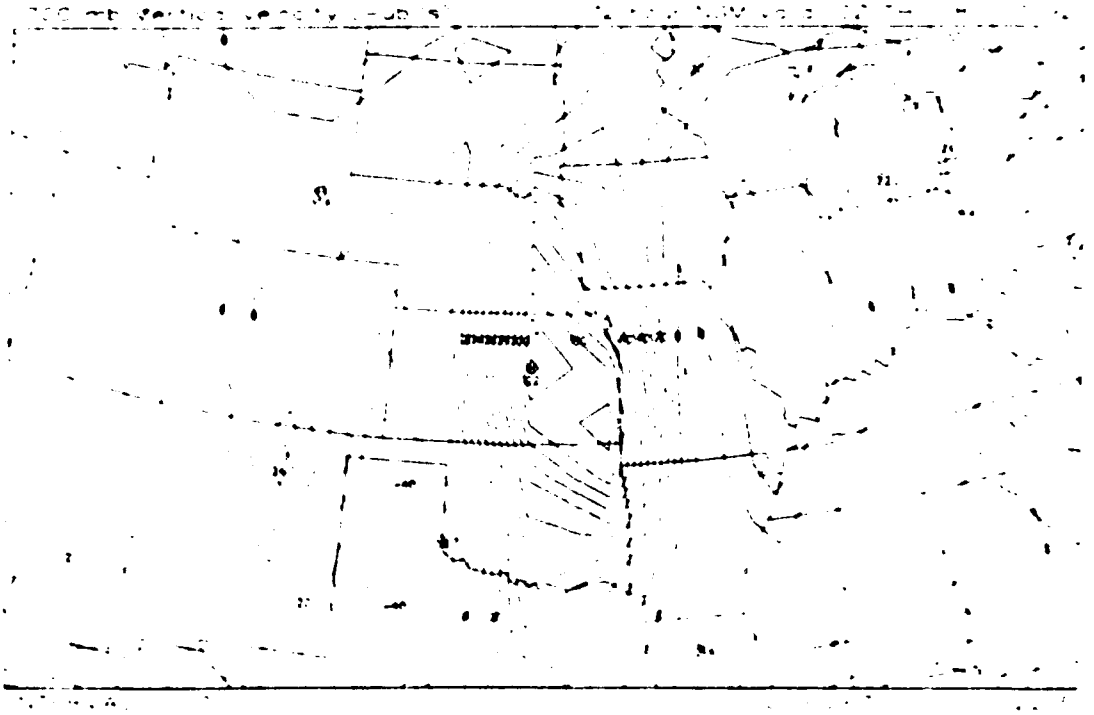

Figure 68: NGM 12 UTC 7 October 1992 forecast of 700 mb vertical velocity (10^{-1}μb/s, or mm/s), valid 00 UTC 8 October 1992.

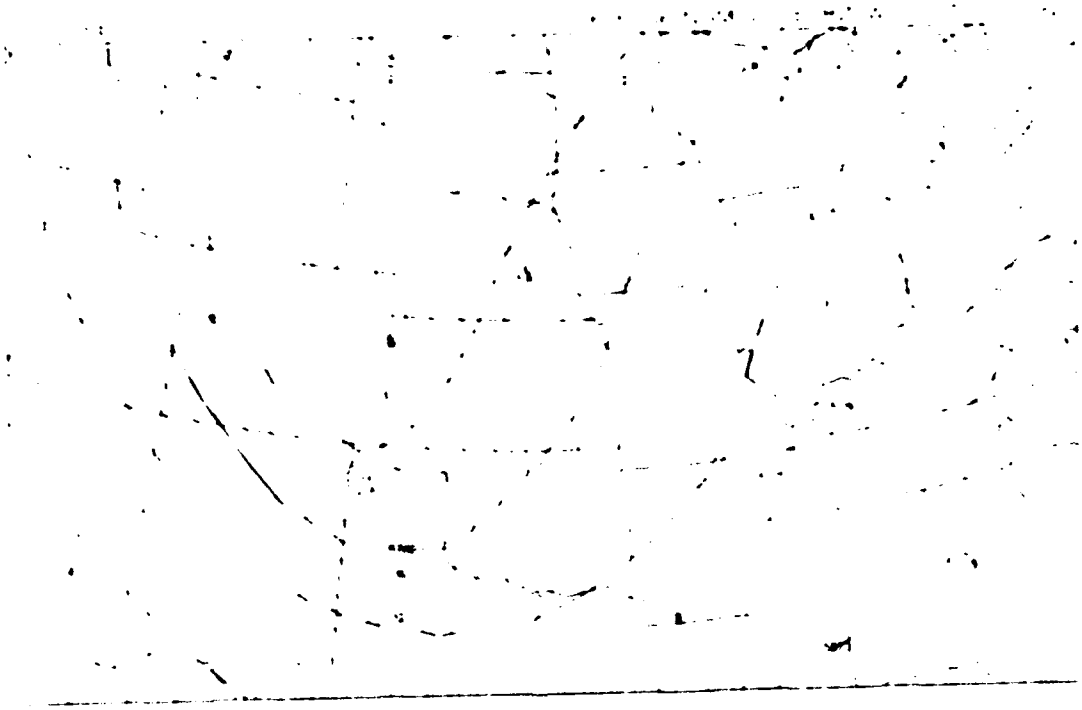

Figure 69: NGM 12 UTC 7 October 1992 forecast of 500 mb height (solid lines) and absolute vorticity (dashed lines), valid 18 UTC 7 October 1992.

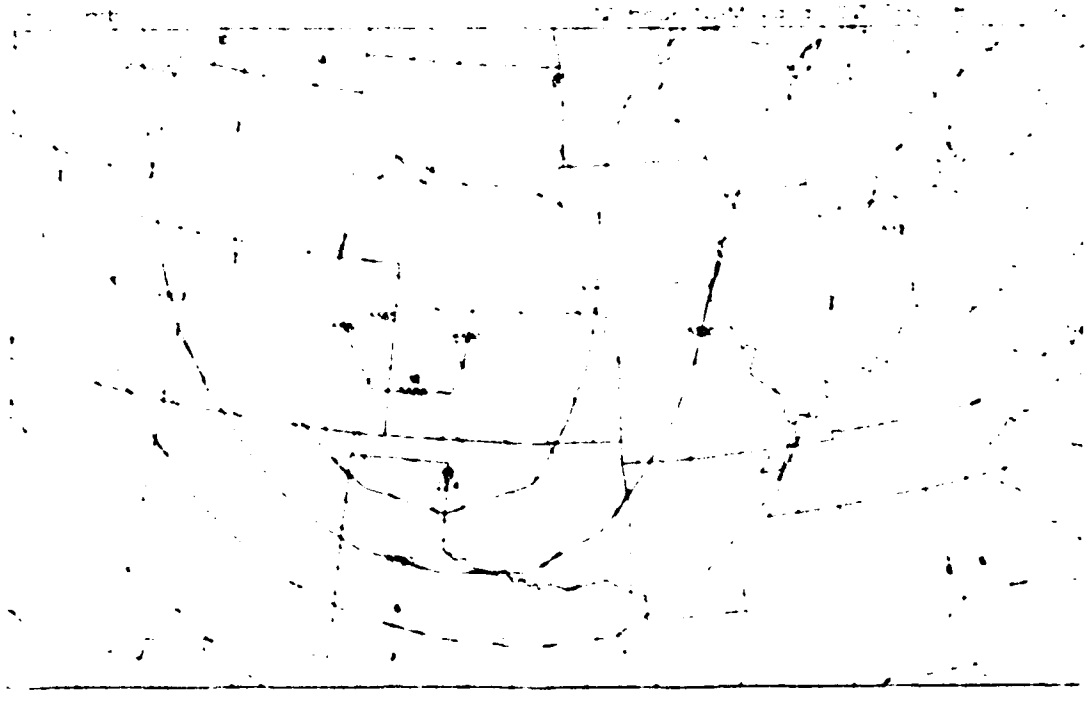

Figure 70: NGM 12 UTC 7 October 1992 forecast of 500 mb height (solid lines) and absolute vorticity (dashed lines), valid 00 UTC 8 October 1992.

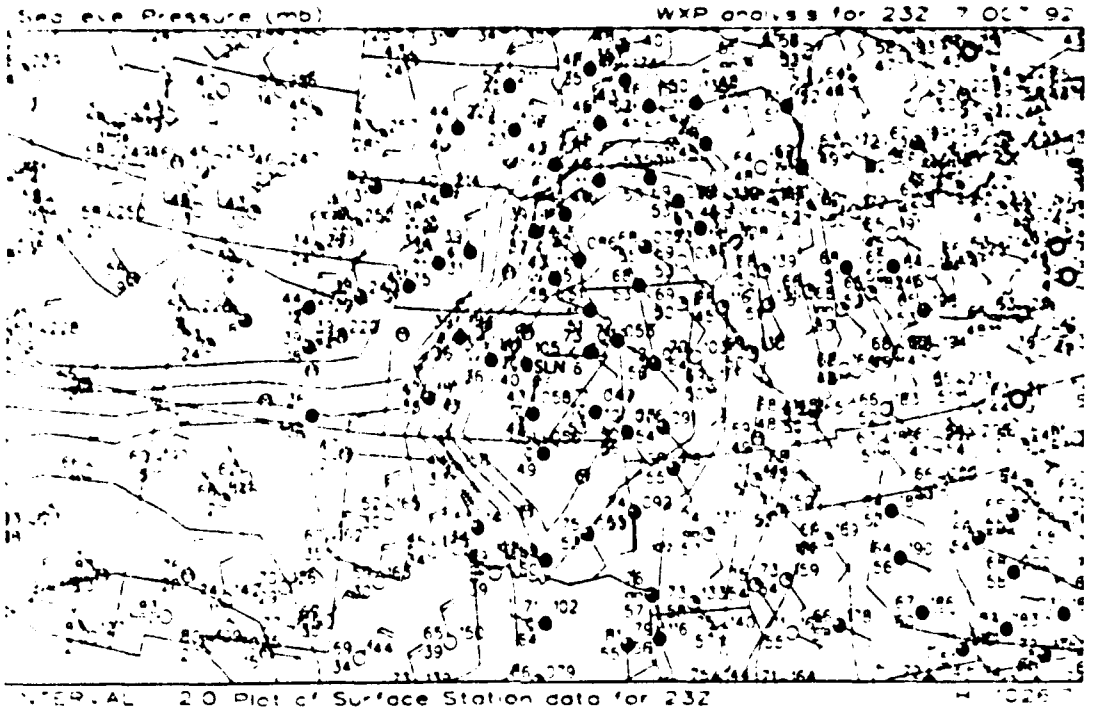

Figure 71: Surface weather map and sea-level pressure analysis for 23 UTC 7 October 1992.

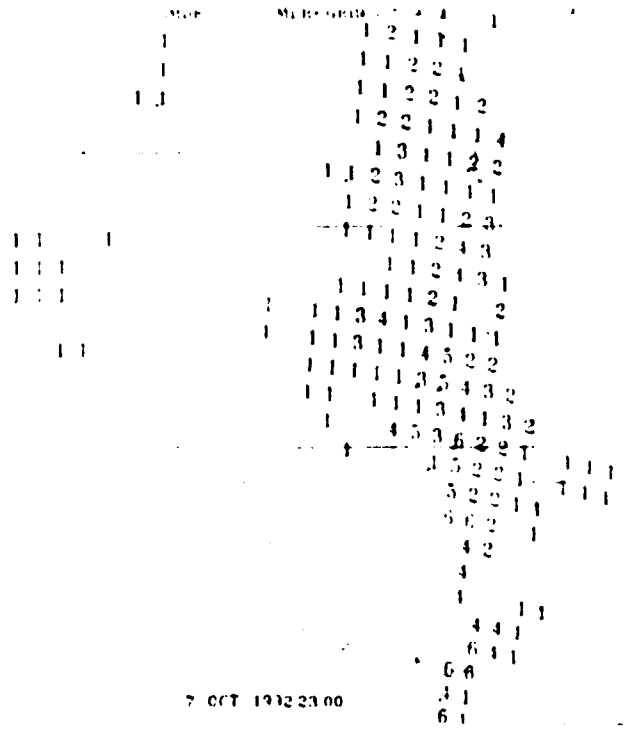

Figure 72: MDR summary for 23 UTC 7 October 1992.

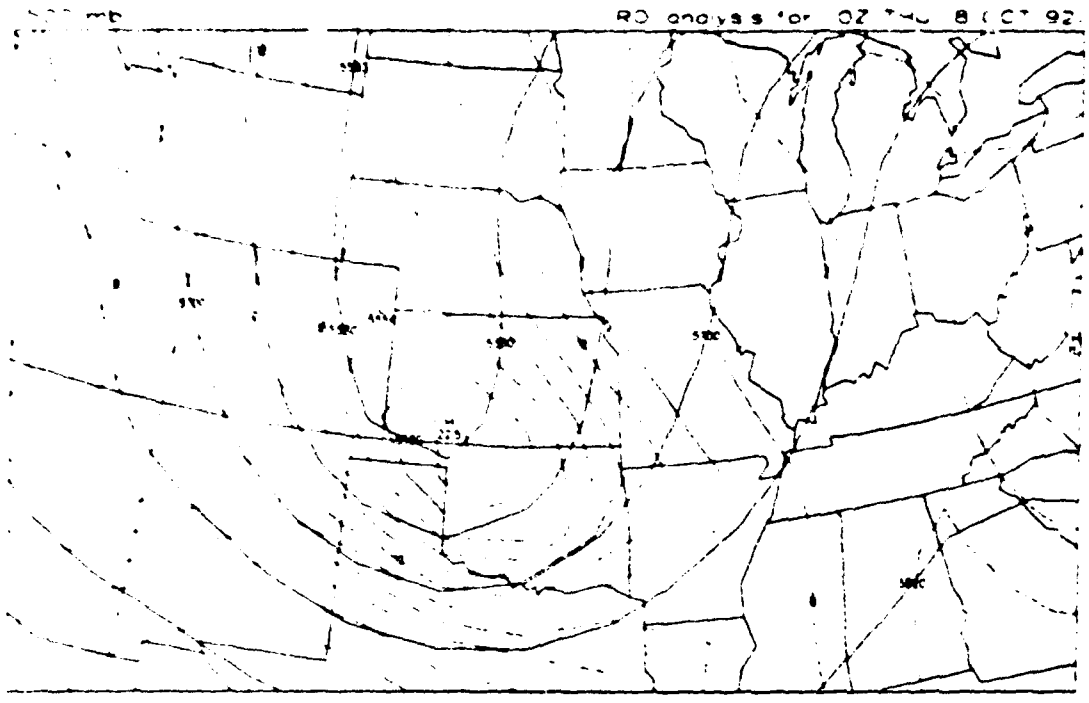

Figure 73: 500 mb analysis of height (solid lines) and absolute vorticity (dashed lines) for 00 UTC 8 October 1992.

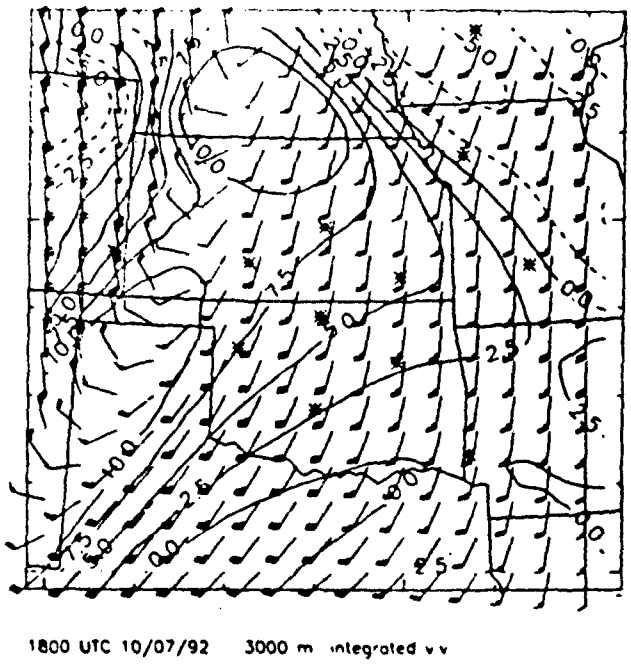

Figure 74: Profiler-derived analysis of winds and integrated vertical velocity (cm/s) at 3000 m for 18 UTC 7 October 1992.

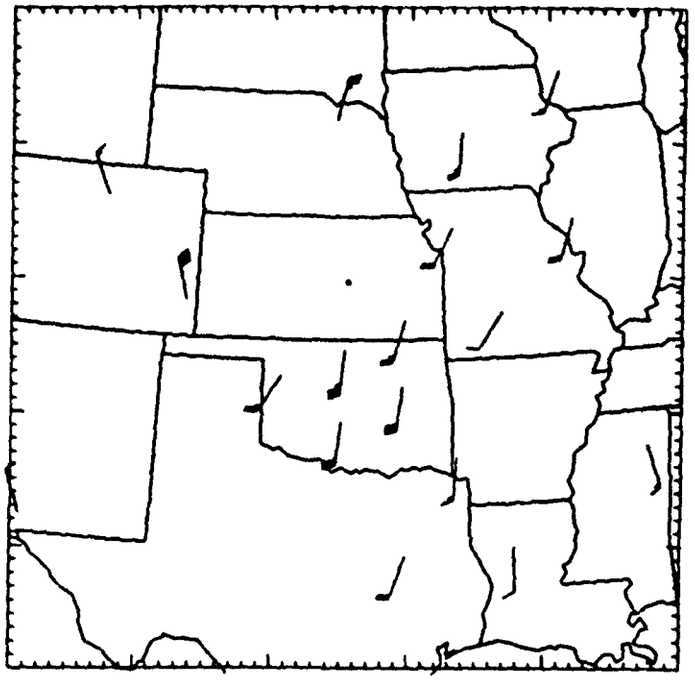

Figure 75: Profiler observations used in the analysis of winds at 1500 m for 18 UTC 7 October 1992.

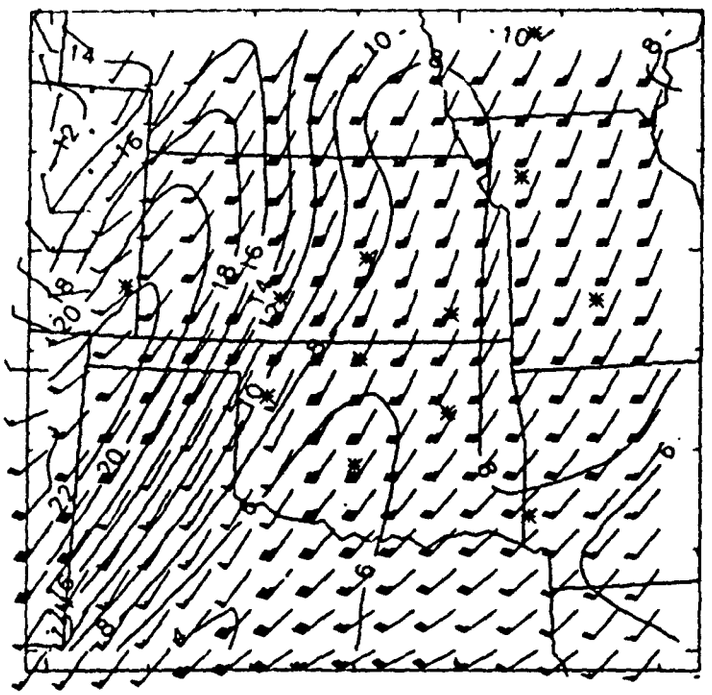

Figure 76: Profiler-derived analysis of winds and absolute vorticity ($10^{-5}s^{-1}$) at 5500 m for 18 UTC 7 October 1992.

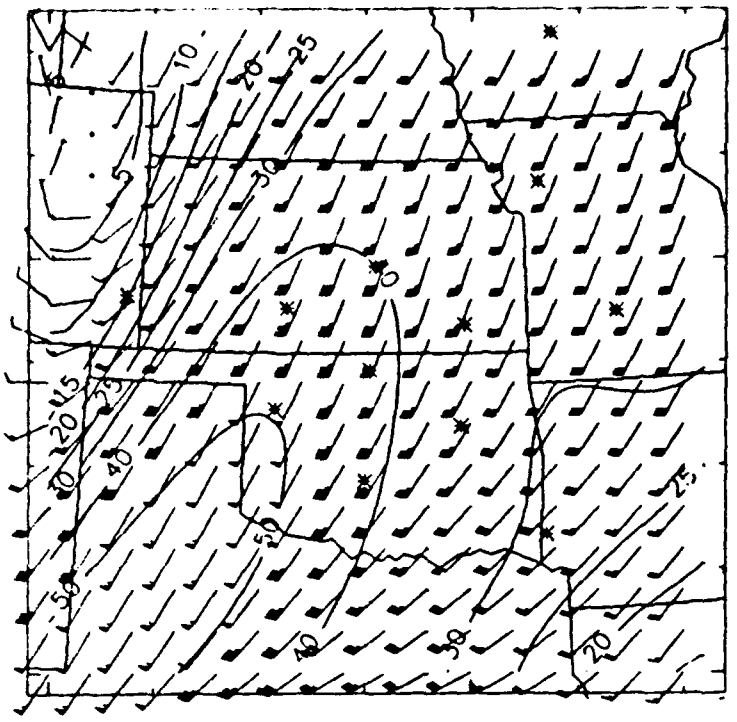

Figure 77: Profiler-derived analysis of winds and wind speed (kts) at 5500 m for 18 UTC 7 October 1992.

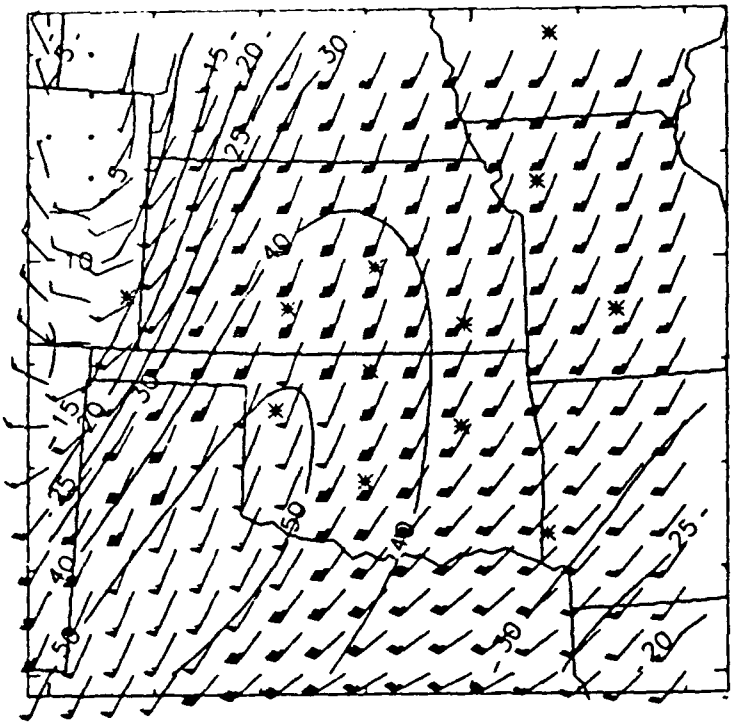

Figure 78: Profiler-derived analysis of winds and wind speed (kts) at 5500 m for 19 UTC 7 October 1992.

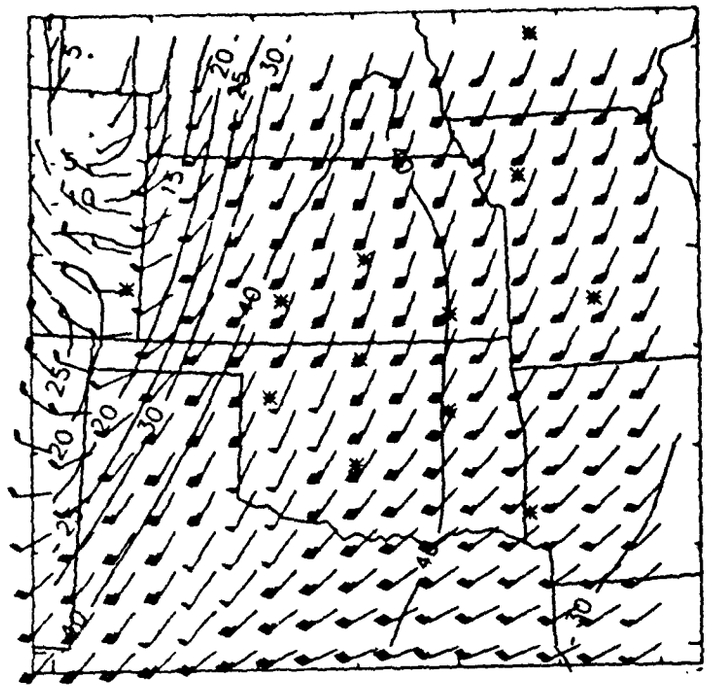

Figure 79: Profiler-derived analysis of winds and wind speed (kts) at 5500 m for 20 UTC 7 October 1992.

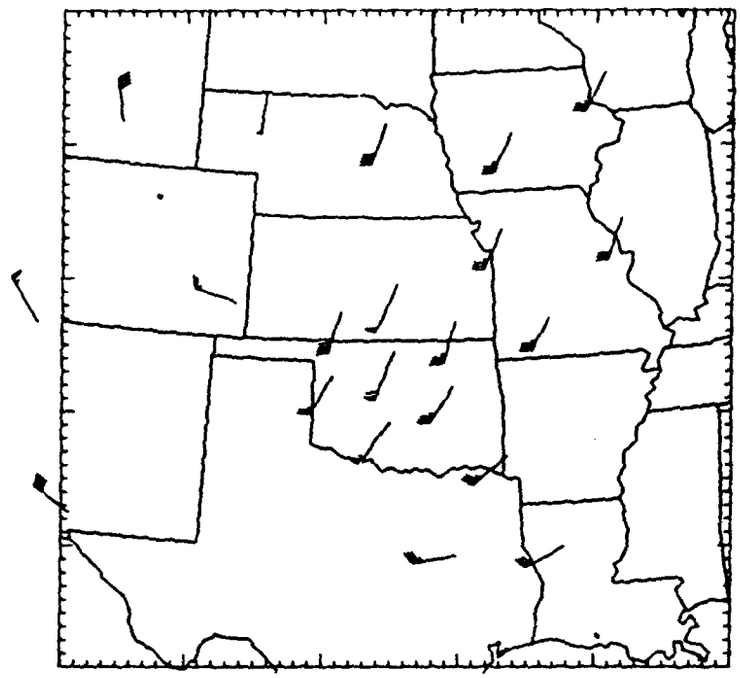

Figure 80: Profiler observations used in the analysis of winds at 5500 m for 20 UTC 7 October 1992.

3.5. November 24, 1992: Kansas/Oklahoma snowstorm

A low moving east from the southern Rockies created blizzard conditions in southwest Kansas between 12 UTC 24 November and 12 UTC 25 November 1992. Garden City, KS (GCK - see Figure 81 for station location) received more than 12" of snow, with the majority falling between 18 and 00 UTC. Snowfall totals of 12"-19" were reported over the Oklahoma panhandle and southwest Kansas. The storm occurred during the heavily traveled two days before Thanksgiving, so an accurate forecast of this event was important. The 6-12 hour NGM guidance failed to forecast the intensity of the precipitation between 18 and 00 UTC. Profiler data and profiler derived quantities are used to identify the NGM forecast errors, and to offset the inaccurate model guidance.

3.5.1. Standard Meteorological Data Available Before the Storm.

The 12 UTC and 15 UTC 24 November surface maps (Figures 81 - 92) show a surface low in north central Texas with light rain falling in the east Texas panhandle, western Oklahoma, and central Kansas. Light snow is falling from the west Texas panhandle to western Kansas. Moderate to strong northerly winds are causing blowing snow. The 15 UTC 24 November manually digitized radar summaries (Figure 83) show level 1-2 echoes in southwest Kansas and the Texas-Oklahoma panhandle. The level 2 echoes decrease between 12 UTC and 15 UTC in the Texas panhandle while showing a slight increase in southwest Kansas.

The 12 UTC 24 November upper air maps show a closed circulation extending from 850 mb (Figure 84) to 500 mb (Figure 85). The center of circulation slopes to the northwest with height, and winds at 500 mb (and 300 mb, not shown) are strongest behind the trough, both indications of a deepening system. Significant 500-300 mb diffluence is occurring over southwest Kansas and the Texas-Oklahoma panhandle ahead of this digging trough, helping to induce upward motion and increase the precipitation intensity in southwest Kansas. The moist layer above the Texas panhandle is deeper (850-500 mb) than that over southwest Kansas (850-700 mb), consistent with the greater number of level 2 radar echoes observed in the former. However, moist advection between 850 and 500 mb over southwest Kansas is deepening their moist layer with time,

and, in concert with the upper level diffluence, leads to the observed intensification of precipitation over southwest Kansas.

The 12 UTC 24 November 500 mb NGM forecast of precipitation for the period 18 UTC - 00 UTC is shown in Figure 86. The NGM forecast the largest precipitation amounts for north central Oklahoma, and only .35" of liquid for GCK between 18 and 00. The 700 mb vertical velocity (Figures 87 - 88) is forecast to be strongest just to the east of the Texas/Oklahoma panhandle area for the entire 12-hour period between 12 UTC and 00 UTC. The 500 mb forecast maps (Figures 89 - 90) show this upward motion to be collocated with the maximum positive vorticity advection at that level. The 850 mb temperature forecasts (not shown) are below 0° C and thus indicate snow for GCK, so a forecast of 4" of snow (assuming a ratio of 1:10) is indicated by the NGM between 18 and 00 UTC.

3.5.2. Information Available During and After the Storm.

The surface maps between 18 UTC (Figure 91) 24 November and 00 UTC 25 November (Figure 92) show light to moderate snowfall in northwest Oklahoma and moderate to heavy snowfall in southwest Kansas as the surface low moves through central Oklahoma. Moderate to strong northerly winds are reducing visibility with blowing snow. The manually digitized radar summaries over this period (Figures 93-94) show level 2 echoes dissipating in southwest Kansas and the Oklahoma-Texas panhandle. Level 1 echoes are decreasing with time in the Oklahoma-Texas panhandle, perhaps due to radar insensitivity to snow or overshooting of the radar beam. GCK reported 12" of snow on the ground at 03 UTC 25 November, with only 2" at 12 UTC the day before; the heaviest snow occurred between 18 UTC and 03 UTC with continuous moderate or heavy snow. Based on the snowfall intensity, a rough estimate for the precipitation between 18 and 00 UTC is 8" of snow, or about .6" of liquid, .25" more than forecast by the NGM. Even more impressive snowfall totals were reported (Weygandt, personal communication) over a number of locations over the Oklahoma panhandle (12" - 19" in most locations) and extreme southwest Kansas (13"-15").

3.5.3. Utility of the Profiler Data.

Figure 95 shows the 18 UTC 24 November 3000 m profiler derived winds and vertical velocities, and Figure 96 the corresponding 5500 m profiler derived

winds and vorticity. The NGM upward motion maximum is located over northwest Oklahoma while the profiler derived upward motion maximum is located over the northwest Texas panhandle. Stronger than forecast upward motion is occurring over GCK, giving a forecaster reason to believe the NGM is underforecasting the amount of precipitation for GCK between 18 and 00 UTC. Subsequent profiler analyses (not shown) indicate that this stronger than forecasted upward motion continues through 00 UTC. Comparison of the observed 500 mb flow in Figure 96 with the NGM forecast (Figure 89) shows a more pronounced trough to the south of the Texas panhandle, resulting in vorticity contours that are more perpendicular to the wind flow in southwest Kansas than forecasted, resulting in greater cross contour flow and positive vorticity advection. This greater PVA explains the greater upward motion and intensified snow fall in southwest Kansas between 18 and 00 UTC.

The analysis of this case provided an interesting illustration of the limitations of the analysis technique, and its potential pitfalls: the 18 UTC profiler analysis at 5500 m turned out to be very sensitive to the buddy-check procedure over west Texas. Shown in Figure 97 is the profiler analysis obtained from an analysis cycle that was started at 12 UTC, which is in striking contrast to the analysis obtained from a cycle started at 14 UTC (shown in Figure 96). The raw profiler winds shown in Figure 98 clearly indicate that the analysis in Figure 96 is in better agreement with the observations. The reason for this discrepancy lies in the fact that the raw profiler winds over Jayton, TX (JTN - see Figure 1 for the station location) shifted from the south-southwest to westerly between 12 UTC and 14 UTC. Since no buddy-checking is performed at the first analysis time in a cycle, starting the analysis at 14 UTC led to an analysis and subsequent first guess with westerly winds over JTN, whereas the 12 UTC analysis cycle flagged JTN as suspect because of the disagreement with the first guess southerly winds, and rejected it because of the lack of verifying "buddies" (nearby observations in agreement). This example underscores the importance of comparing the profiler derived analyses with the supporting observations, and indicates the potential for further refinements in the buddy-check procedure.

In summary, the NGM 6-12 hour forecast of an intensifying low over Texas/Oklahoma placed the maximum upward motion at 700 mb too far to the south and east, resulting in an underforecast of precipitation over southwest

Kansas and the Texas/Oklahoma panhandle, which experienced blizzard conditions because of heavy snowfalls and strong winds. This forecast error was related to errors in the vorticity advection pattern at 500 mb. The 18 UTC profiler derived analyses for the 700 mb vertical velocity, and 500 mb vorticity, allow identification of these errors, and would help to issue an improved forecast at that time. This case also provided an example of erroneous rejection of good data by the buddy check procedure, due to shifting winds at a profiler station near the edge of the network.

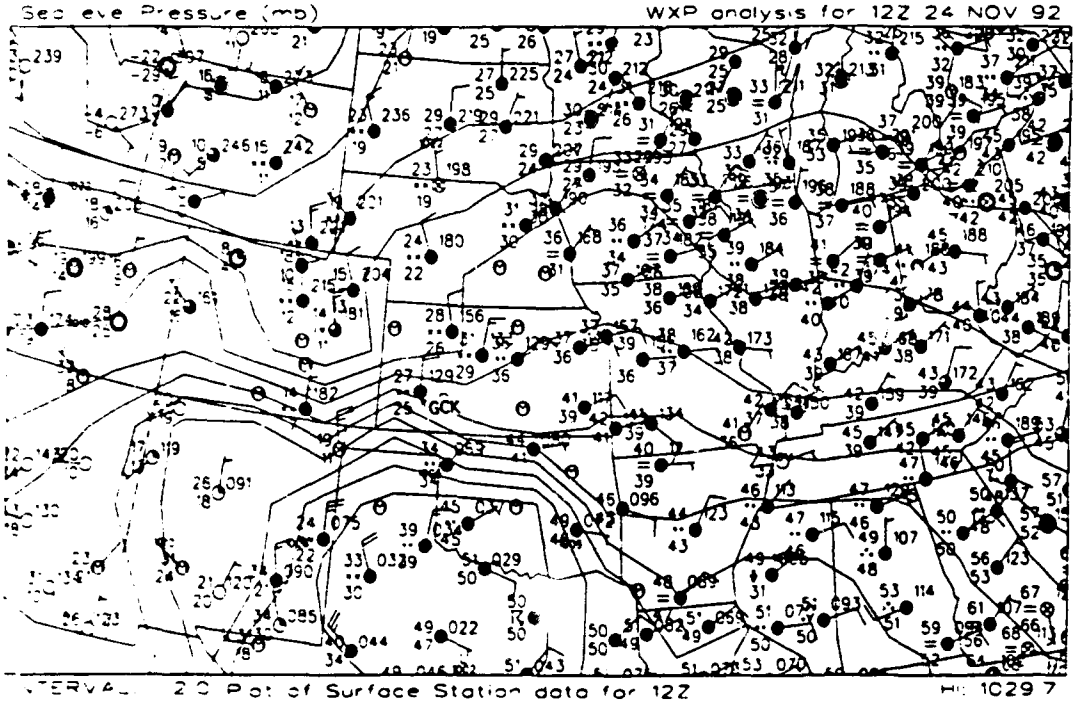

Figure 81: Surface weather map and sea-level pressure analysis for 12 UTC 24 November 1992.

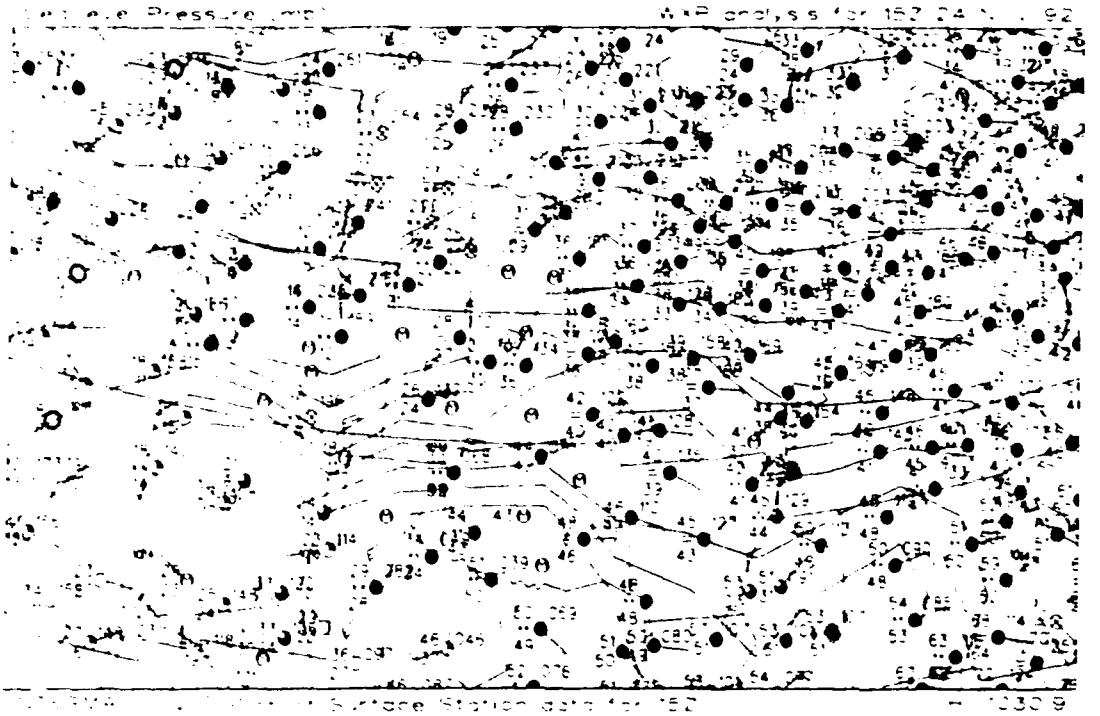

Figure 82: Surface weather map and sea-level pressure analysis for 15 UTC 24 November 1992.

Figure 83: MDR summary for 15 UTC 24 November 1992.

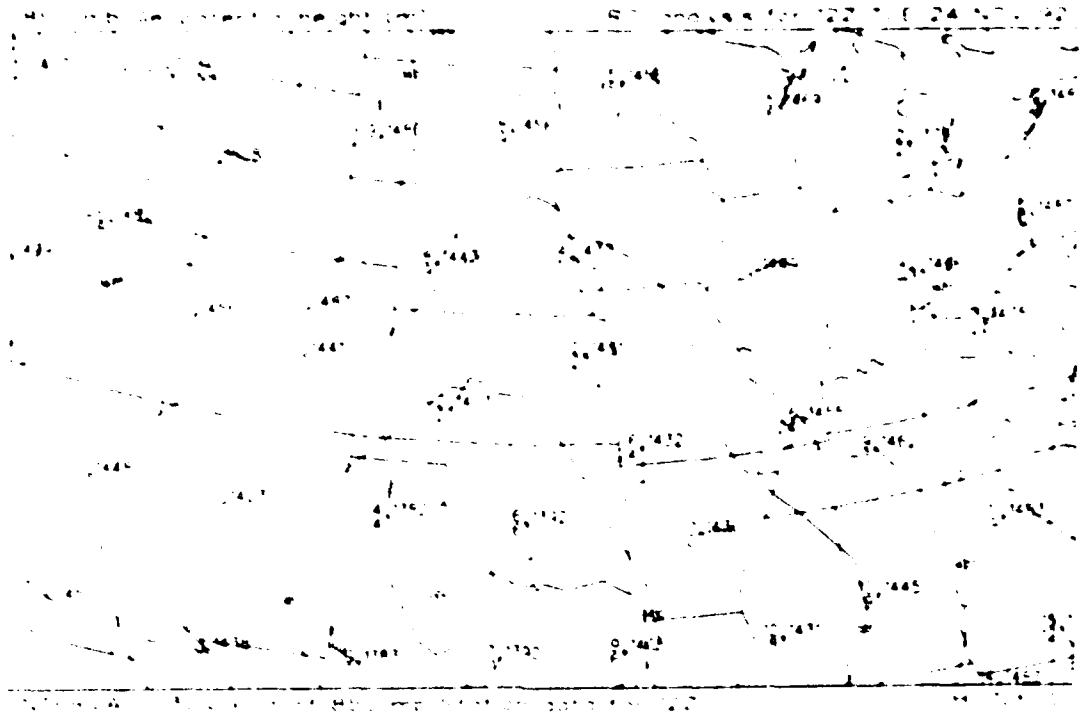

Figure 84: 850 mb weather map and height analysis for 12 UTC 24 November 1992.

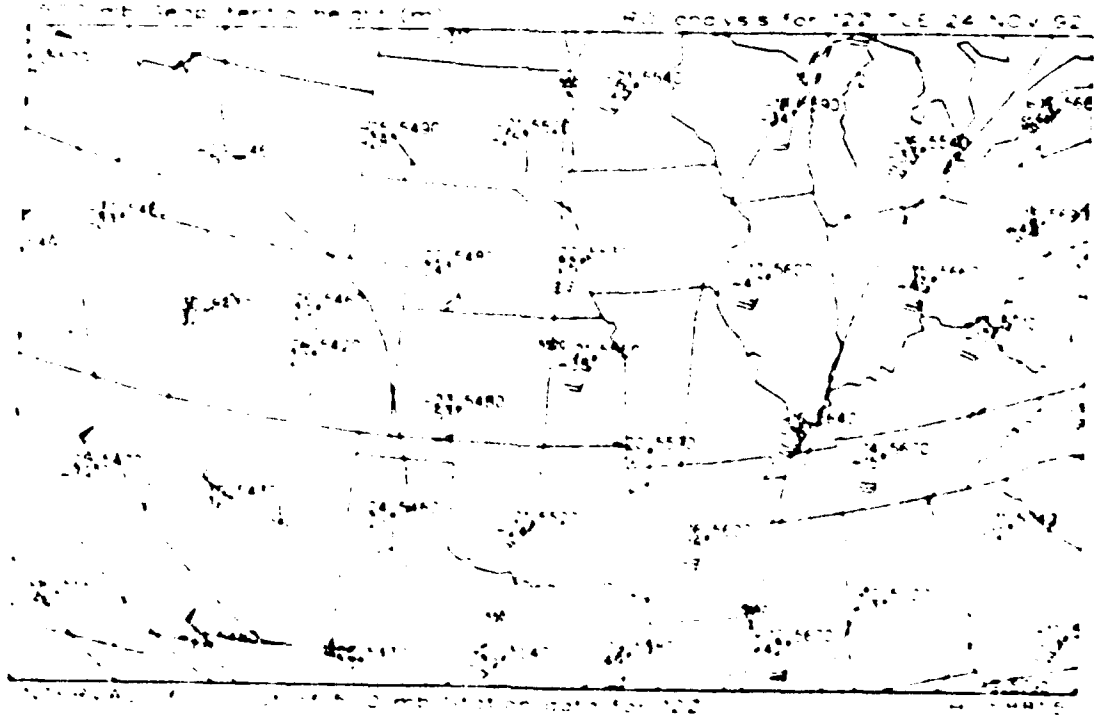

Figure 85. 500 mb weather map and height analysis for 12 UTC 24 November 1992.

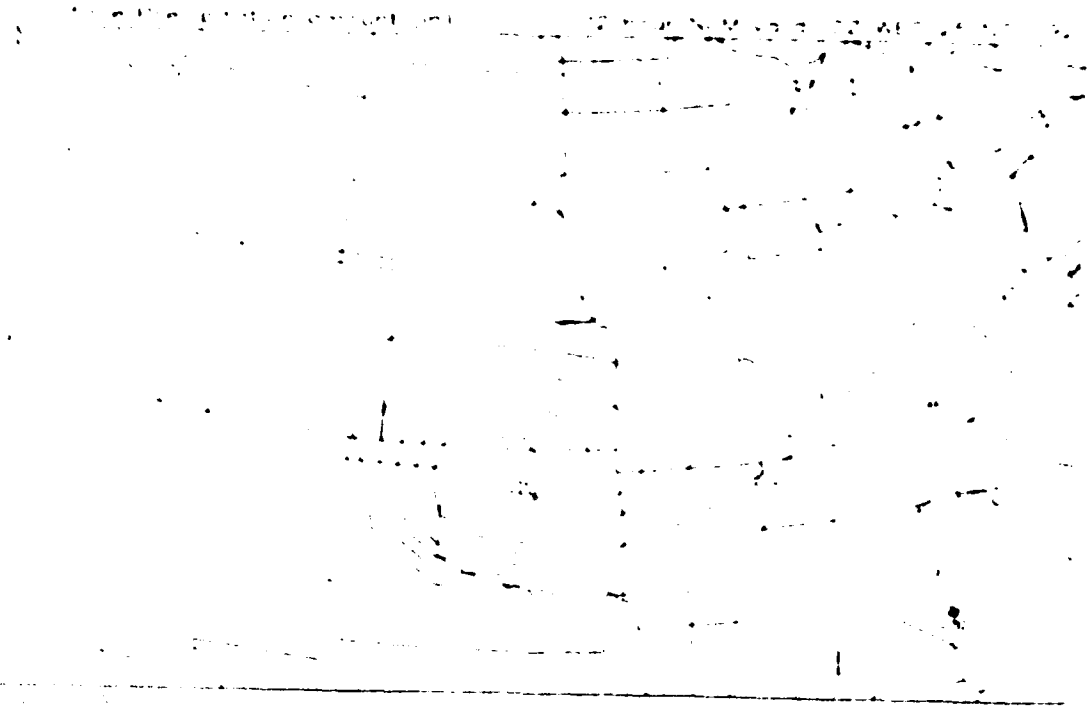

Figure 86: NGM 12 UTC 24 November 1992 forecast of 6-hour accumulated precipitation, valid 00 UTC 25 November 1992.

Figure 87: NGM 12 UTC 24 November 1992 forecast of 700 mb vertical velocity (10^{-1} μb/s, or mm/s), valid 18 UTC 24 November 1992.

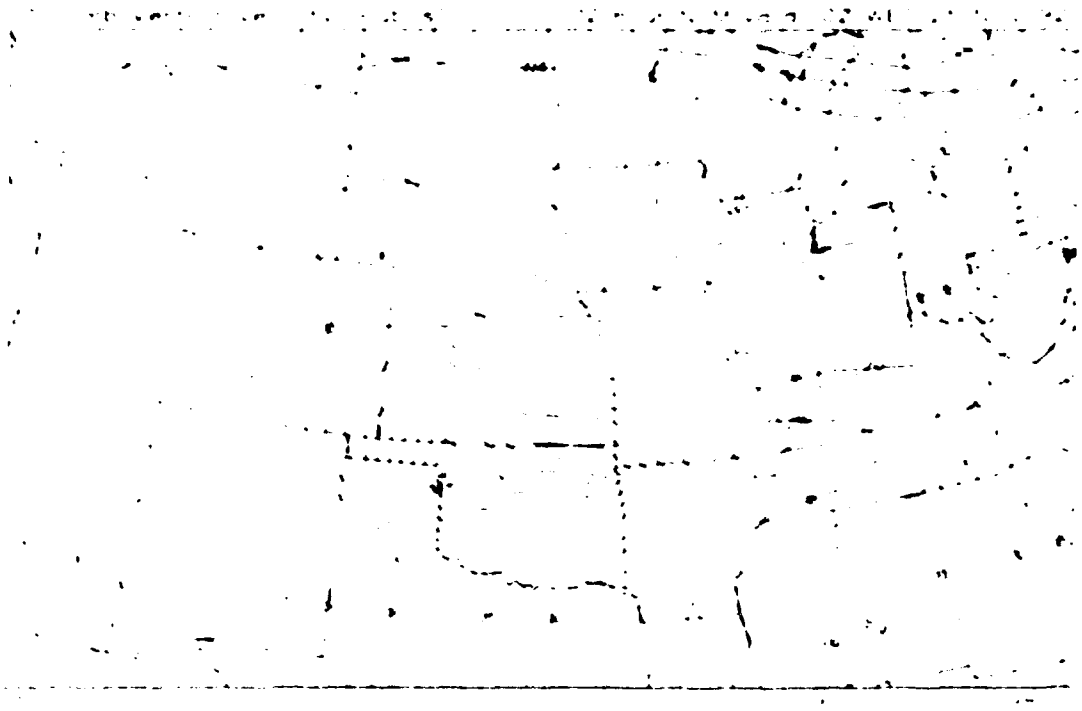

Figure 88. NGM 12 UTC 24 November 1992 forecast of 700 mb vertical velocity ($10^{-1}\mu b/s$, or mm/s), valid 00 UTC 25 November 1992.

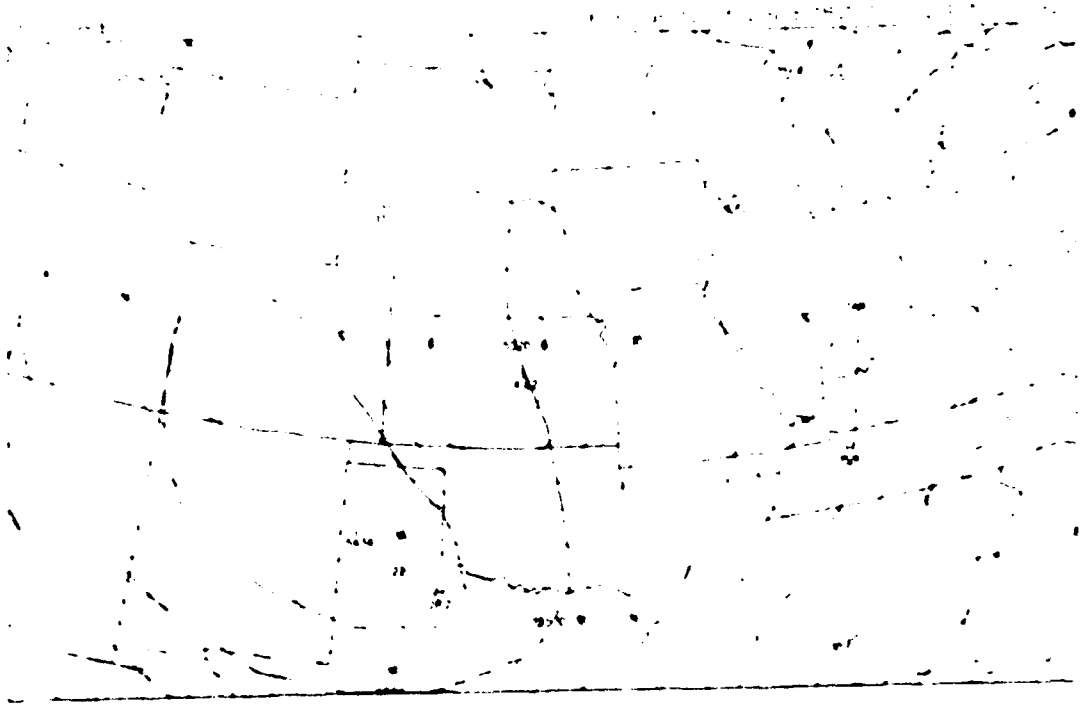

Figure 89: NGM 12 UTC 24 November 1992 forecast of 500 mb height and absolute vorticity, valid 18 UTC 24 November 1992.

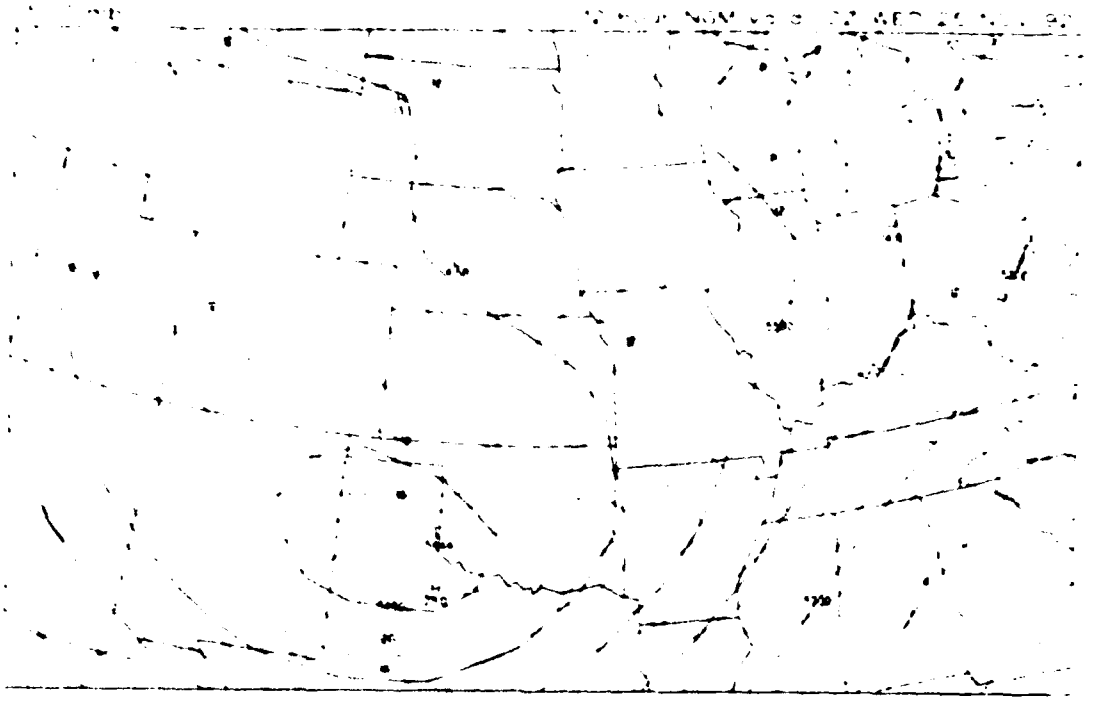

Figure 90: NGM 12 UTC 24 November 1992 forecast of 500 mb height and absolute vorticity, valid 00 UTC 25 November 1992.

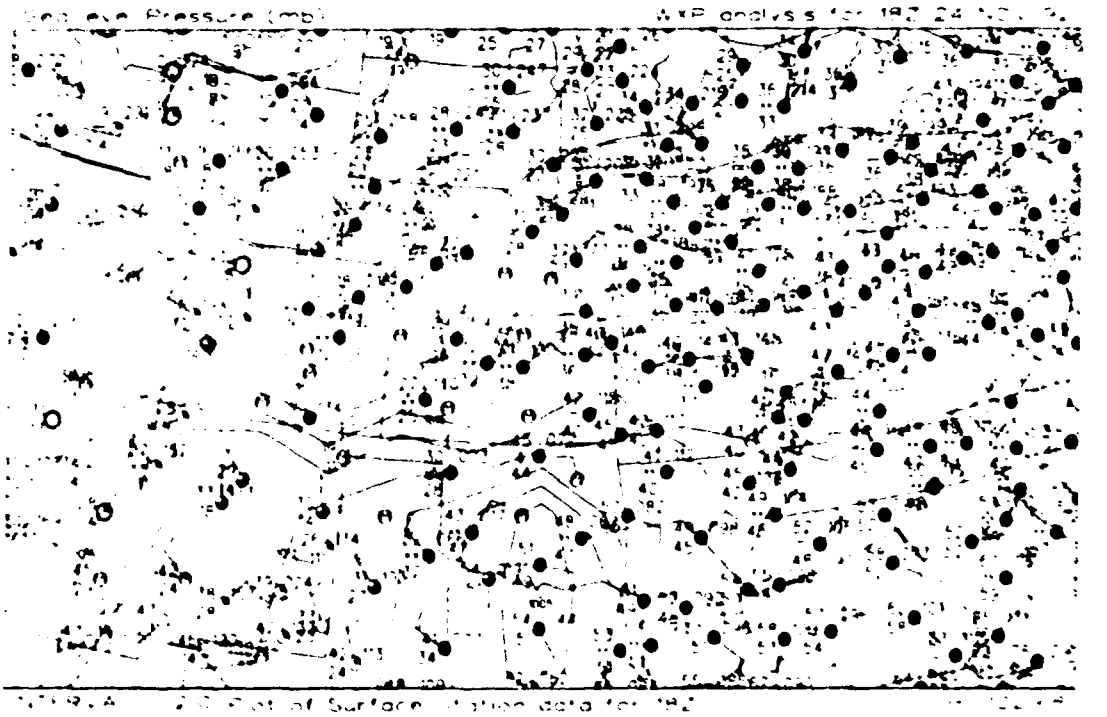

Figure 91: Surface weather map and sea-level pressure analysis for 18 UTC 24 November 1992.

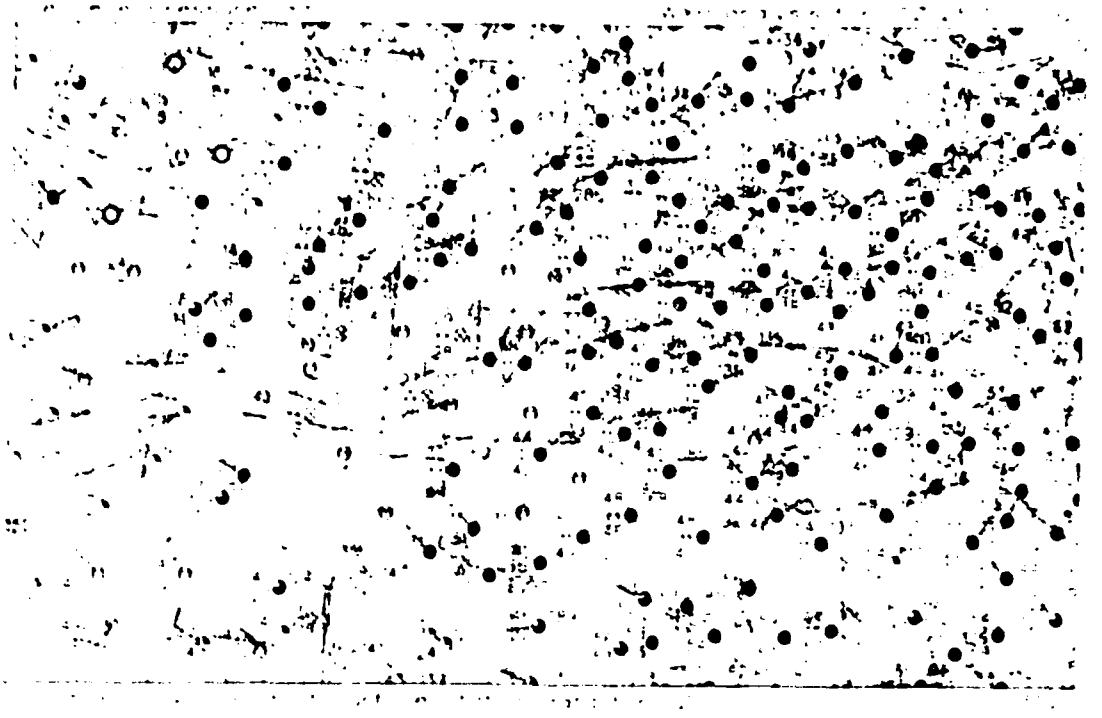

Figure 92: Surface weather map and sea-level pressure analysis for 00 UTC 25 November 1992.

Figure 93: MDR summary for 18 UTC 24 November 1992.

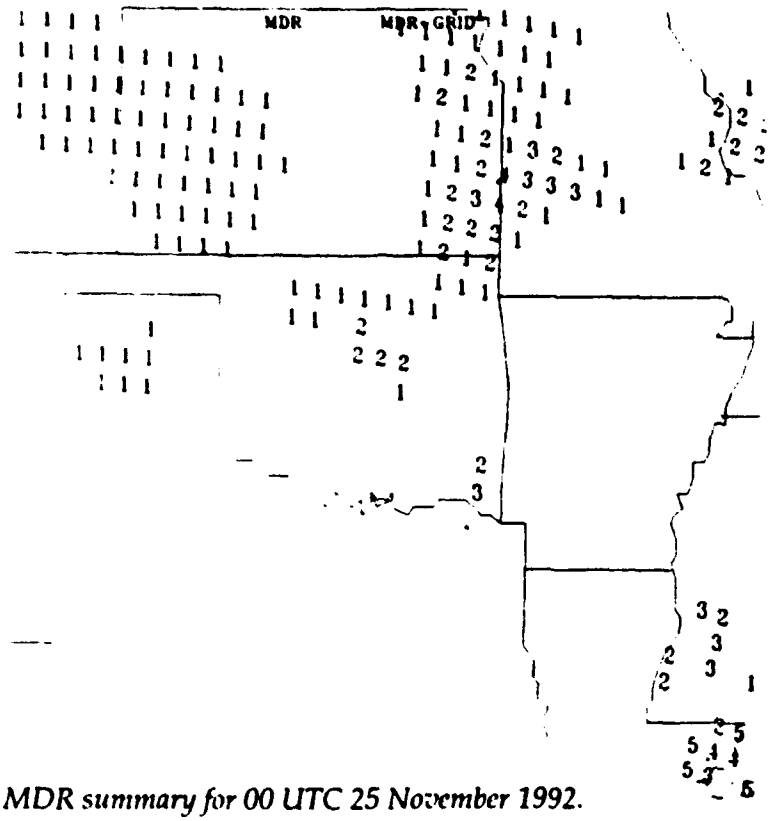

Figure 94: MDR summary for 00 UTC 25 November 1992.

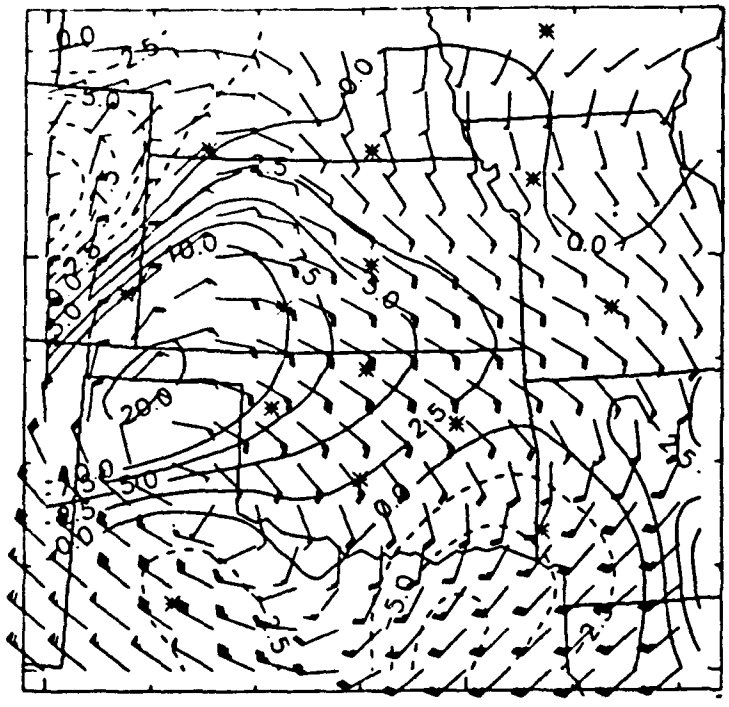

Figure 95: Profiler-derived analysis of winds and vertical velocity (cm/s) at 3000 m for 18 UTC 24 November 1992.

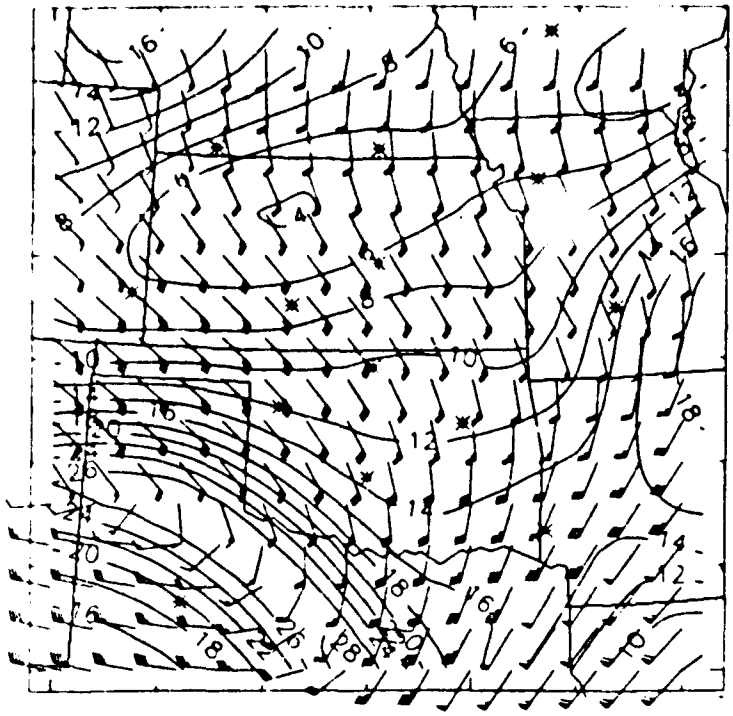

Figure 96: Profiler-derived analysis of winds and absolute vorticity (in $10^{-5}s^{-1}$) at 5500 m for 18 UTC 24 November 1992. Analysis cycle started at 14 UTC.

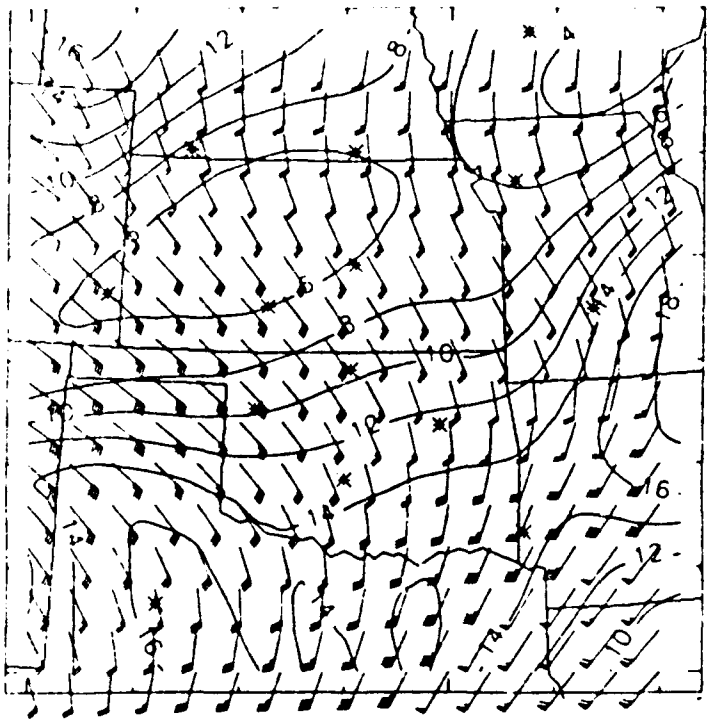

Figure 97: Same as Figure 96, except analysis cycle started at 12 UTC.

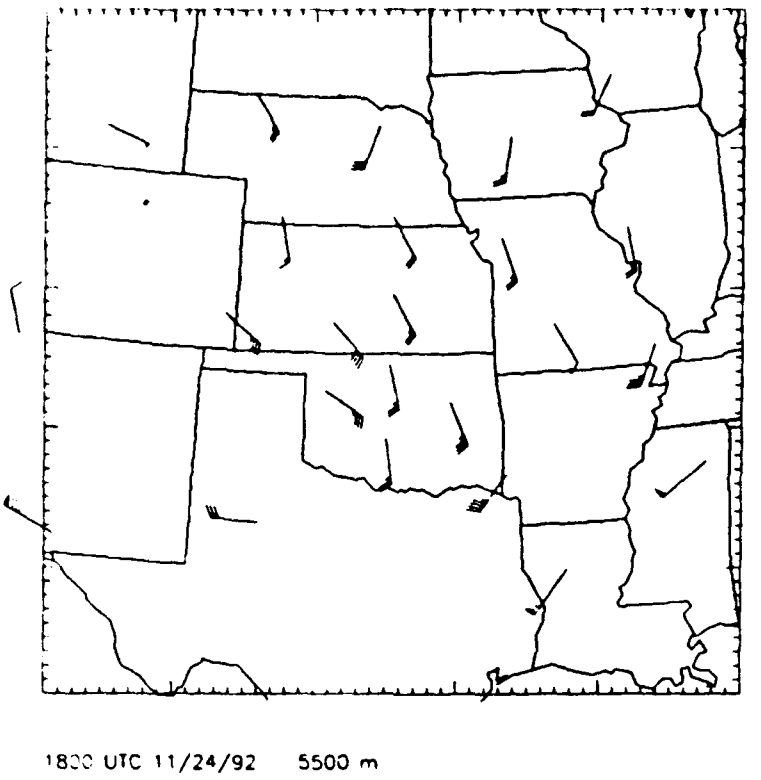

Figure 98: Profiler data used in the analysis shown in Figures 96 and 97.

3.6. November 25, 1992: Iowa snowstorm

Between 12 UTC 25 November and 00 UTC 26 November 1992, the same storm that led to blizzard conditions in the Kansas/Oklahoma region the day before caused moderate to heavy snowfall across a narrow corridor from southwest to northeast Iowa, including Des Moines (DSM - see Figure 99 for station location). Because this snowstorm corresponded with the heavily traveled Thanksgiving Eve time period, a reliable forecast of this type of event would be useful to the general public. However, the 6-12 hour model guidance failed to forecast the intensity and duration of this localized snow event. The utility of wind profiler data in improving the 6-12 hour forecast, particularly for the period 18 UTC to 00 UTC, is demonstrated in this case.

3.6.1. Standard Meteorological Data Available Before the Storm.

The 12 UTC 25 November surface map (Figure 99) shows an elongated surface low in northeast Oklahoma and southwest Missouri. Light to moderate snow is falling in southwest Iowa with light snow falling to the west and light rain and drizzle to the south. The 12 UTC 25 November manually digitized

rain and drizzle to the south. The 12 UTC 25 November manually digitized radar summary (Figure 100) shows an area of level 2 echoes over south central Iowa. At 15 UTC (not shown), moderate snow is reported at DSM, and there are some level 2-3 echoes with cloud top reports of 19,000 and 20,000 feet in northwest Missouri which appear to be moving toward south central Iowa.

The 12 UTC 25 November upper air maps show a deep moist layer from 850 mb (Figure 101) to 500 mb (Figure 102) over eastern Kansas and eastern Nebraska, with a noticeable 700 mb dry surge over southwest Missouri. An 850-300 mb closed circulation exists over the eastern Kansas-Oklahoma border with 500-300 mb diffluence helping to produce upward motion over Missouri and Iowa The NGM forecast maps of 6-hour precipitation accumulation ending at 18 UTC (Figure 103) and 00 UTC (Figure 104) show about .35" of liquid for DSM between 12 UTC and 00 UTC. The NGM forecast maps of 700 mb vertical velocity (Figures 105 and 106) show the greatest upward motion southeast of DSM. The corresponding 500 mb forecast maps (Figures 107 and 108) show that this predicted vertical velocity maximum is associated with 500 mb positive vorticity advection (PVA). Most of the precipitation at DSM is forecast to fall between 12 UTC and 18 UTC. The 850 mb temperature and 1000-500 mb thickness forecasts (not shown) indicate snow for DSM, so a forecast of 3-4" of snow by 18 UTC with little additional accumulation thereafter seemed reasonable based on the NGM guidance.

3.6.2. Information Available During and After the Storm.

The surface maps between 18 UTC 25 November (Figure 109) and 00 UTC 26 November (Figure 110) show a narrow band of moderate to heavy snow from southwest to northeast Iowa. The surface low is moving northeast across Missouri and into western Illinois. Moderate northerly winds are helping to reduce visibility with blowing snow in the central plains. The radar summaries show level 2 echoes remaining in the DSM vicinity between 17 UTC (Figure 111) and 21 UTC (Figure 112), and dissipating thereafter. The hourly observations for DSM show moderate or heavy snow between 15 UTC and 23 UTC, with heavy snow between 17 UTC and 19 UTC. Seven inches of snow is reported on the ground at 00 UTC. A total of 1.06" of liquid precipitation falls between 12 UTC and 00 UTC, .45" during the first 6 hours and .61" during the latter six hours. The

precipitation by .56". Figures 113 and 114 show the 6 hour observed precipitation totals over the midwest for 18 and 0 UTC. The observed precipitation amounts are heavier than and to the NW of the NGM forecast maximum (viz. Figures 103 and 104).

Figure 115 shows the 500 mb 00 UTC 26 November height and vorticity analysis. The vorticity gradient over the DSM vicinity is greater than that forecasted by the NGM (see Figure 108), suggesting greater PVA and vorticity induced upward vertical motion than forecast during the previous 12 hours. This northwest deviation of the vorticity gradient from the NGM forecast is probably responsible for the more prolonged and heavier than forecasted precipitation over the DSM vicinity.

3.6.3. Utility of the Profiler Data.

Figure 116 shows the 18 UTC profiler derived 3000 m winds and vertical velocity. A band of upward motion of > 2.5 cm/s extends across southern Iowa and into eastern Nebraska, suggesting a continuation of significant snow in DSM beyond 18 UTC. This is contrary to the NGM vertical velocity and precipitation forecasts (Figures 104 and 106), which indicate little snowfall after 18 UTC. The time-height cross section of vertical velocity over DSM (Figure 117) shows a deep layer of > 2.5 cm/s upward motion moving over by 16 UTC with moderate snow, and continuing with moderate to heavy snow through 21 UTC.

Figure 118 shows the profiler-derived 5500 m wind and relative vorticity analysis for 18 UTC 25 November. The vorticity maximum and associated vorticity gradient is north of the forecast position (see Figure 107), with subsequently stronger PVA over the DSM vicinity. Thus, 18 UTC profiler derived vorticity advection indicates PVA which is stronger than forecasted by the NGM, a trend which continues for the following 6 hours (see the 00 UTC plots in Figures 108 and 115). Figure 119 shows the 15 UTC profiler derived 5500 m winds and relative vorticity which would be available around the same time the NGM 12 UTC guidance would be. The profiler analysis already shows the center of circulation to the north of the forecasted position at 18 UTC. This provides an early clue to the forecaster that the NGM is tracking the vorticity gradient too far to the south.

In summary, the NGM underforecasted snow amounts at DSM, particularly for the time period 18 UTC 25 November and 00 UTC 26 November, because it placed the 500 mb vorticity maximum, and the associated PVA and upward motion, too far to the south and east. This forecast error is clearly evident in the 18 UTC profiler analyses, and indications of it are present as early as 15 UTC. The forecast for the 18 UTC to 00 UTC time period could thus have been corrected shortly before and at the beginning of the forecast period.

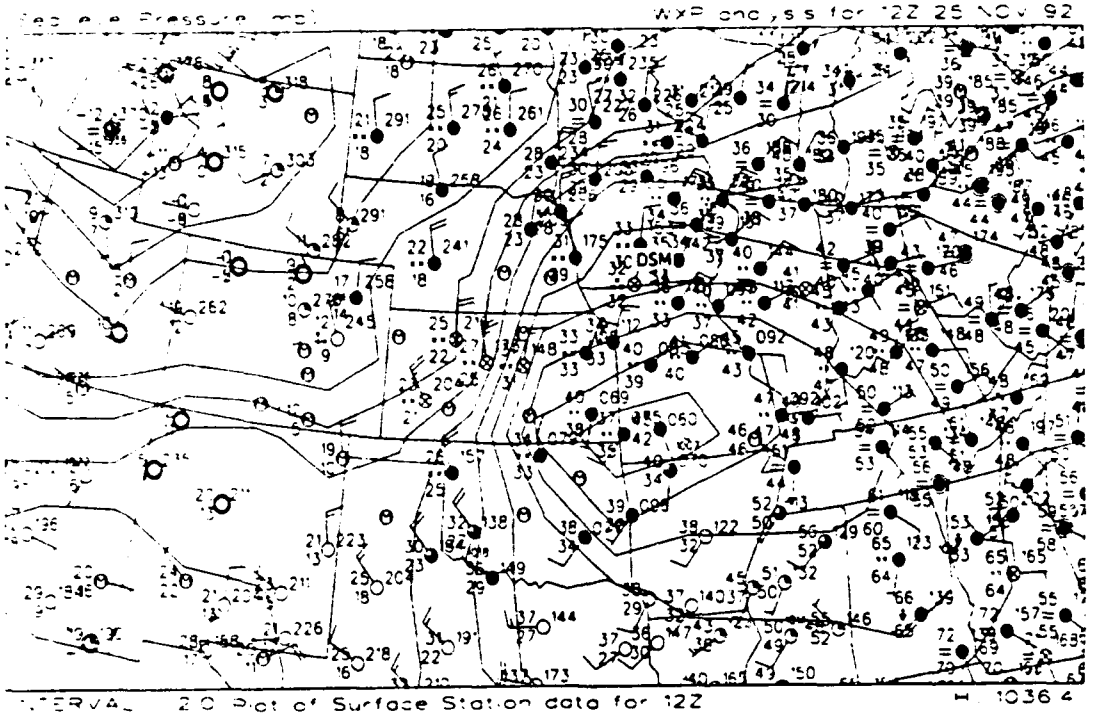

Figure 99: Surface weather map and sea-level pressure analysis for 12 UTC 25 November 1992.

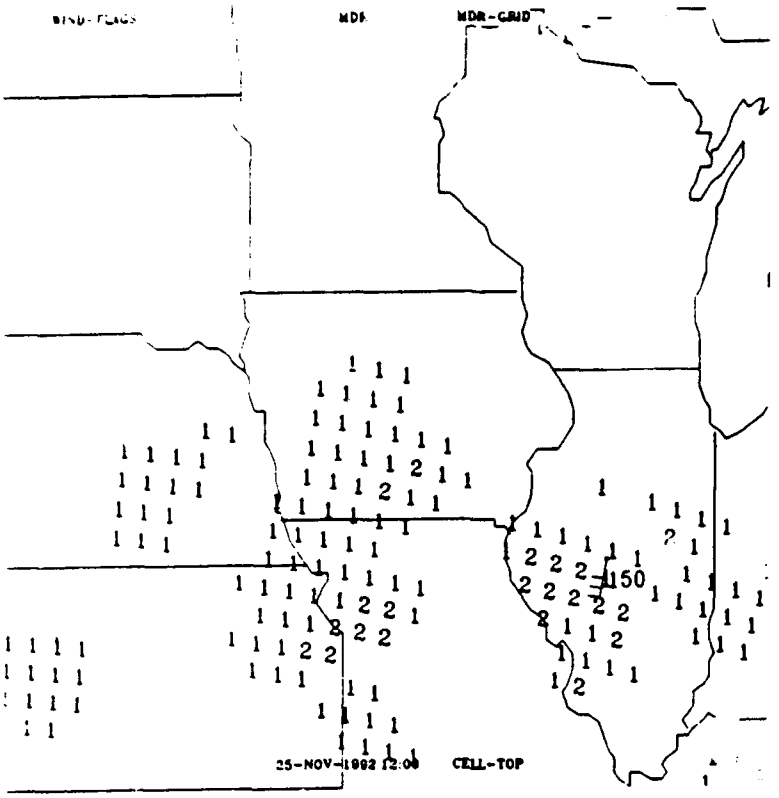

Figure 100: MDR summary for 12 UTC 25 November 1992.

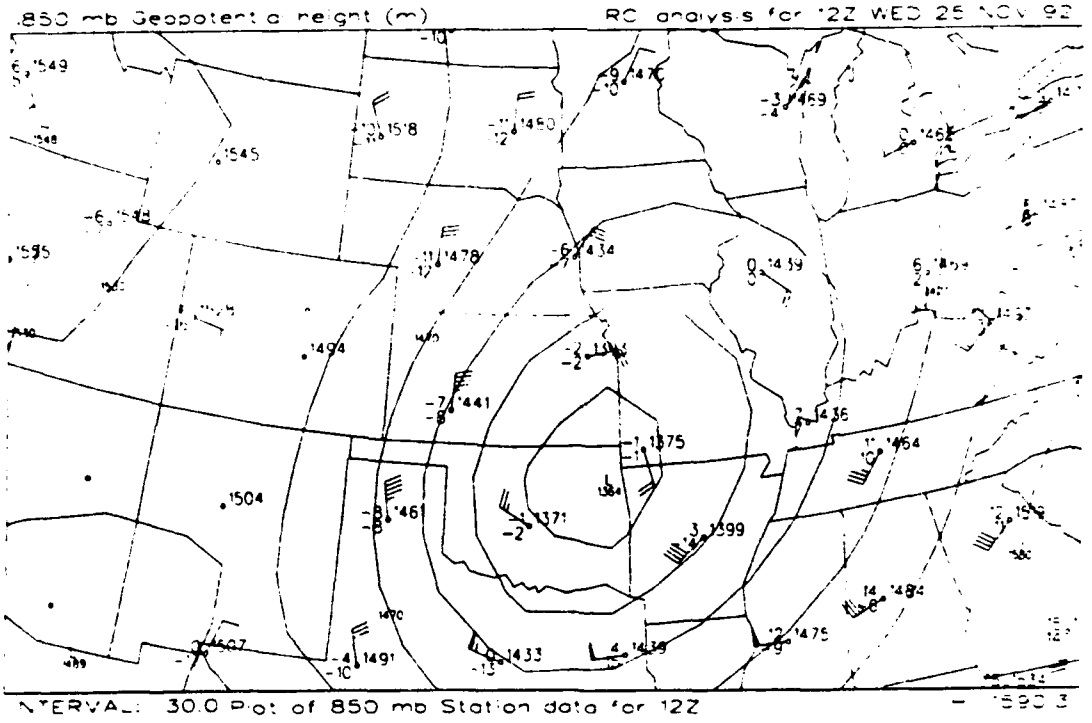

Figure 101: 850 mb weather map and height analysis for 12 UTC 25 November 1992.

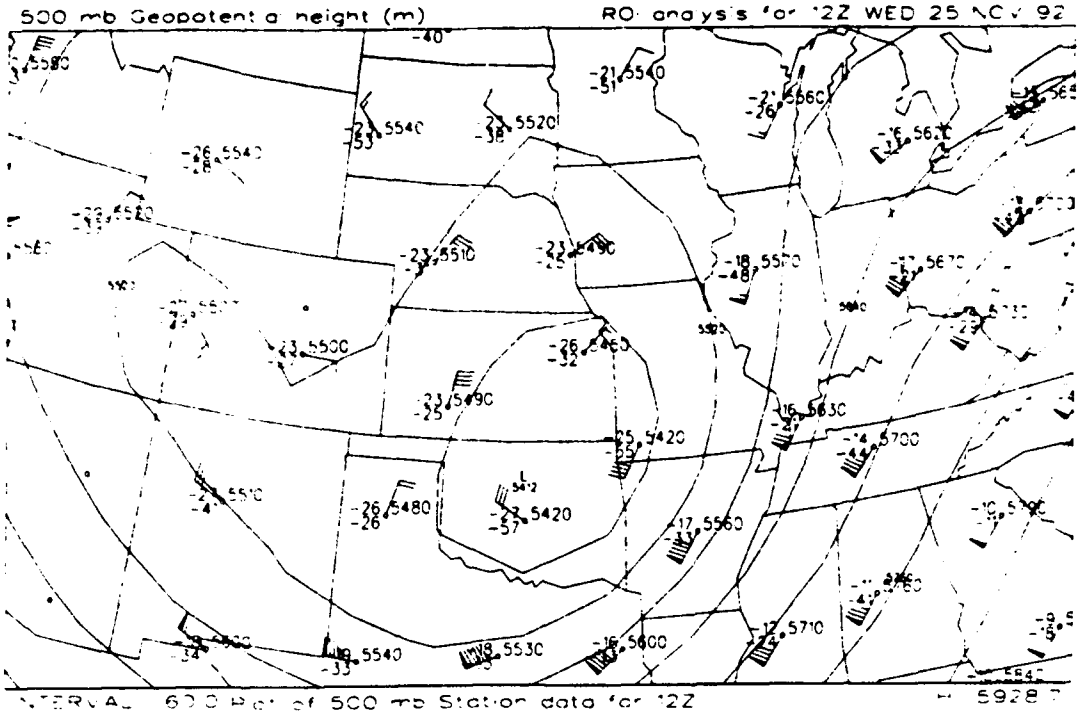

Figure 102: 500 mb weather map and height analysis for 12 UTC 25 November 1992.

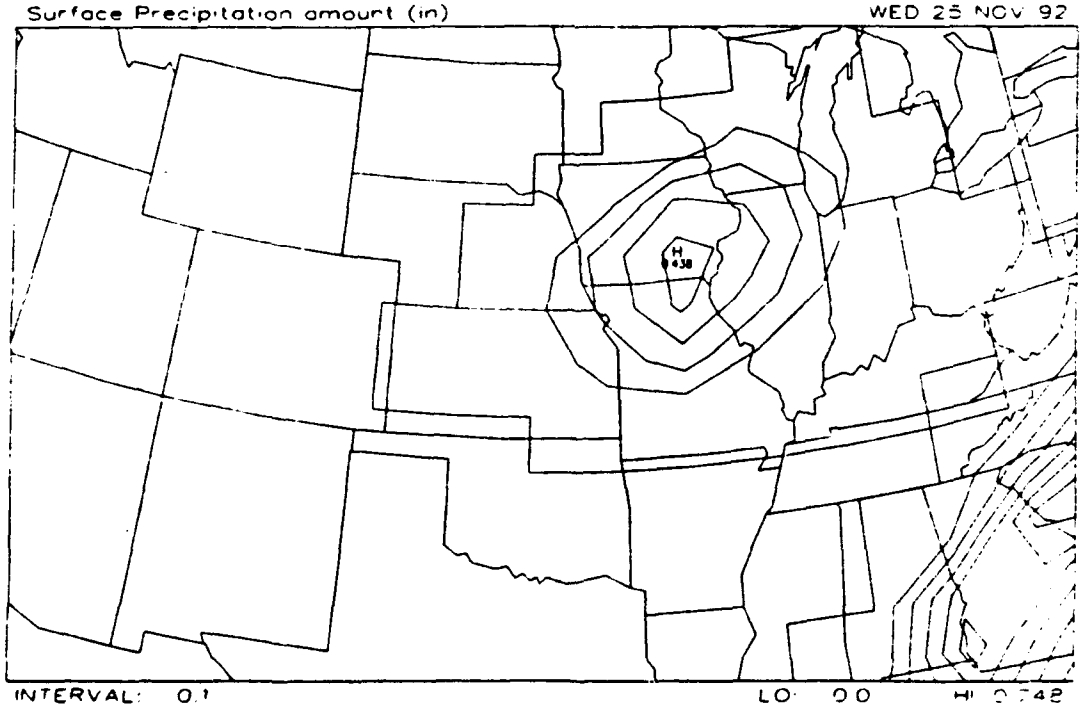

Figure 103: NGM 12 UTC 25 November 1992 forecast of 6-hour accumulated precipitation, valid 18 UTC 25 November 1992.

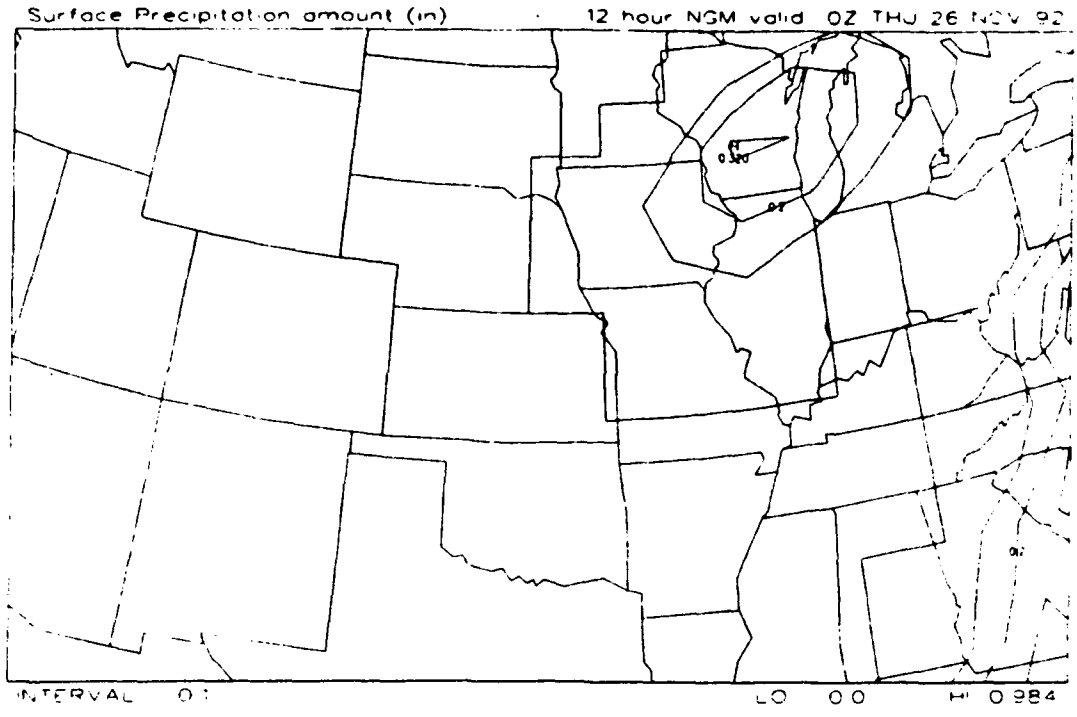

Figure 104: NGM 12 UTC 25 November 1992 forecast of 6-hour accumulated precipitation, valid 00 UTC 26 November 1992.

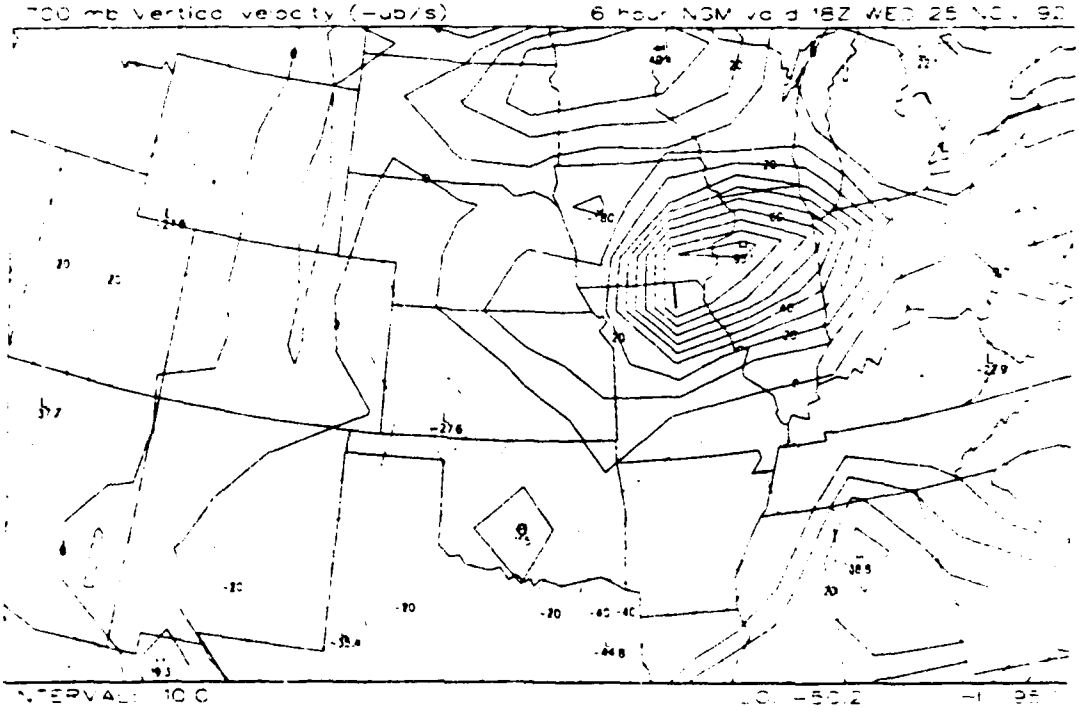

Figure 105: NGM 12 UTC 25 November 1992 forecast of 700 mb vertical velocity (10^{-1} μb/s, or mm/s), valid 18 UTC 25 November 1992.

Figure 106: NGM 12 UTC 25 November 1992 forecast of 700 mb vertical velocity (10^{-1} μb/s, or mm/s), valid 00 UTC 26 November 1992.

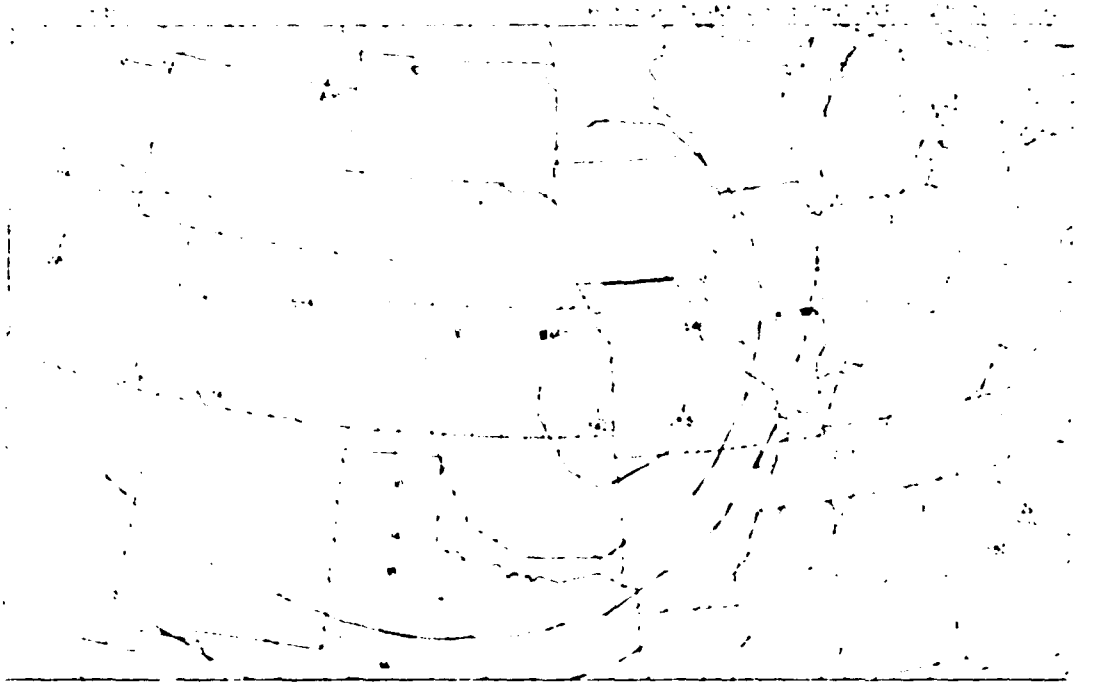

Figure 107: NGM 12 UTC 25 November 1992 forecast of 500 mb height (solid lines) and absolute vorticity (dashed lines), valid 18 UTC 25 November 1992.

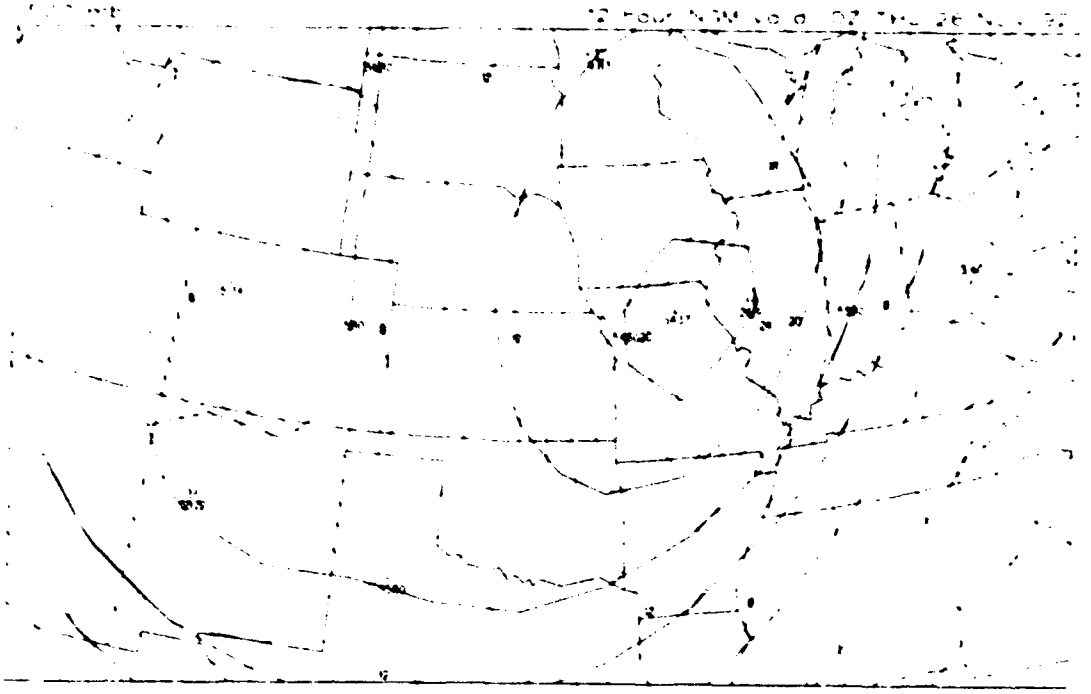

Figure 108: NGM 12 UTC 25 November 1992 forecast of 500 mb height (solid lines) and absolute vorticity (dashed lines), valid 00 UTC 26 November 1992.

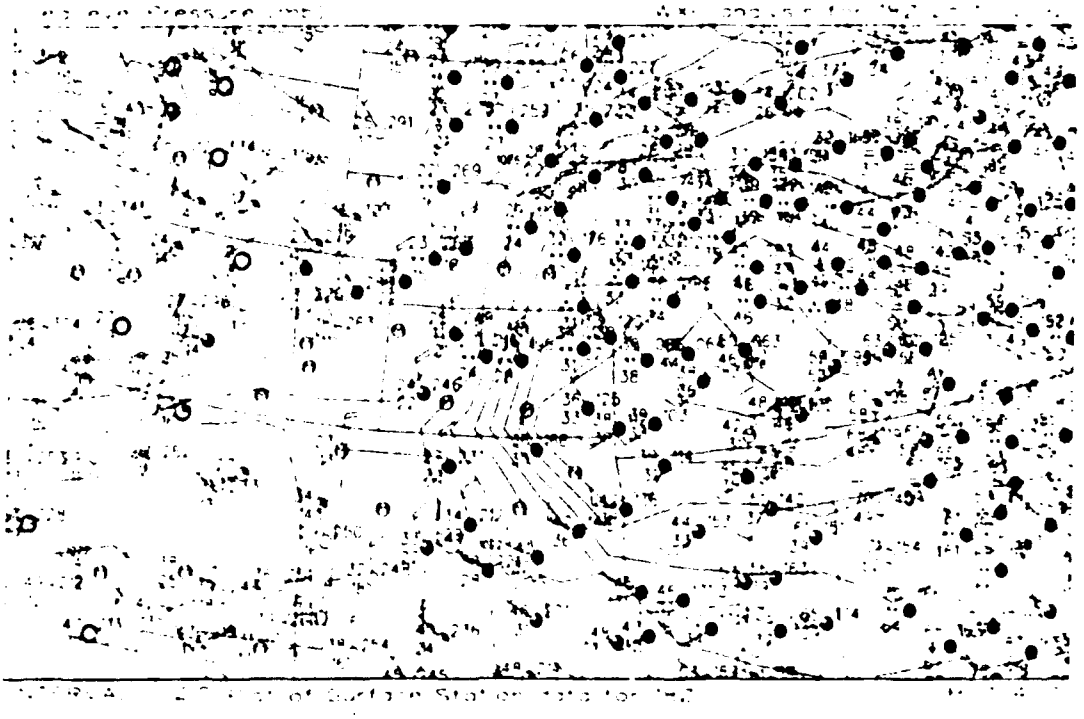

Figure 109: Surface weather map and sea-level pressure analysis for 18 UTC 25 November 1992.

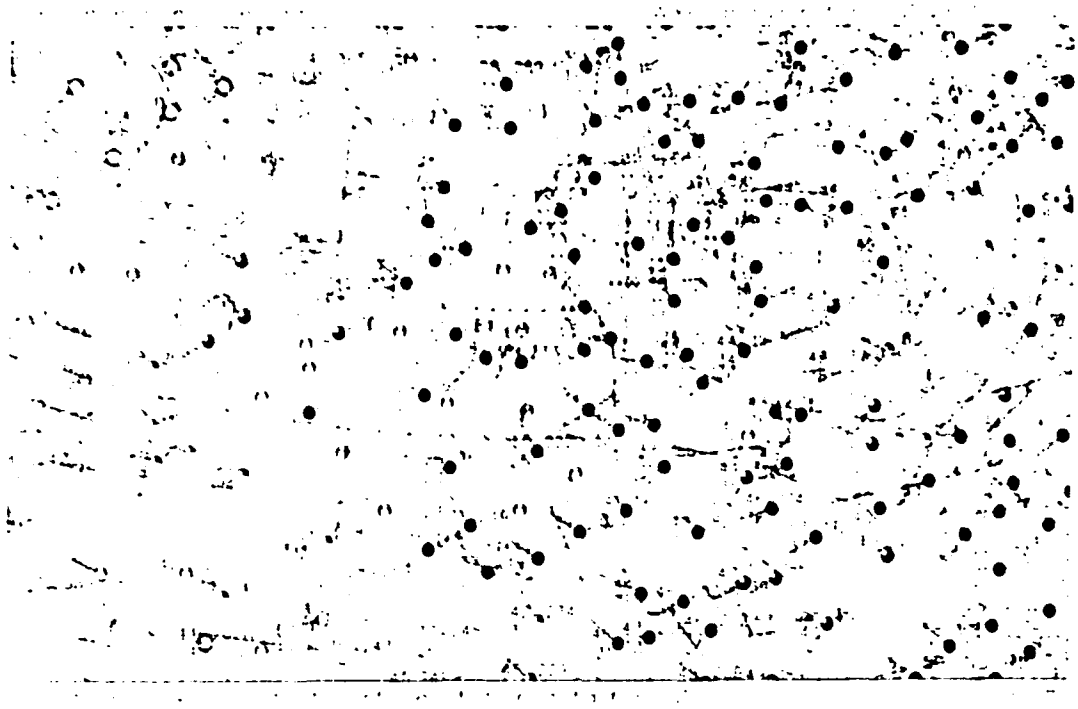

Figure 110: Surface weather map and sea-level pressure analysis for 00 UTC 26 November 1992.

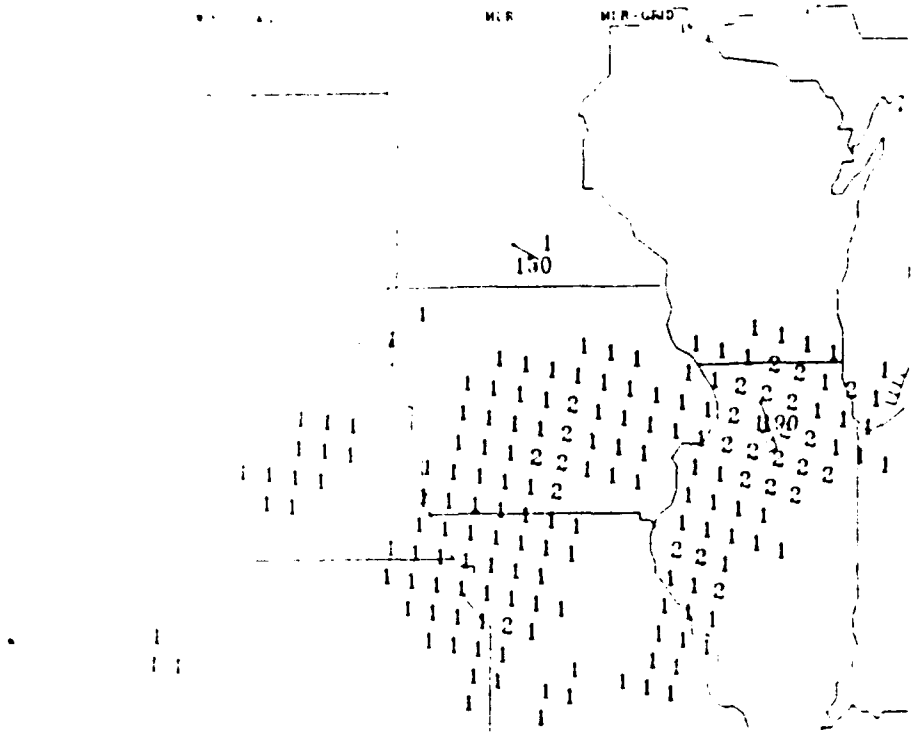

Figure 111. MDR summary for 17 UTC 25 November 1992.

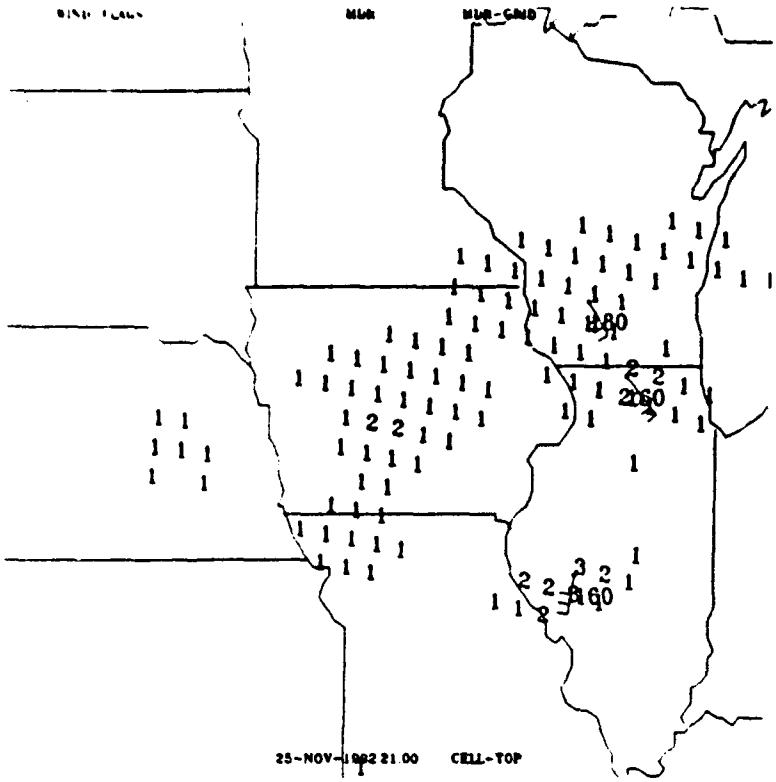

Figure 112: MDR summary for 21 UTC 25 November 1992.

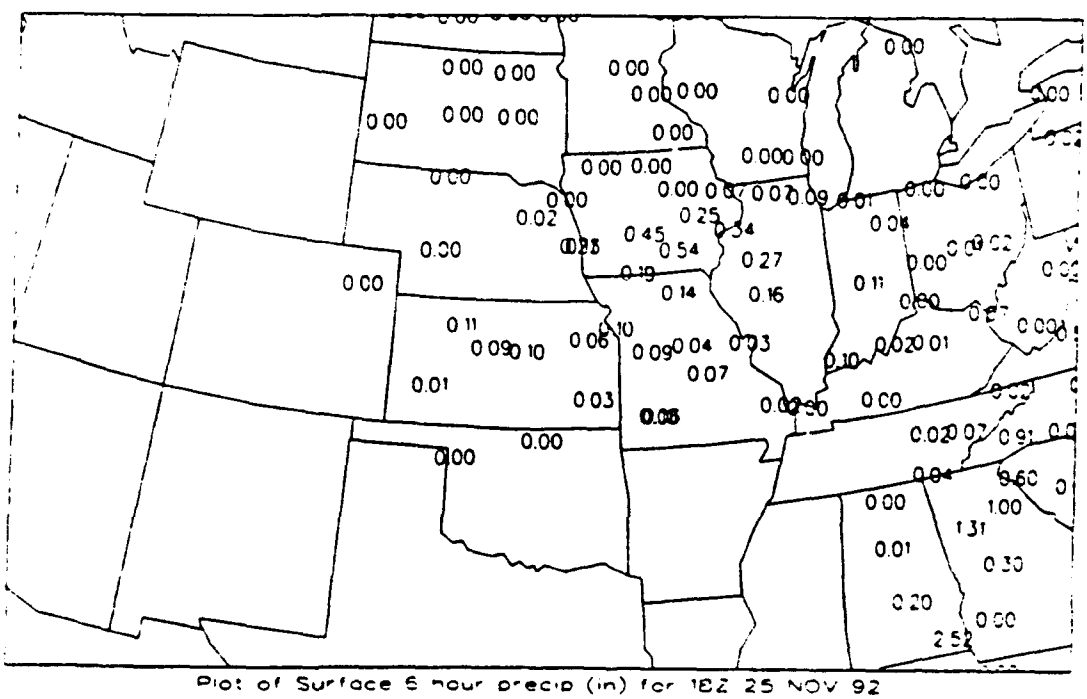

Figure 113: Observed 6-hour precipitation accumulation (in) ending 18 UTC 25 November 1992.

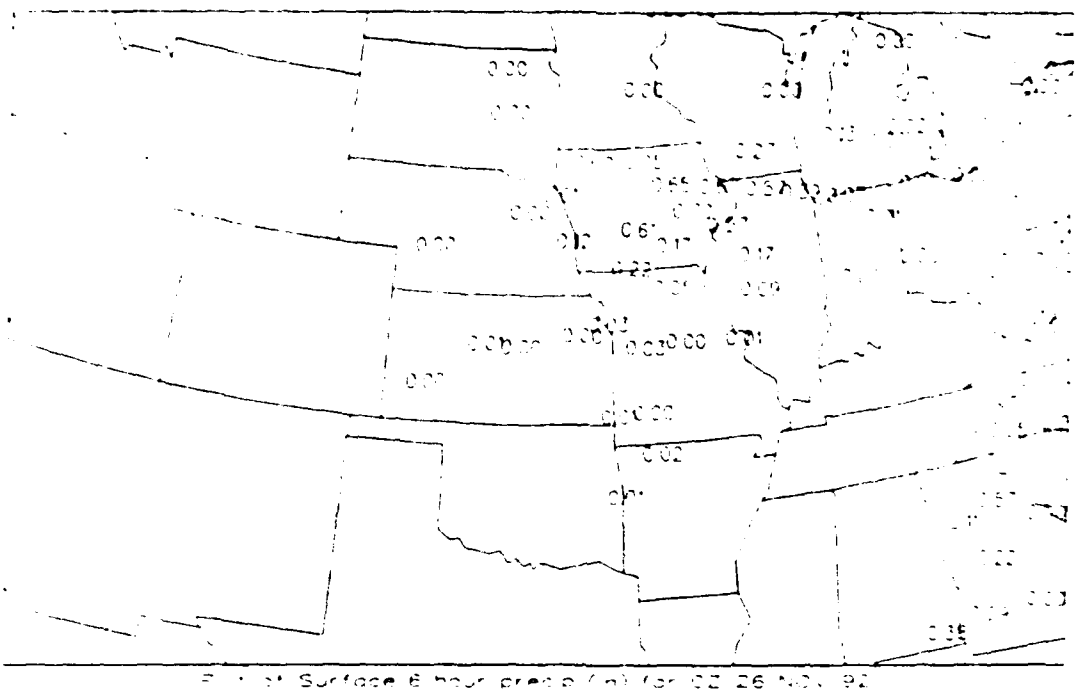

Figure 114: Observed 6-hour precipitation accumulation (in) ending 00 UTC 26 November 1992.

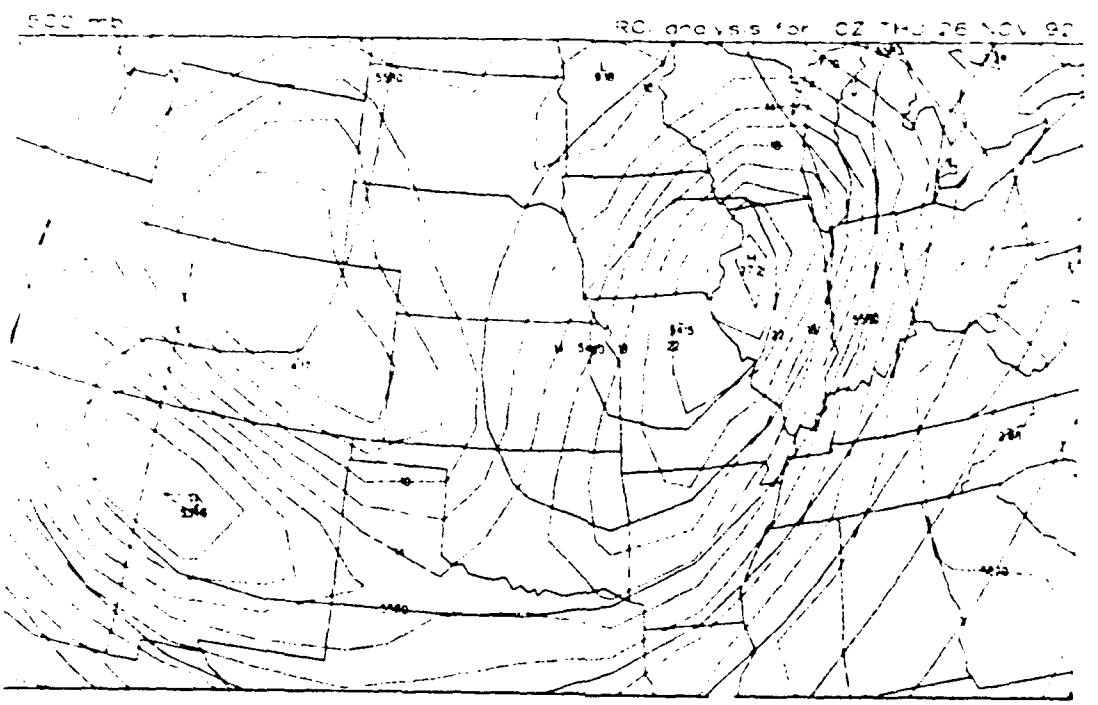

Figure 115: 500 mb analysis of height (solid lines) and absolute vorticity (dashed lines) for 00 UTC 26 November 1992.

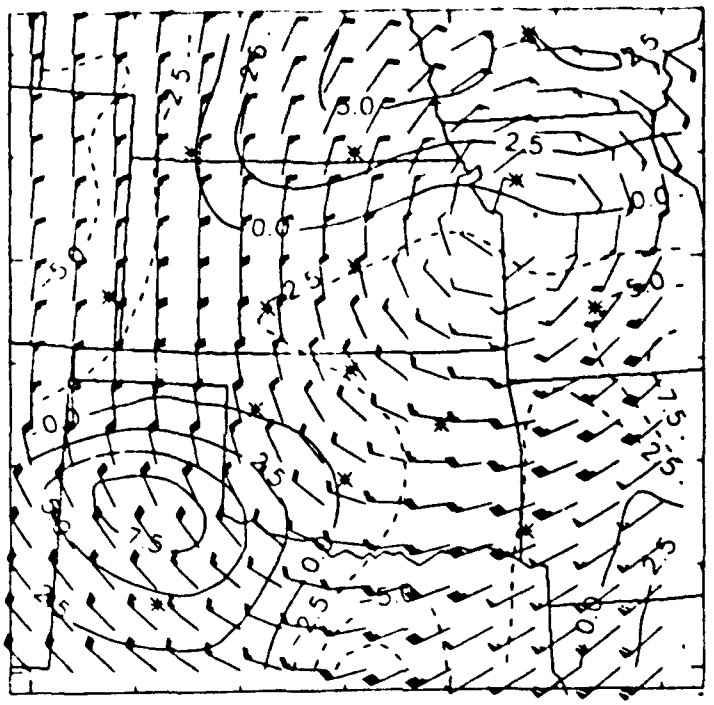

Figure 116: Profiler-derived analysis of winds and integrated vertical velocity (cm/s) at 3000 m for 18 UTC 25 November 1992.

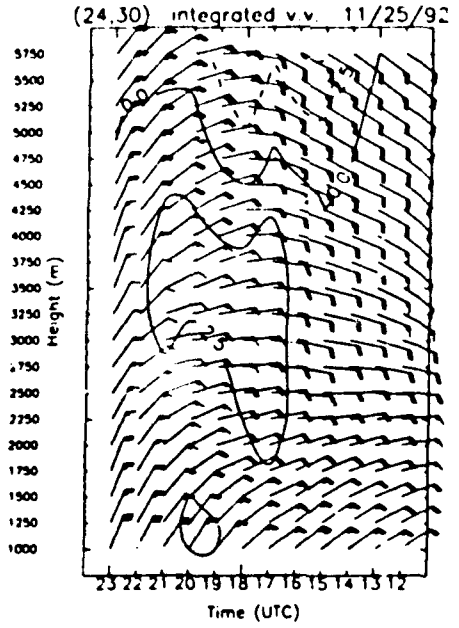

Figure 117: Time-height cross section of profiler-derived winds and integrated vertical velocity (cm/s) for DSM for 12-23 UTC 25 November 1992.

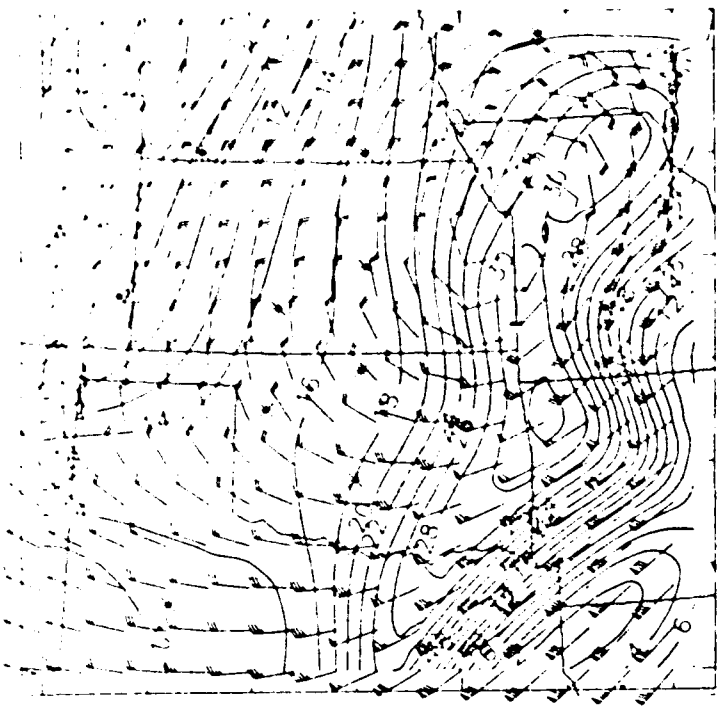

Figure 118: Profiler-derived analysis of winds and absolute vorticity ($10^{-5}s^{-1}$) at 5500 m for 18 UTC 25 November 1992.

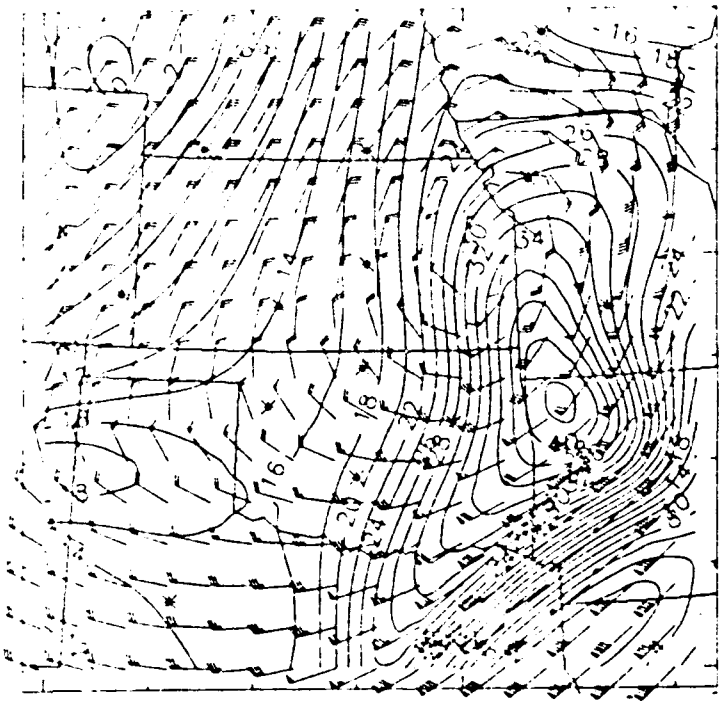

Figure 119: Profiler-derived analysis of winds and absolute vorticity ($10^{-5}s^{-1}$) at 5500 m for 15 UTC 25 November 1992.

3.7. December 9, 1992: Oklahoma/Texas rain event

Between 00 and 12 UTC 9 December 1992 an area of rain and embedded thunderstorms associated with a strong mid-level short wave trough deposited .5-1" of rain in central and eastern Oklahoma with local amounts up to 1.46" reported in southeastern Oklahoma. The NGM made a good precipitation forecast between 00 and 06 UTC, but was too quick in moving the heaviest rainfall to the east after 06 UTC, underforecasting the rainfall in southeastern Oklahoma between 06 and 12 UTC by more than an inch. Profiler data available for this case was unable to resolve this problem due to missing observations and the highly localized nature of the heaviest rainfall.

3.7.1 Standard Meteorological Data Available Before the Storm.

The 00 and 06 UTC surface analyses in Figures 120 and 121 show a low moving from southwest Texas to the Texas panhandle with a moist southeast flow ahead of it. The NMC analyses for those times (not shown) indicated an occluded front extending southeastward from the center of the low. Rain and thunderstorms are occurring to the north and east of this occluded front in northern Texas. The manually digitized radar summaries (shown in Figure 122 for 06 UTC) show an eastward moving area of rain streching from Kansas to Texas. The heaviest rainfall is occuring across northern Texas along the occluded front.

The 00 UTC upper air maps show a short-wave trough, tilting back from the Texas/New Mexico border at 850 mb (Figure 123) to central New Mexico at 500 mb (Figure 124). Ahead of this trough, the low level is characterized by a moist atmosphere over Oklahoma and northern Texas, with 850 mb southerly flow from the Gulf of Mexico resulting in warm and moist advection. At 500 mb and 300 mb (not shown), diffluence over northern Texas and Oklahoma contributes to upward motion.

The 00 UTC NGM 6 and 12 hour forecasts of 6 hour precipitation for Oklahoma in Figures 125 and 126 show .2-.5" between 00 and 06 UTC and less than .3" between 06 and 12 UTC. The corresponding forecasts of 700 mb vertical velocity in Figures 127 and 128 show a band of maximum upward motion from north central Texas to south central Kansas at 06 UTC moving to the east with the

maximum upward motion over northeast Texas by 12 UTC. The precipitation forecasts do not correspond as well to the vertical velocity forecasts as in some of the other cases: decreasing precipitation intensity is forecast over northeast Texas, southeast Oklahoma at the same time when the upward motion intensities over this area, and the precipitation maximum at 12 UTC to the east does not correspond to any feature in the vertical velocity forecast. Examination of the forecast moisture fields (not shown) did not reveal the reason for the apparent discrepancy. Apparently, other factors (possibly related to convective precipitation) determined the NGM precipitation forecast. The 00 UTC NGM 6 and 12 hour forecasts of 500 mb height and vorticity in Figures 129 and 130 show the short wave trough moving across northern Texas and Oklahoma with little change in intensity. The associated positive vorticity advection is moving from north central Texas at 06 UTC to southeast Oklahoma at 12 UTC, consistent with the vertical velocity forecast.

3.7.2. Information Available During and After the Storm.

The low pressure area in the Texas panhandle, and the associated occluded front through northeast Texas, moves east by very little between 06 and 12 UTC, as can be seen in the surface map for 12 UTC in Figure 131. Rain and thunderstorms continue along and to the north and east of the occluded front. The 10 UTC radar summary in Figure 132 shows a large area of rain and embedded thunderstorms from northeast Texas northward to Missouri and eastward to Mississippi. The most widespread heavy rainfall is occurring in northeast Texas where the NGM forecasted the maximum upward motion.

The verifying 12 UTC analysis of 500 mb height and vorticity in Figure 133 shows a slightly deeper than forecast trough, but an otherwise very accurate 12 hr forecast over southeast Oklahoma and northeast Texas. The forecasted and verifying patterns of vorticity advection (not shown) agree to within 10%. In spite of this good forecast of the flow field, the NGM precipitation forecast was not accurate for the 06 to 12 UTC time period: only .25" of rain for northeast Texas and southeast Oklahoma was forecasted, when .5-1.5" actually fell, and the forecast precipitation maximum was too far to the east in Mississippi. The reasons for the apparent discrepancy between the vertical motion and

precipitation forecast, and thus the precipitation forecast error, are not entirely clear.

3.7.3. Utility of the Profiler Data.

The profiler analyses for this case suffered from missing observations at a number of sites: both profilers in northern Texas (JTN and PAT), the site in northern New Mexico (TUC), and sites in eastern Oklahoma (HKL) and Kansas (NDS). As a result, details of the circulation over Texas are not observed at all, resulting in poor estimates of derived quantities over this region. However, the remaining observations allow reliable analyses of the wind and convergence fields over southeast Oklahoma, where the greatest rainfall was reported.

The 06 and 12 UTC profiler analysis of 3000 m horizontal winds and vertical velocities in Figures 134 and 135 show ascent over eastern Oklahoma, in general agreement with the corresponding NGM forecasts. The ascent intensifies with time. The time-height cross section of horizontal winds and vertical velocity over McAlester, OK (MLC - see Figure 131 for station location) in Figure 136 shows descent between 00 and 06 UTC, and intensifying ascent afterwards. This pattern corresponds well to the hourly observations from MLC, which indicated not more than a trace of precipitation before 06 UTC, and continued rain producing 1.46" between 07 and 12 UTC. Thus, the profiler-derived vertical velocity analysis is in agreement with the NGM vertical velocity forecast, and consistent with the observations of precipitation. Since the NGM precipitation forecast was poor for reasons other than errors in the wind field, this information is not useful for correcting the NGM forecast of precipitation.

The profiler derived analyses of the 500 mb flow are less than helpful in this case. The 12 UTC analysis of 5500 m horizontal winds and vorticity shown in Figure 137 deviates from the corresponding Raob based analysis (Figure 133) in some important details over the data-void region: the trough axis is too far to the west, and the curvature of the flow over northeast Texas has the wrong sign, resulting in an erroneous vorticity pattern, and vorticity advection of the wrong sign over northeast Texas and southeast Oklahoma.

In summary, the NGM forecast of precipitation for northeast Texas/southeast Oklahoma was too low for the time period 06 UTC to 12 UTC in this case, in spite of a generally accurate forecast of the flow field and vertical velocity pattern. The cause of the forecast error was not apparent. Profiler analyses of low level vertical velocity over Oklahoma are in general agreement with the NGM forecast, and thus not helpful in identifying the NGM forecast error in precipitation. Missing data made profiler analyses over Texas unreliable, and resulted in an erroneous pattern of vorticity advection over Texas and southeast Oklahoma.

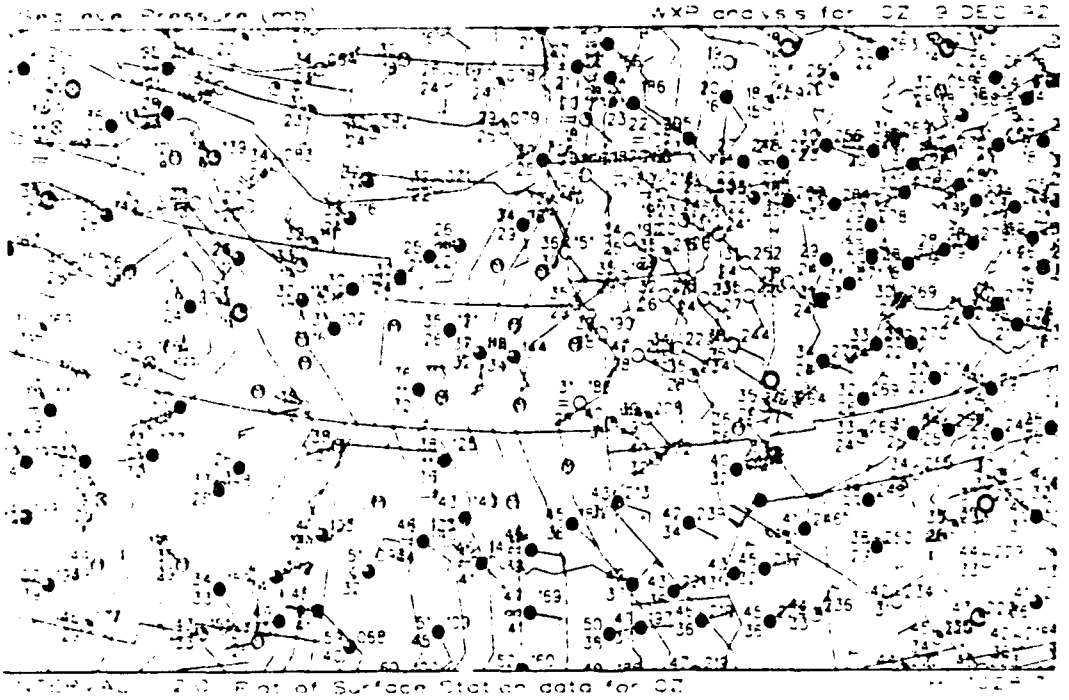

Figure 120: Surface weather map and sea-level pressure analysis for 00 UTC 9 December 1992.

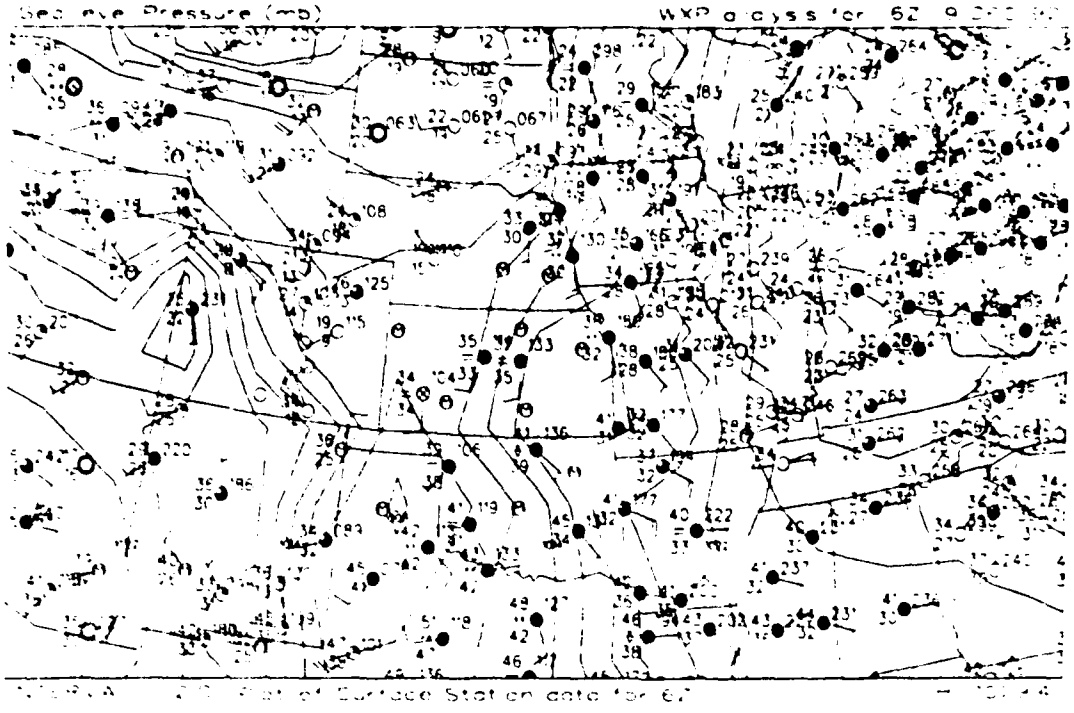

Figure 121: Surface weather map and sea-level pressure analysis for 06 UTC 9 December 1992.

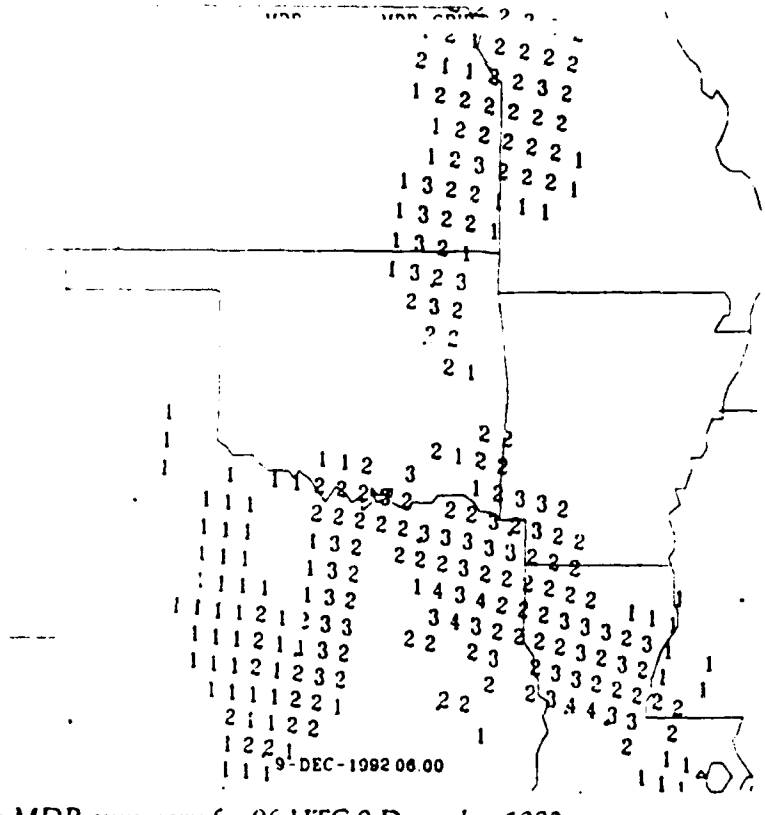

Figure 122: MDR summary for 06 UTC 9 December 1992.

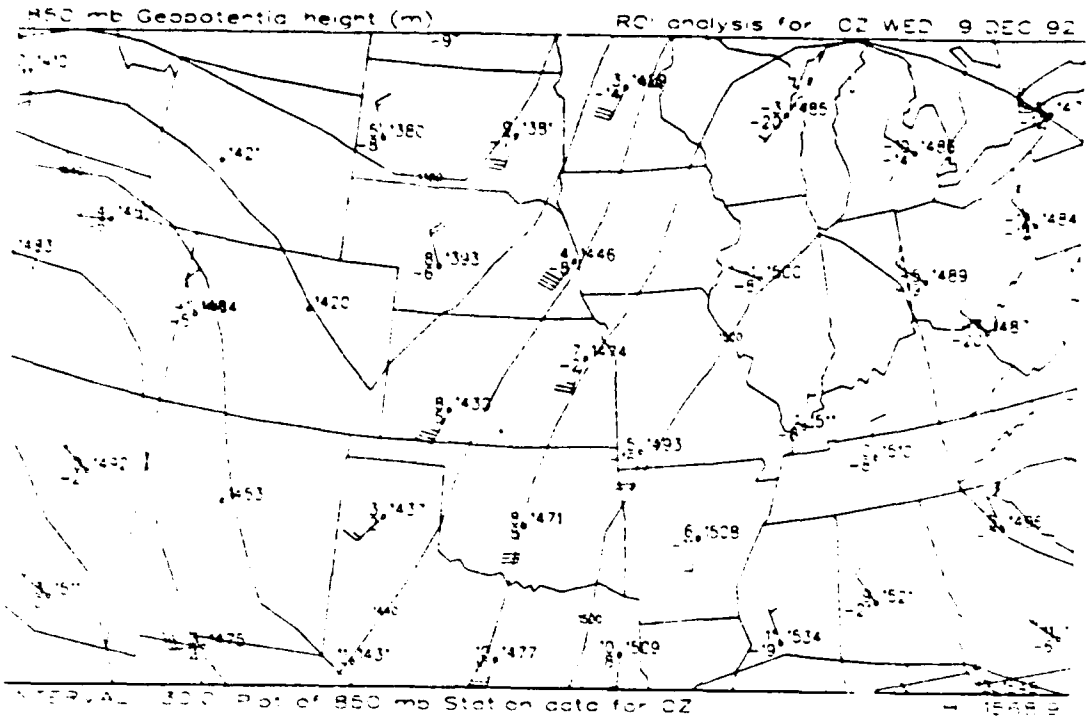

Figure 123: 850 mb weather map and height analysis for 00 UTC 9 December 1992.

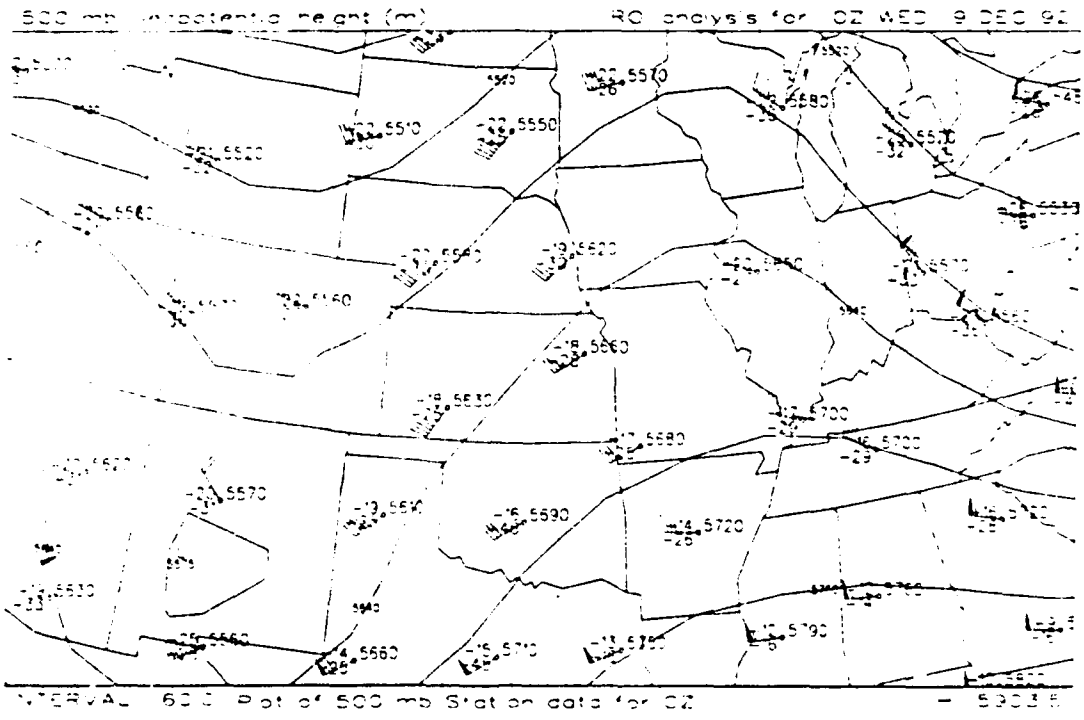

Figure 124: 500 mb weather map and height analysis for 00 UTC 9 December 1992.

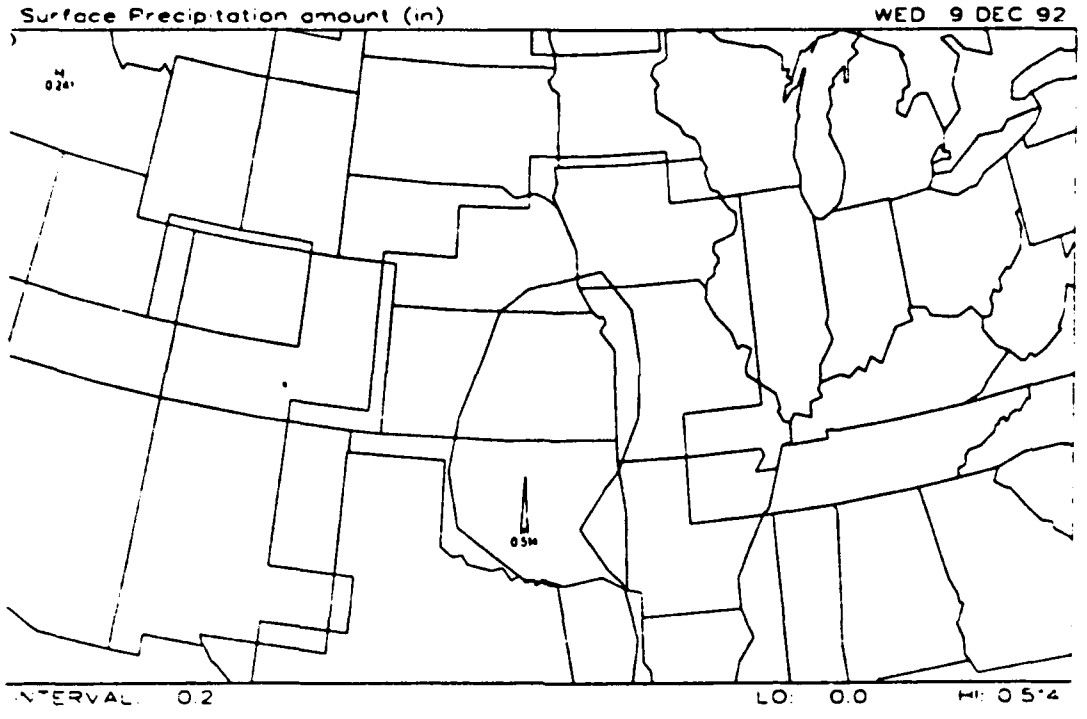

Figure 125: NGM 00 UTC 9 December 1992 forecast of 6-hour accumulated precipitation, valid 12 UTC 9 December 1992.

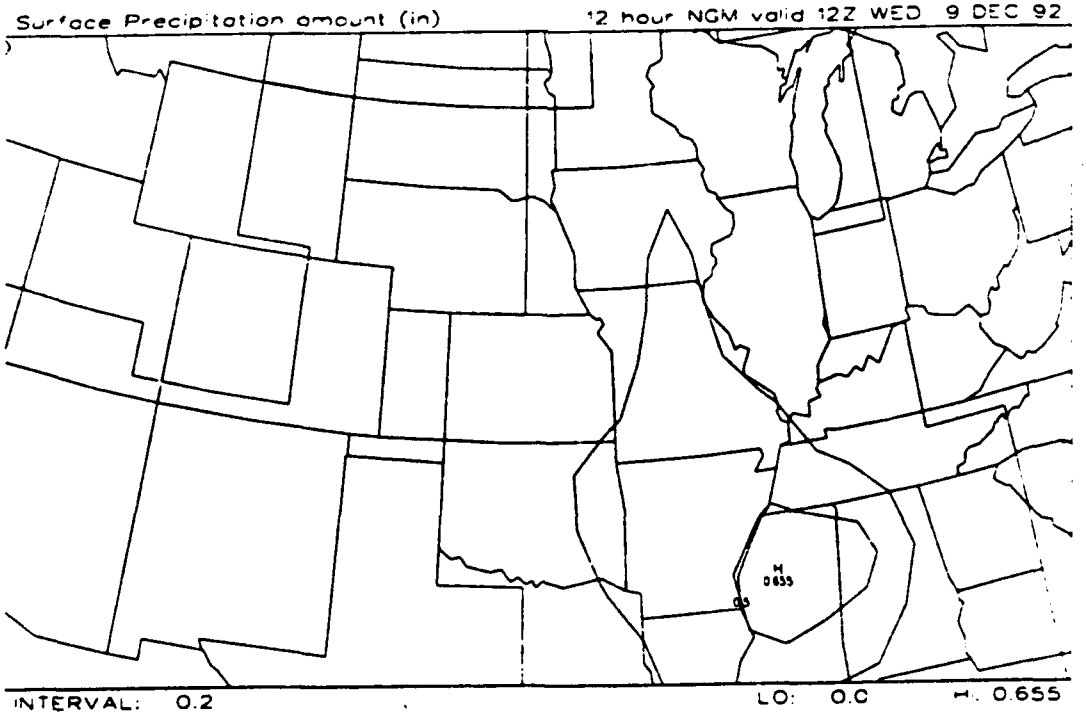

Figure 126: NGM 00 UTC 9 December 1992 forecast of 6-hour accumulated precipitation, valid 06 UTC 9 December 1992.

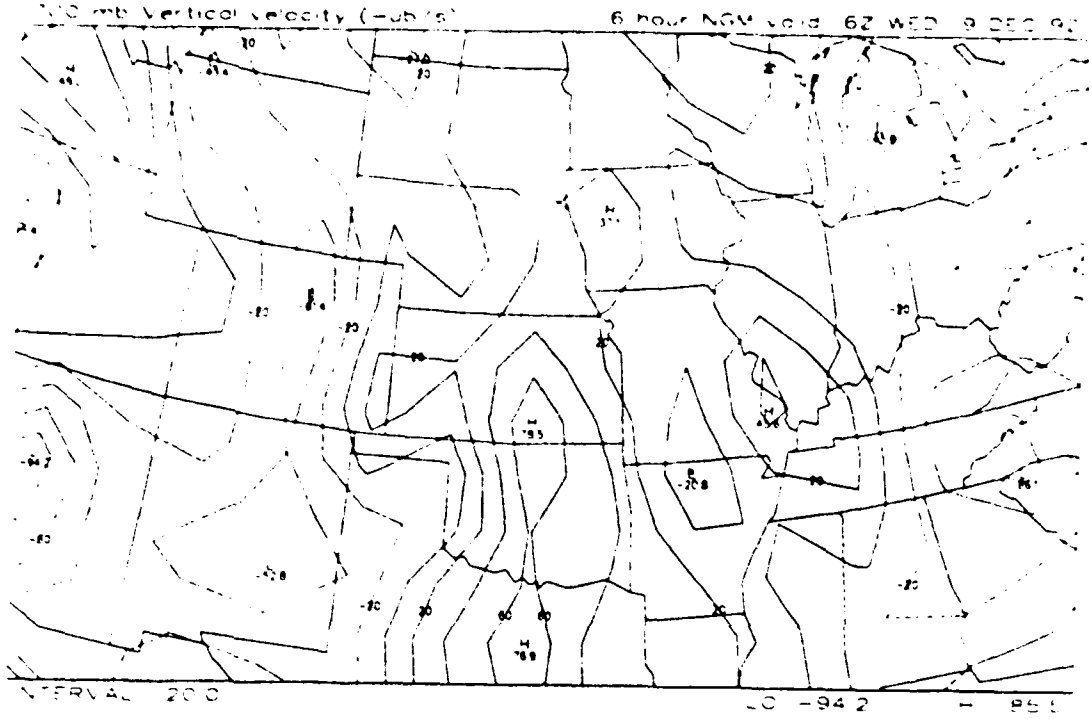

Figure 127: NGM 00 UTC 9 December 1992 forecast of 700 mb vertical velocity (10^{-1} μb/s, or mm/s); valid 06 UTC 9 December 1992.

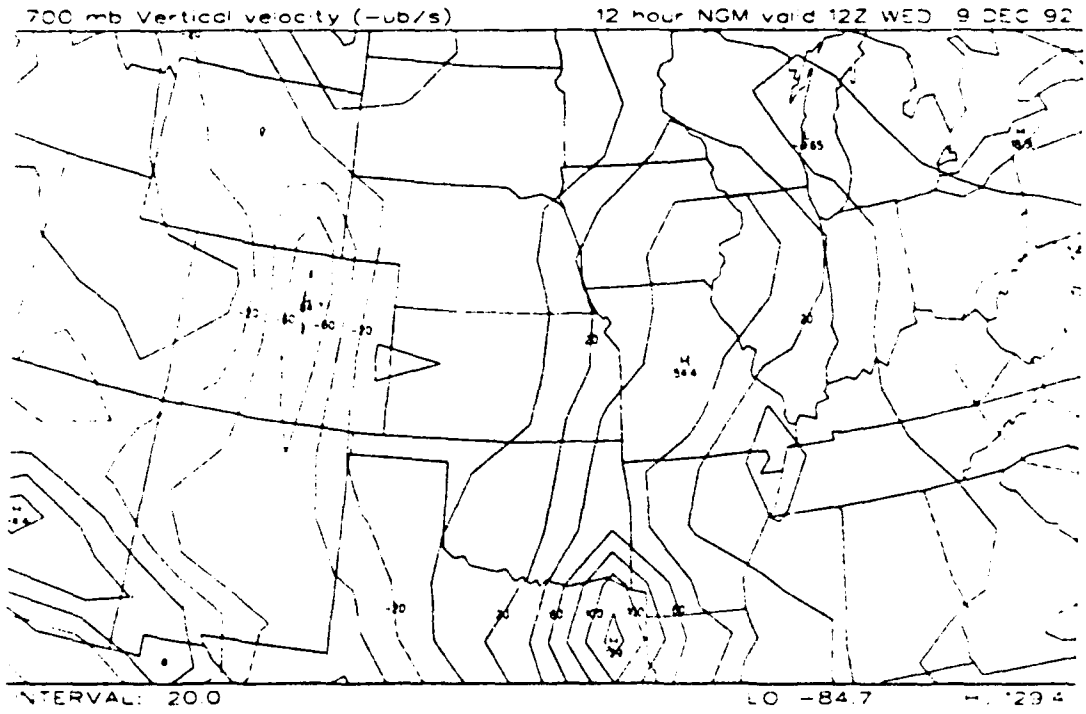

Figure 128: NGM 00 UTC 9 December 1992 forecast of 700 mb vertical velocity (10^{-1} μb/s, or mm/s), valid 12 UTC 9 December 1992.

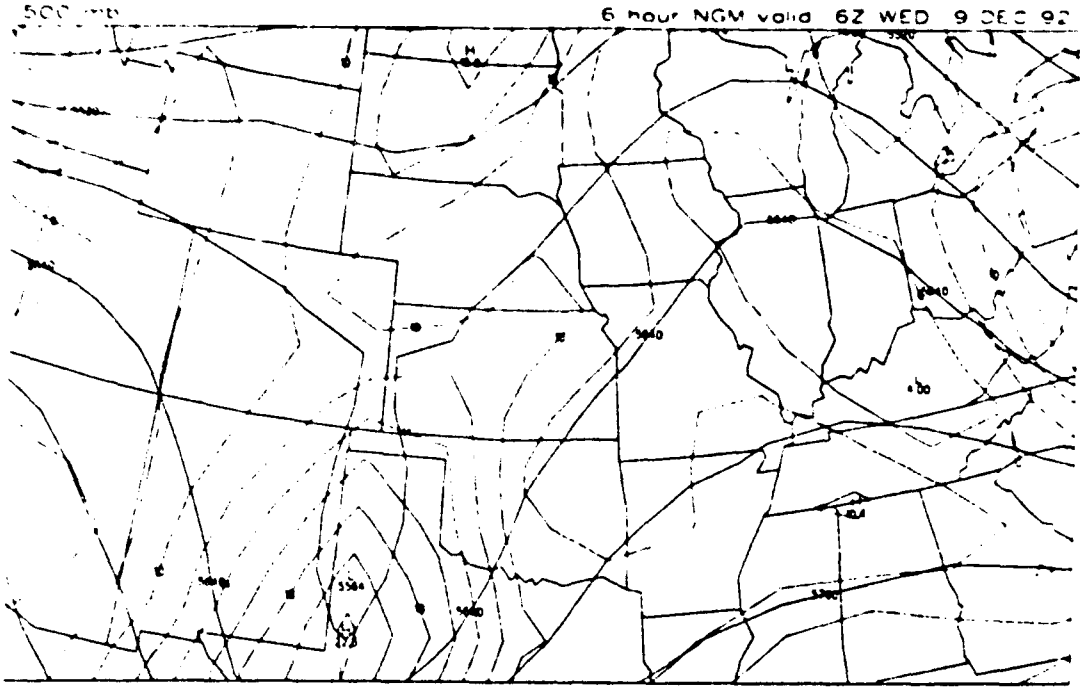

Figure 129: NGM 00 UTC 9 December 1992 forecast of 500 mb height (solid lines) and absolute vorticity (dashed lines), valid 06 UTC 9 December 1992.

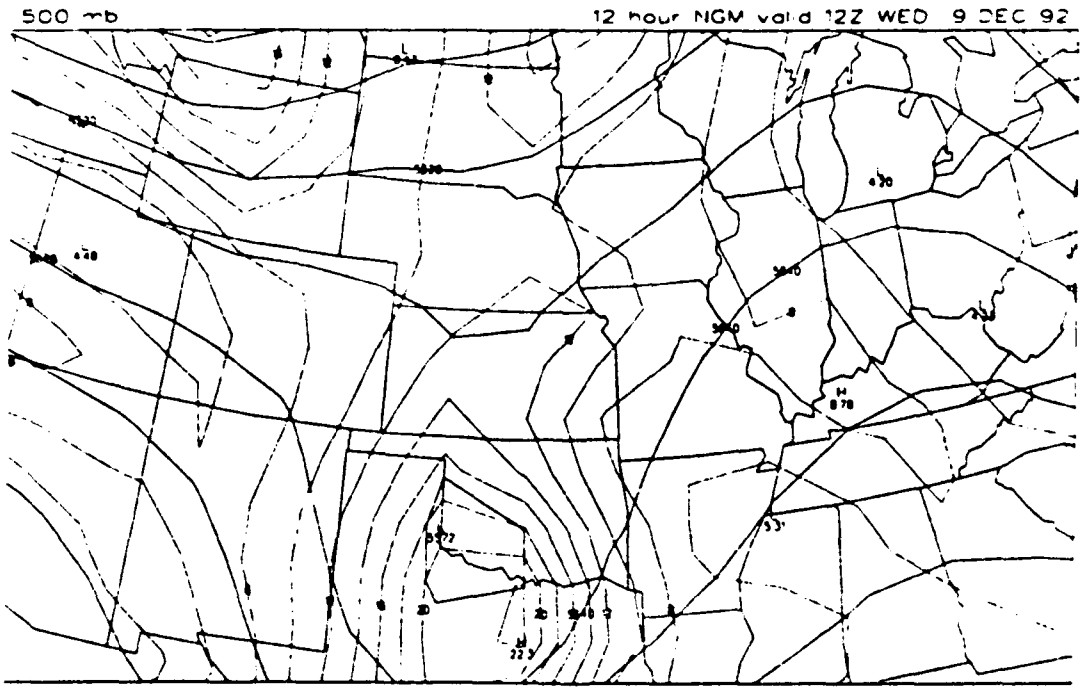

Figure 130: NGM 00 UTC 9 December 1992 forecast of 500 mb height (solid lines) and absolute vorticity (dashed lines), valid 12 UTC 9 December 1992.

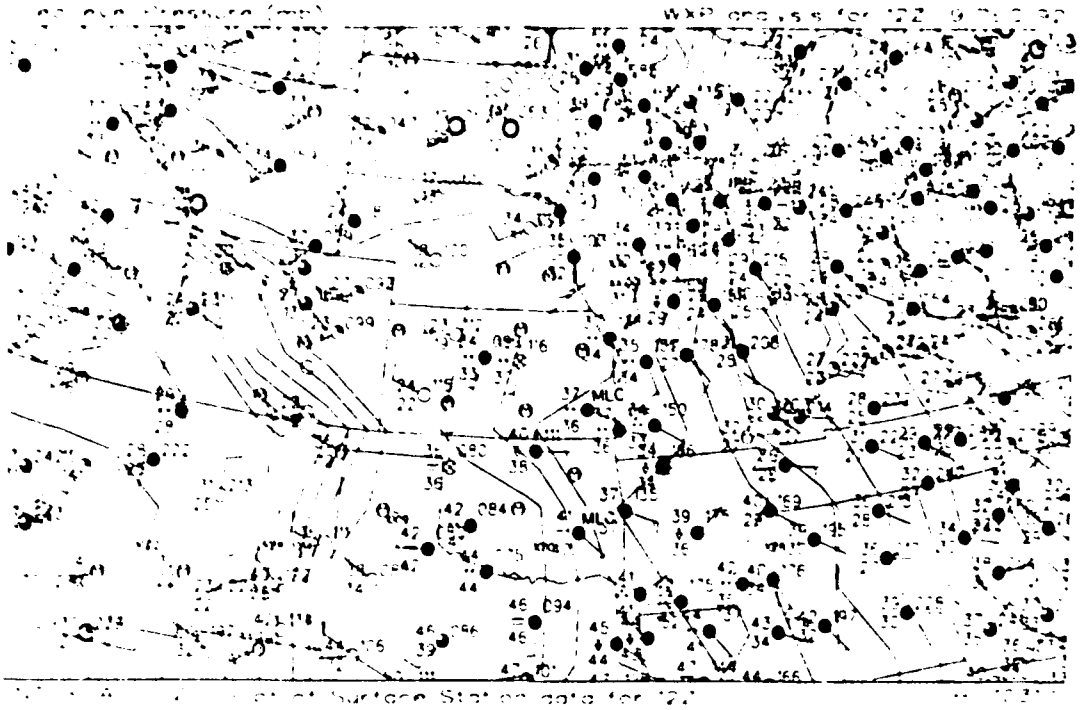

Figure 131: Surface weather map and sea-level pressure analysis for 12 UTC 9 December 1992.

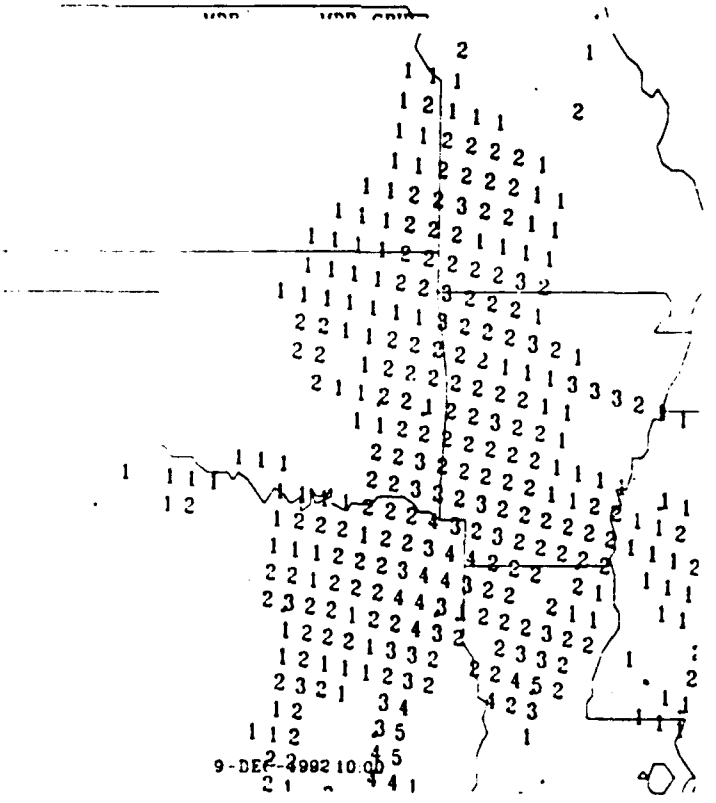

Figure 132: MDR summary for 10 UTC 9 December 1992.

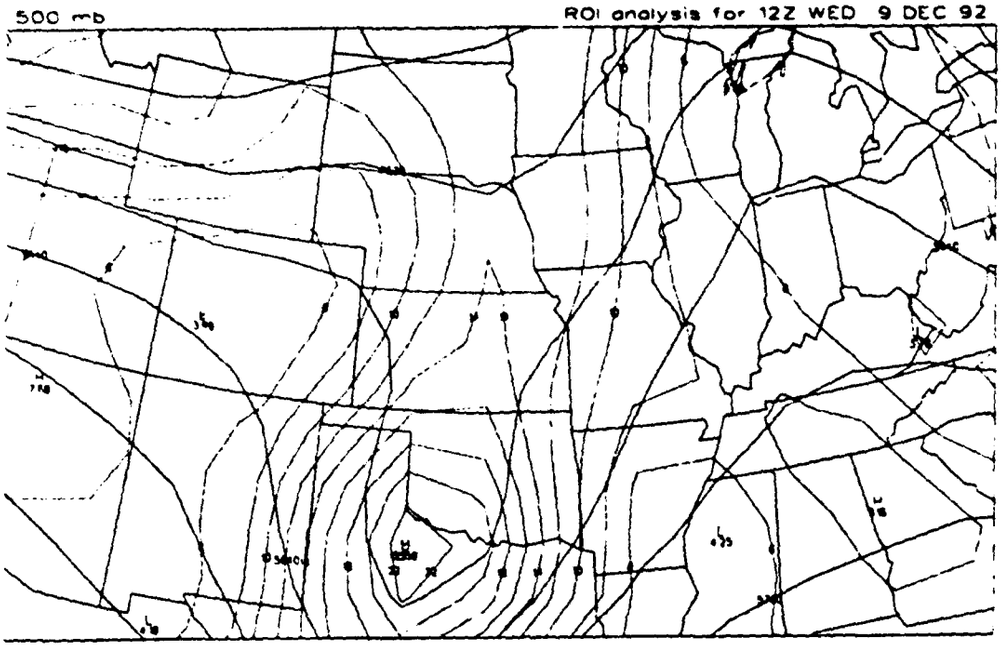

Figure 133: 500 mb analysis of height (solid lines) and absolute vorticity (dashed lines) for 12 UTC 9 December 1992.

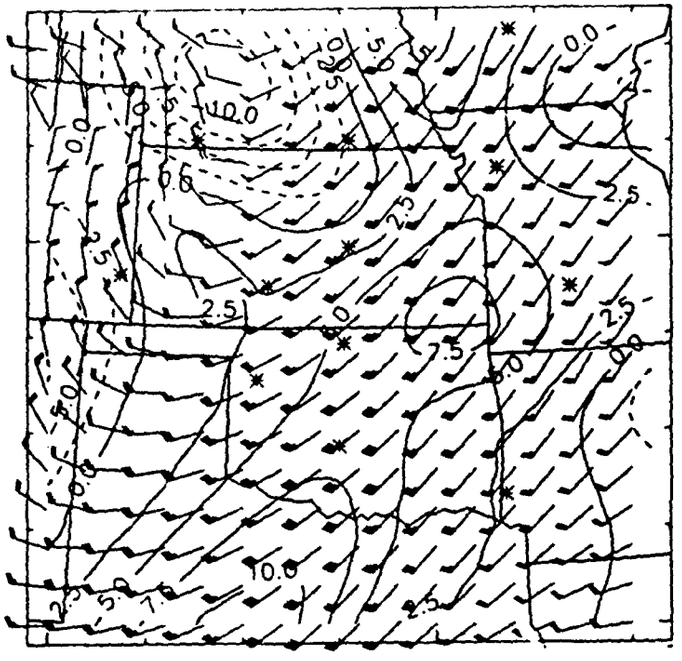

Figure 134: Profiler-derived analysis of winds and integrated vertical velocity (cm/s) at 3000 m for 06 UTC 9 December 1992.

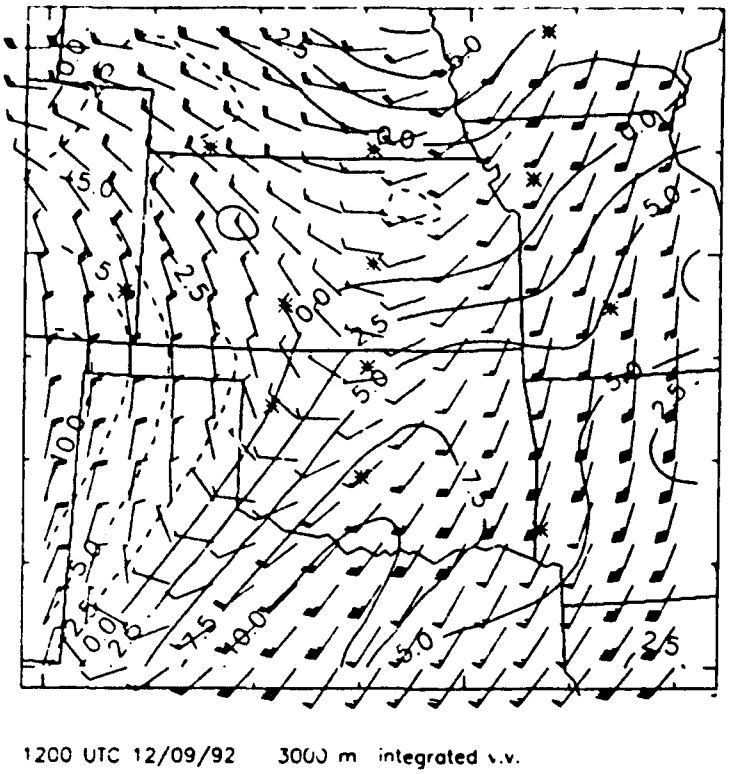

Figure 135: Profiler-derived analysis of winds and integrated vertical velocity (cm/s) at 3000 m for 12 UTC 9 December 1992.

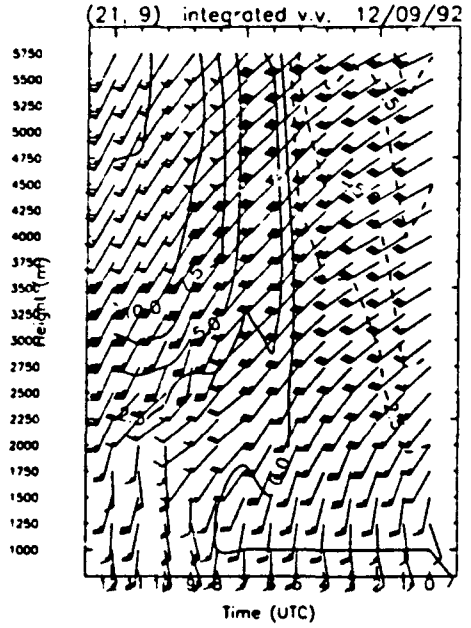

Figure 136: Time-height cross section of profiler-derived winds and integrated vertical velocity (cm/s) for MLC for 00-12 UTC 9 December 1992.

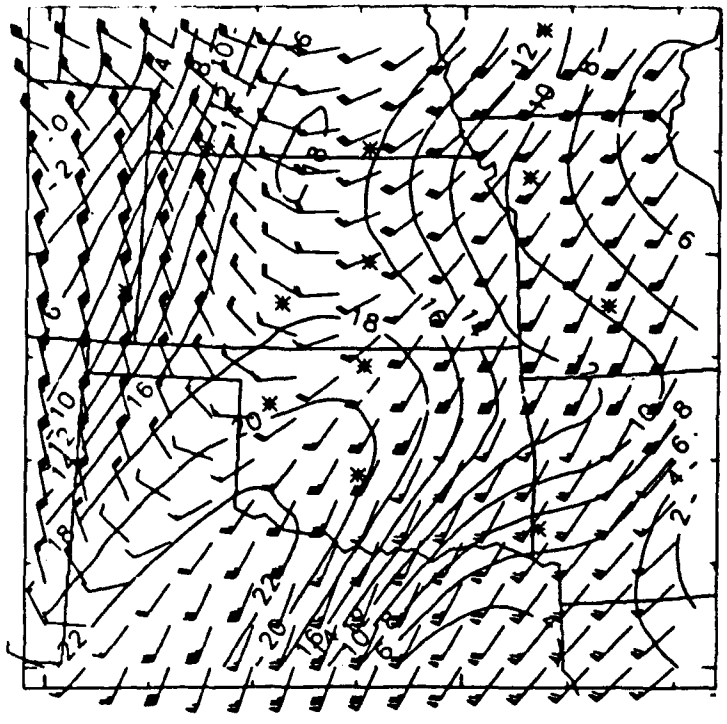

Figure 137: Profiler-derived analysis of winds and absolute vorticity ($10^{-5}s^{-1}$) at 5500 m for 12 UTC 9 December 1992.

3.8. April 24, 1993: Tulsa, Oklahoma tornado

At approximately 2350 UTC 24 April 1993 a strong tornado plowed through eastern Tulsa, Oklahoma (OK), and nearby suburb Catoosa, killing 10 people and injuring 50 (AP 1993). Though the National Severe Storms Forecast Center (NSSFC) had issued tornado watch boxes for the area and chasers from the University of Oklahoma knew enough to be near Tulsa, the tornado still surprised the local citizenry because it and its parent supercell developed quickly and because the tornado was obscured by heavy rain (personal communication, Steven Weygandt 1993). NSSFC discussed their use of profiler data in determining a watch area, but their use was limited to raw profiler data, not on any synthesized analyses or derived products. Considering the isolated nature of this particular storm, wind profiler analyses would prove useful here if it could aid in predicting this narrow area where convection occurred. The case study shows how products derived from the wind analyses could aid in making this forecast.

3.8.1. Standard Meteorological Data Available Before the Storm.

Doppler radar data was not available to us for this case study, but most other standard information was available. Figures 138-139 show surface plots in the OK region for 18 and 23 UTC 24 April 1993. The feature of most interest is the small wave on the cold front, which at 18 UTC stretches from the Texas panhandle to the northeast, crossing through western OK into southeast Kansas (KS). The front is marked by a dramatic wind shift (northerly flow north of the cold front, southerly flow to the south), and a drop in temperatures and dewpoints. The wave moves to the northeast, so at 23 UTC (Figure 139) it is just to the southeast of Tulsa, with the trailing front extending SSW through central OK. 12 UTC 24 April 1993 850, 700, 500, and 300 mb facsimile maps are shown in Figures 140-143. Both 850 mb and 700 mb flow over OK is dominated by a strong southwesterly flow, and the 850 mb air is very dry at Oklahoma City/Norman (OUN) , indicating the elevated mixed layer extends below 850 mb here. The air at 500 mb is relatively cool at OUN; the area to the west is characterized by more cool air extending into New Mexico and an approaching jet streak seen at both 500 and 300 mb. Skew-T's at 12 UTC for OUN (Figure 144), and UMN (Monett, Missouri; Figure 145) showed a difference in the depth of the moist air, which extended only to about 900 mb at OUN and to about 750 mb at UMN. If parcels were able to break through the lid, there was ample convective available potential energy (CAPE) available, as indicated by the negative lifted indices. UMN had CAPE of 998 J kg^{-1} and a -5 lifted index (LI) already at 12 UTC, while OUN similarly had 702 J kg^{-1} and a -2 LI.

Satellite information showed scattered cloudiness over OK. Looping the satellite imagery, through 22 UTC 24 April, no deep convection was evident, but the clouds over OK were moving quickly to the northeast, indicating strong southwesterly winds at cloud level. Ground observers reported towering cumulus with strong tilt during the pre-tornadic time period, but no thunderstorms were obvious, as shown in the 22 UTC GOES IR image (Figure 146 (a)).

The 12 UTC NGM 12-hour forecast maps, valid at 00 UTC 25 April, almost the exact time of the tornado, are shown in Figures 147-150. The NGM forecast maps give hints of conditions favorable for severe thunderstorm development; at 00 UTC 25 April a 500 mb vorticity maximum is quickly approaching from the west,

and there is a surface low in central Oklahoma with a warm front draped northeast from the low, toward another low in upper Michigan. There is also a local 700 mb vertical velocity maximum in north central OK. The precipitation forecast, however, did not indicate much rainfall through 00 UTC. A forecaster might take this as a hint of the inability for convection to penetrate the lid on this day.

3.8.2. Information Available During and After the Storm.

The isolated thunderstorm spawning the tornado is obvious in the GOES imagery. Figures 146 (b) - (d) show IR imagery for 23 UTC 24 April 1993 and for 00 and 01 UTC 25 April 1993. The satellite data show the rapid development of a thunderstorm in northeastern Oklahoma and the quick spread of the anvil.

3.8.3. Utility of the Profiler Data.

One of the obvious uses of the profiler analyses is to compare the vorticity as derived from the profiler network to the NGM fields. The software can animate a time series of the analyses, both for horizontal and vertical cross sections, showing the hour-by-hour movement of vorticity. Horizontal plots of absolute vorticity at 5500 m (approximately 500 mb) derived from the profilers are shown in Figures 151 (a) - (b) for 21 and 23 UTC 24 April 1993, respectively. As shown, there is a concentrated vorticity maximum in western KS moving east, with a broad area of positive vorticity advection ahead of this maximum. Assuming less vorticity advection below, by quasigeostrophic theory this area should have strong upward motion. This seems to be in agreement with the NGM's 700 mb vertical velocity forecast for 00 UTC 25 April (Figure 150), which shows north central OK experiencing the strongest upward motion. Thus, from both profilers and numerical forecasts, at first glance eastern OK and Tulsa does not appear to be at the center of strongest upward motion; the area further west and north does. However, Figure 152 (a) - (b) show cross sections of vertical velocities at 21 and 23 UTC derived from the divergence equation and taken along the dashed line in Figure 151. Tulsa is marked with a dot on Figure 143, and a "T" on Figure 144. As shown in Figure 144, there is a localized *lower-tropospheric* maximum of vertical velocity over eastern OK at approximately the elevation of the lid. This may have been key to forecasting this event; since the entire Oklahoma area was strongly capped, the area (eastern OK) with stronger upward motion at the level

of the cap was more likely to experience penetrative convection. Further evidence for the sustained, localized nature of the upward motion at lid elevation can be seen by examining the horizontal plots of 700 mb vertical velocity for 2000 -2300 UTC 24 April, shown in Figure 153 (a) - (d), respectively. In each of the plots, eastern OK is again experiencing the strongest upward motion of any of the areas along the frontal zone. The consistency of upward motion from hour to hour in eastern OK and its slight southeastward displacement from the NGM forecast position should indicate to the forecaster this area could preferentially break through the lid and develop deep convection, especially the area in eastern OK along the front.

This analysis was aided by hindsight, but even so, a talented forecaster may well have found supplemental evidence in the profiler network analyses to indicate severe weather potential and narrow down the tornado watch area to a smaller area.

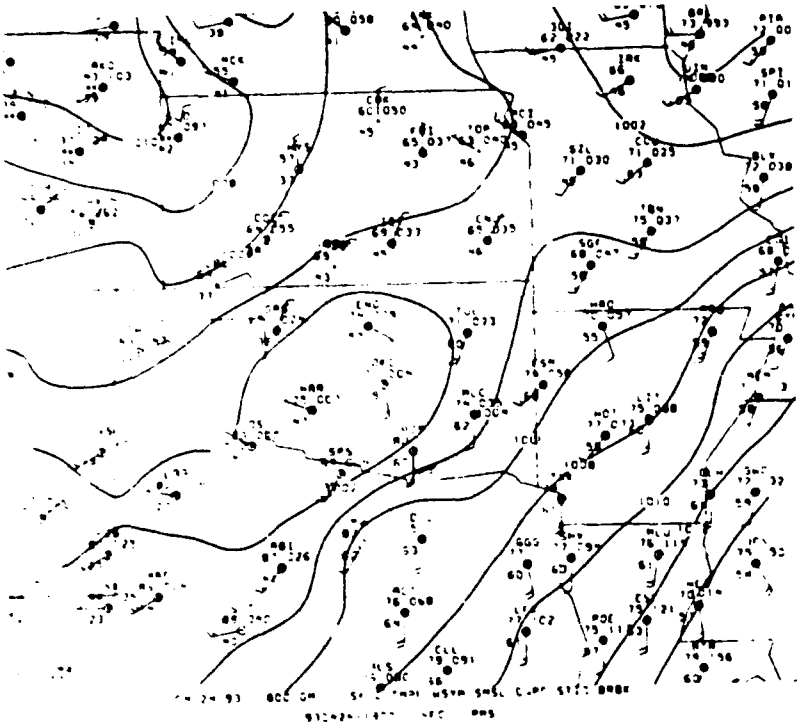

Figure 138: Surface plot for 1800 UTC 24 April 1993. Winds are shown by full barb (~5 ms^{-1}) and half barb (~2.5 ms^{-1}).

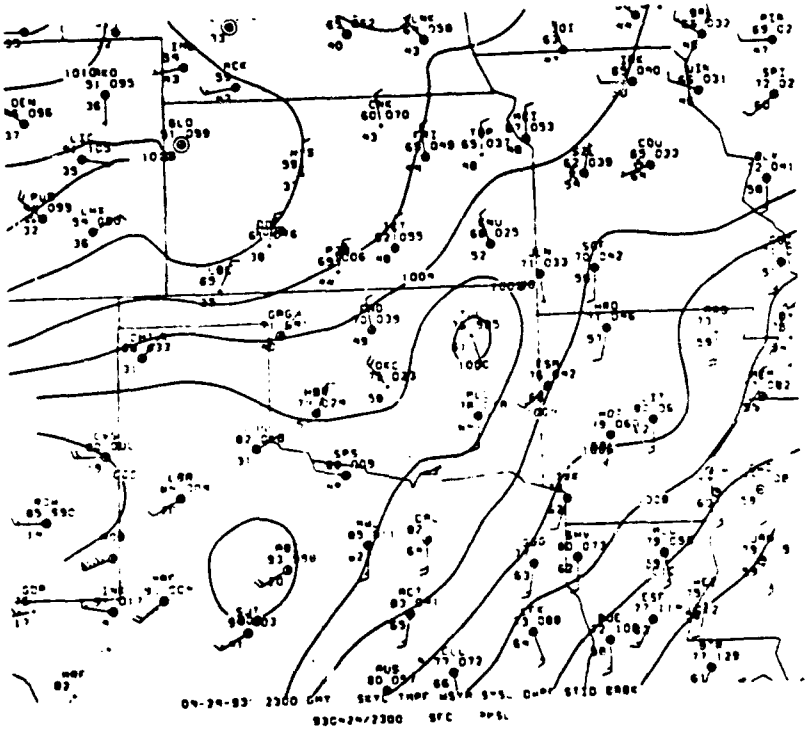

Figure 139: Surface plot for 2300 UTC 24 April 1993.

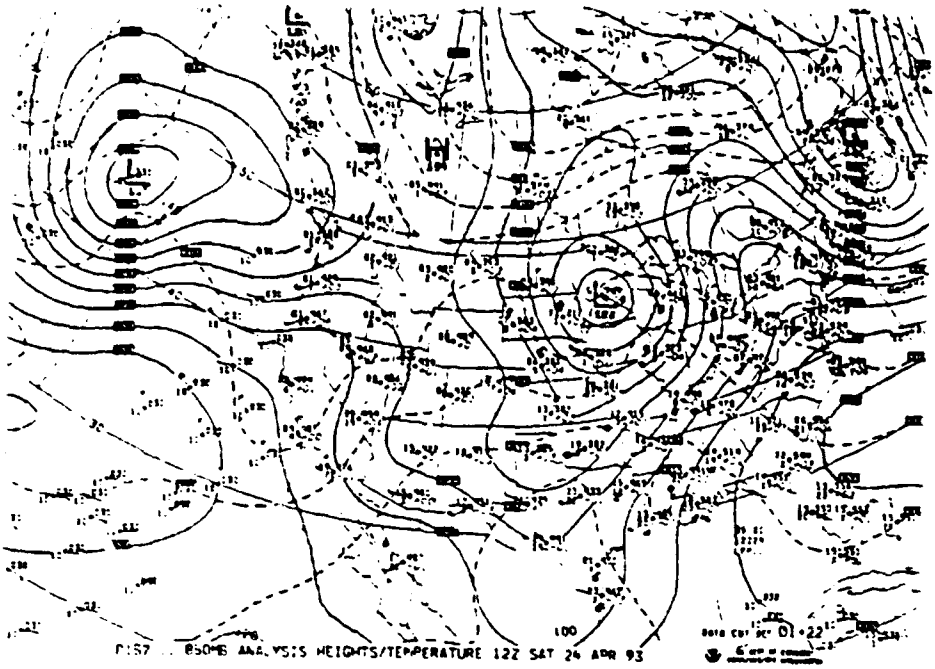

Figure 140: 1200 UTC 24 April 1993 850 mb geopotential height and temperature analysis.

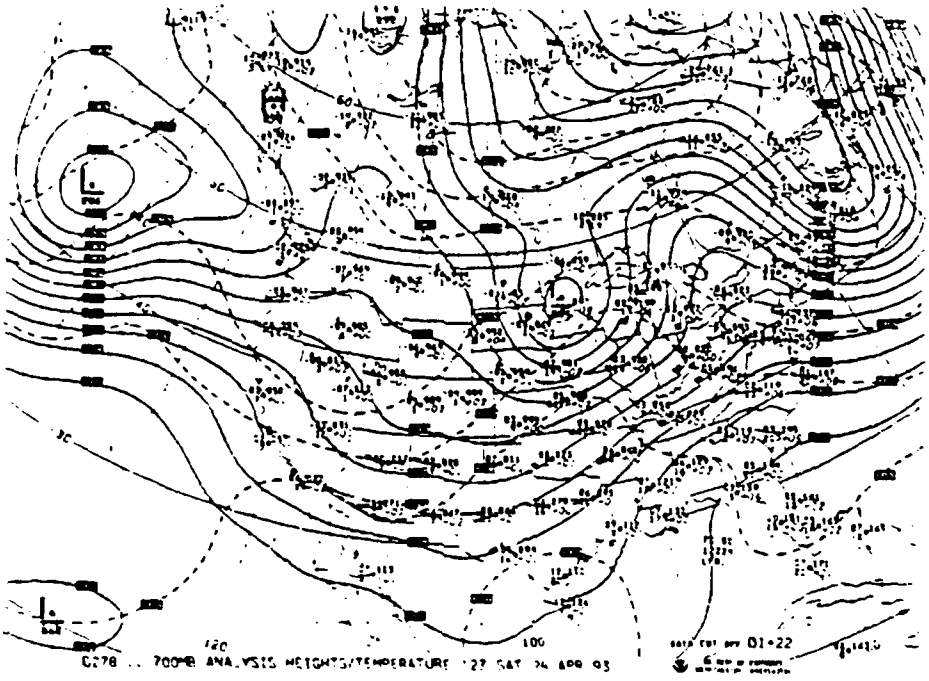

Figure 141: 1200 UTC 24 April 1993 700 mb geopotential height and temperature analysis.

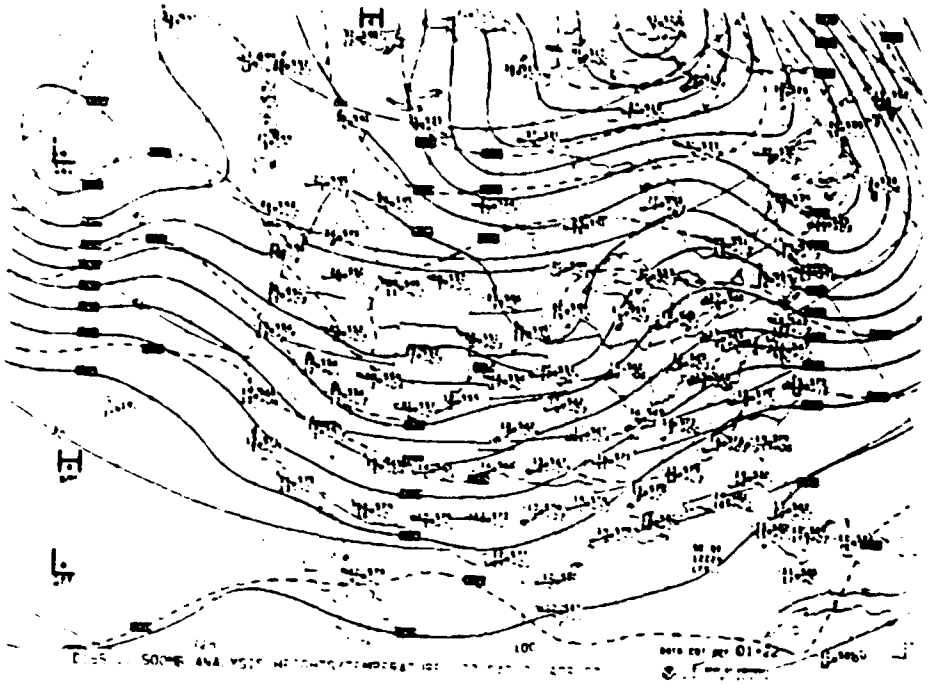

Figure 142: 1200 UTC 24 April 1993 500 mb geopotential height and temperature analysis.

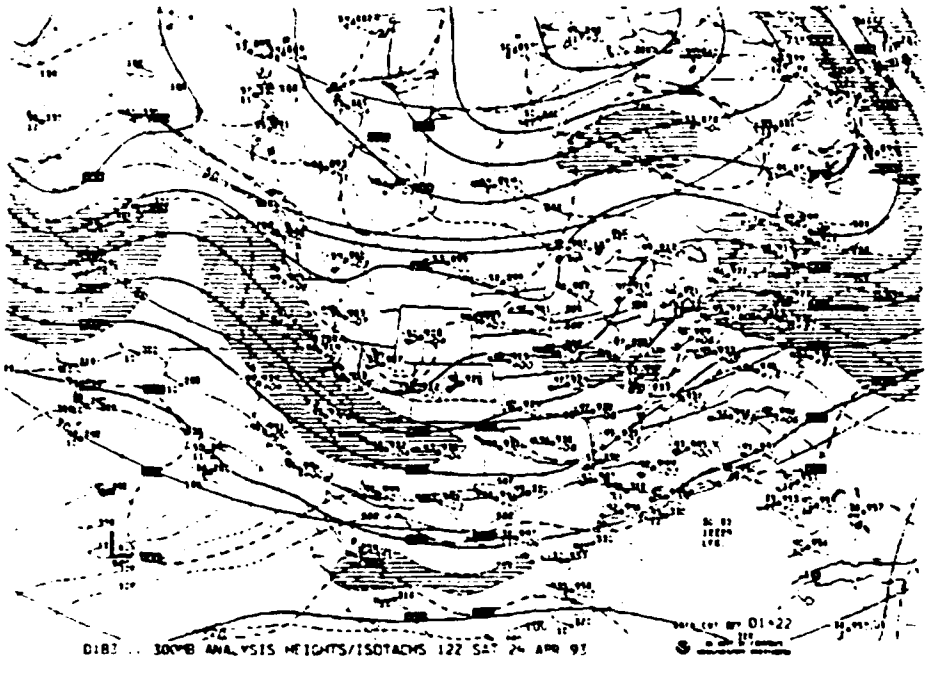

Figure 143: 1200 UTC 24 April 1993 300 mb geopotential height and temperature analysis.

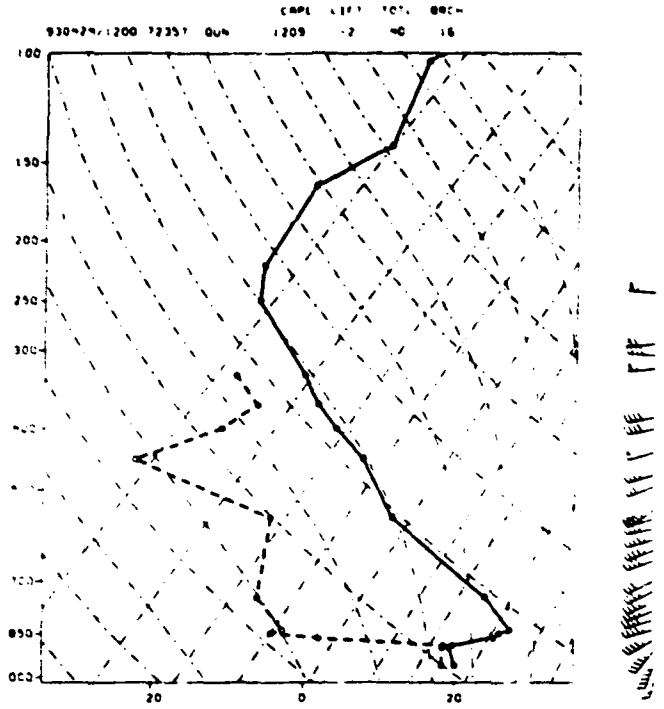

Figure 144: 1200 UTC 24 April 1993 Skew-T plot for Norman, OK.

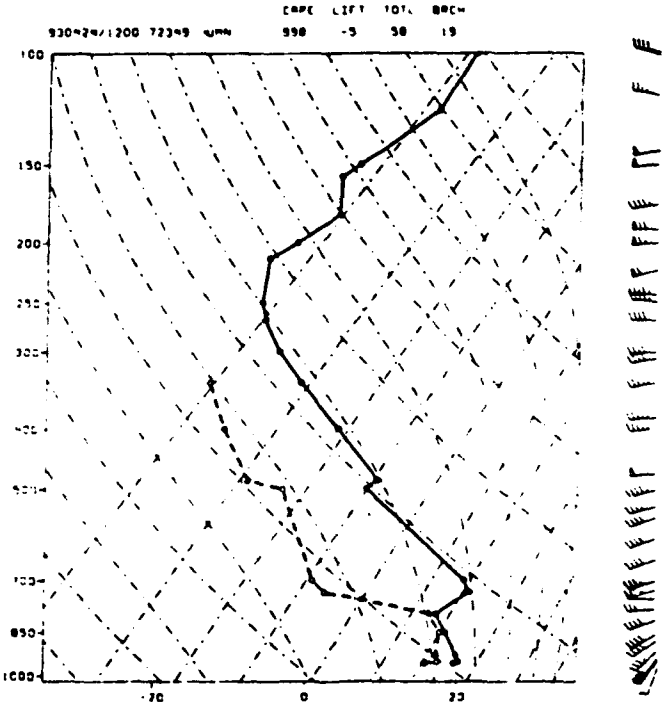

Figure 145: 1200 UTC 24 April 1993 Skew-T plot for Monett, MO.

(a)

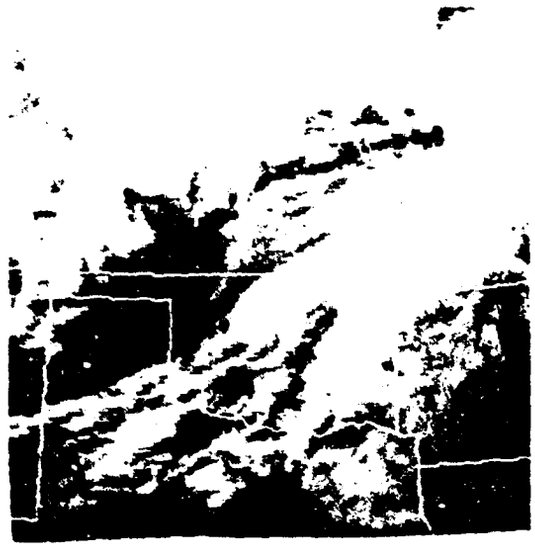

(b)

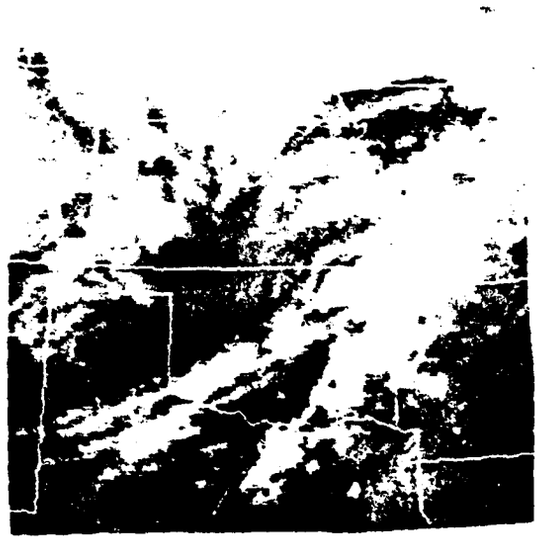

Figure 146: Remapped GOES IR imagery valid at (a) 2200 UTC 24 April 1993; (b) 2300 UTC 24 April 1993; (c) 0000 UTC 25 April 1993; (d) 0100 UTC 25 April 1993.

(c)

(d)

Figure 146 (continued): Remapped GOES IR imagery valid at (a) 2200 UTC 24 April 1993; (b) 2300 UTC 24 April 1993; (c) 0000 UTC 25 April 1993; (d) 0100 UTC 25 April 1993.

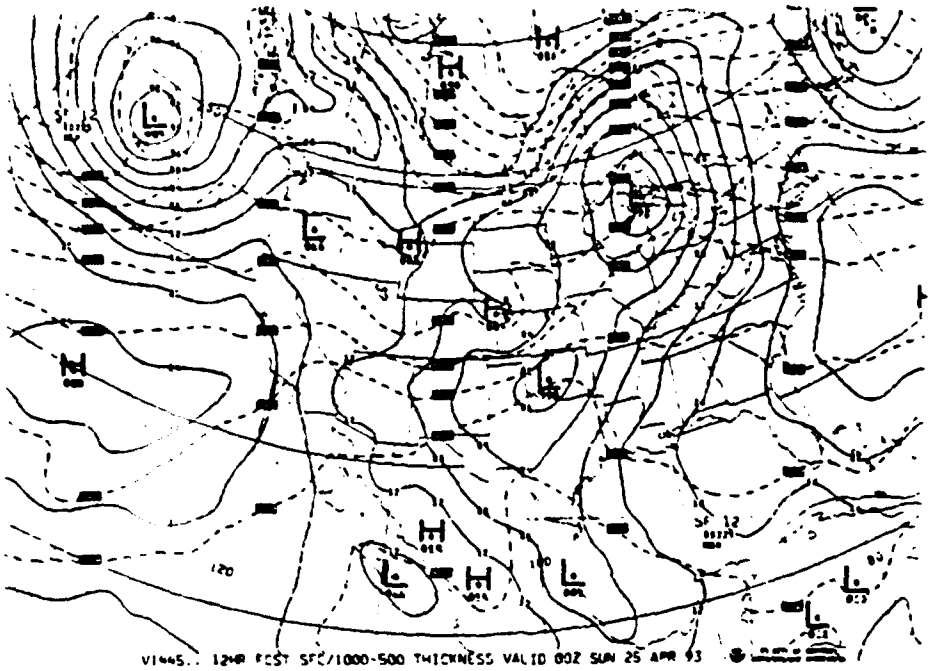

Figure 147: 12-hour NGM forecast of surface pressure and 1000-500 mb thickness valid at 0000 UTC 25 April 1993.

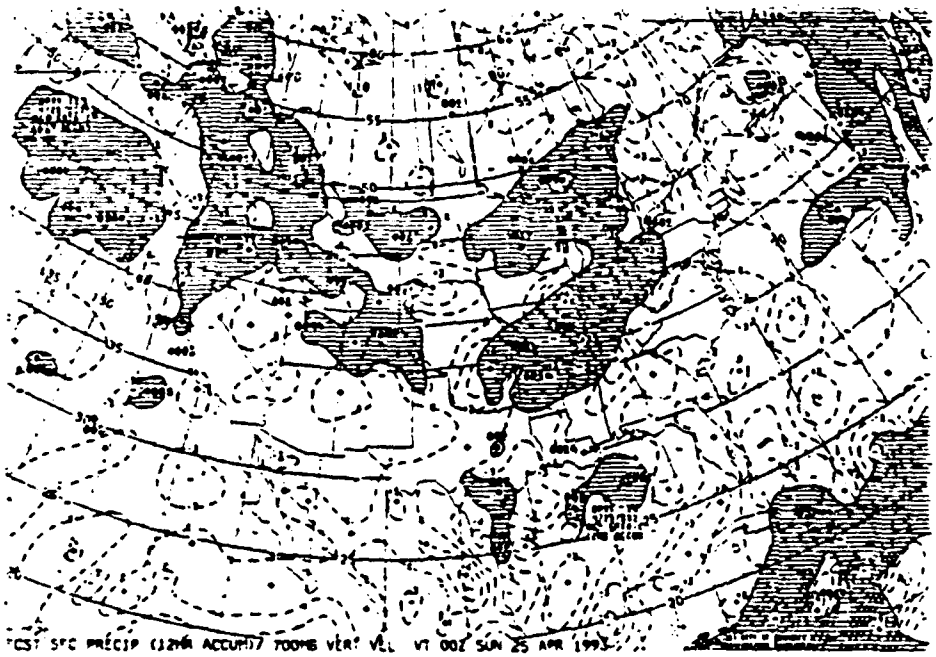

*Figure 148: 12-hour NGM forecast of vertical velocity (μP/s) and precipitation amount (inches*100) valid at 0000 UTC 25 April 1993.*

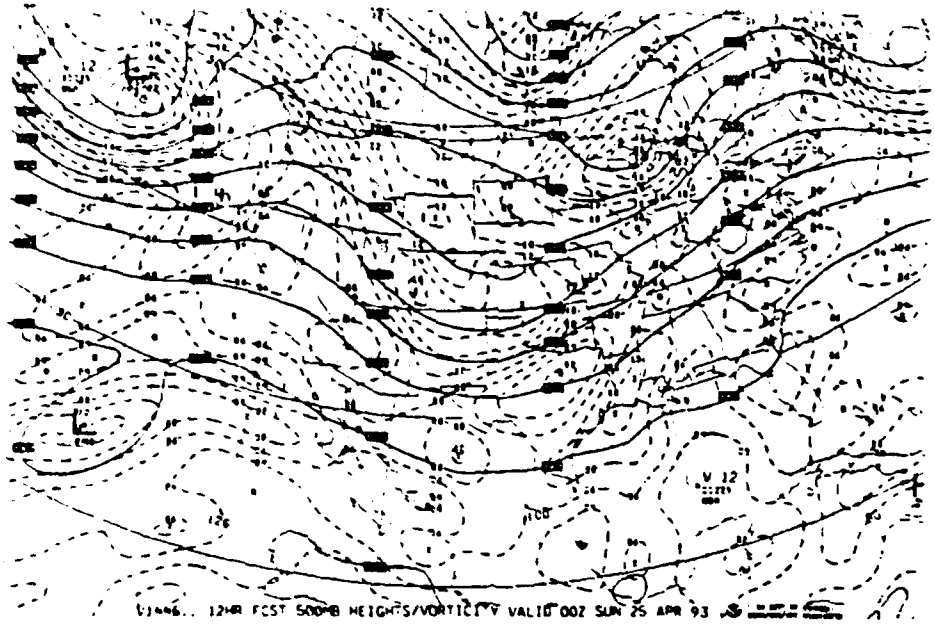

*Figure 149: 12-hour NGM forecast of 500 mb geopotential heights (dm) and absolute vorticity (sec-1*10^5) valid at 0000 UTC 25 April 1993.*

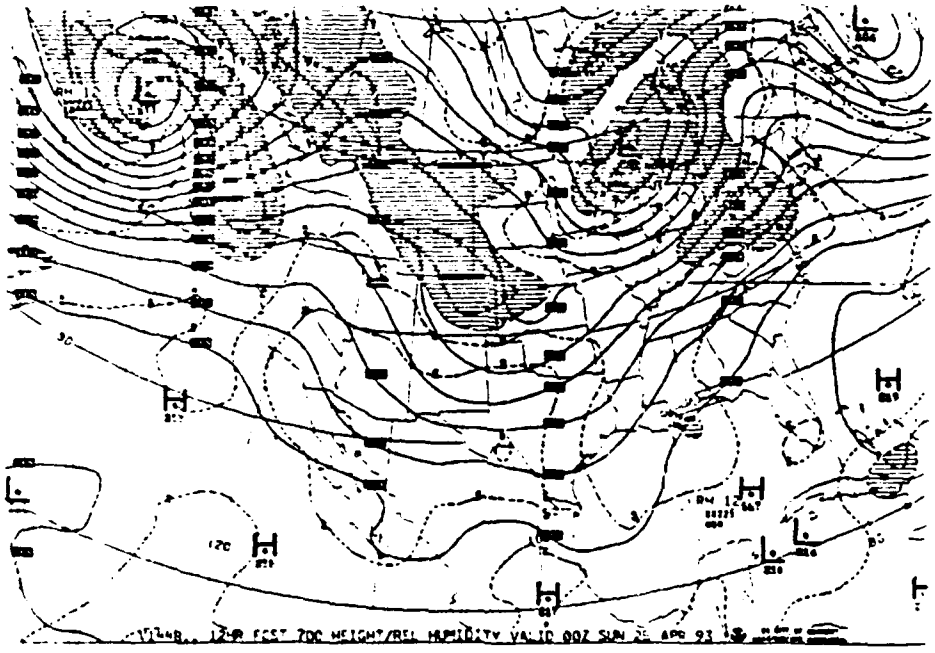

Figure 150: 12-hour NGM forecast of 700 mb geopotential heights (dm) and relative humidity (percent) valid at 0000 UTC 25 April 1993.

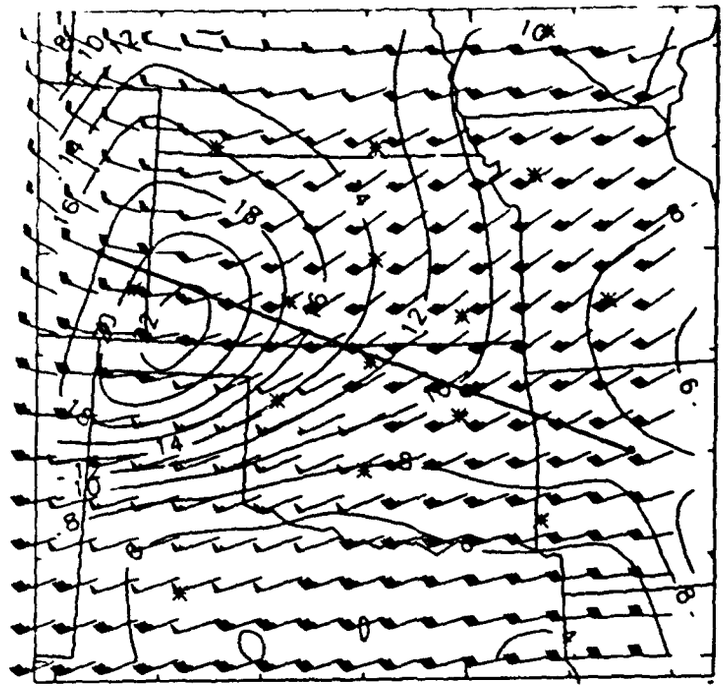

a)

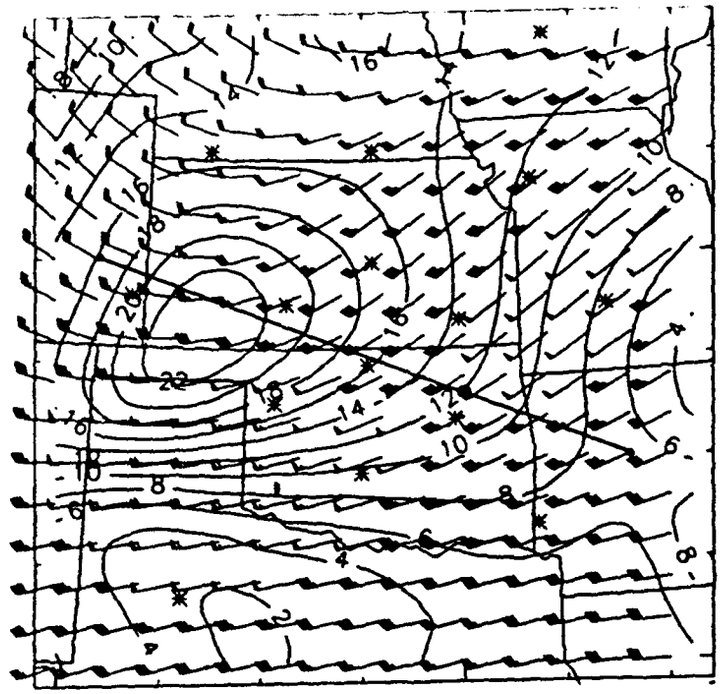

b)

Figure 151: Profiler network analysis horizontal plot of absolute vorticity (10^5 s^{-1}*) data at 5500 m, or approximately 500 mb, at: (a) 2100 UTC 24 April 1993; (b) 2300 UTC 24 April 1993. Line indicates location of cross section in Figure 144.*

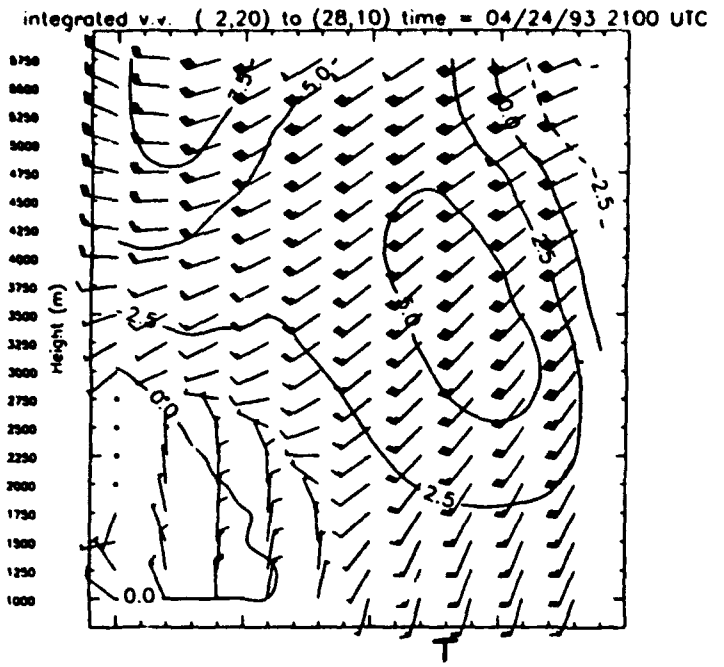

a)

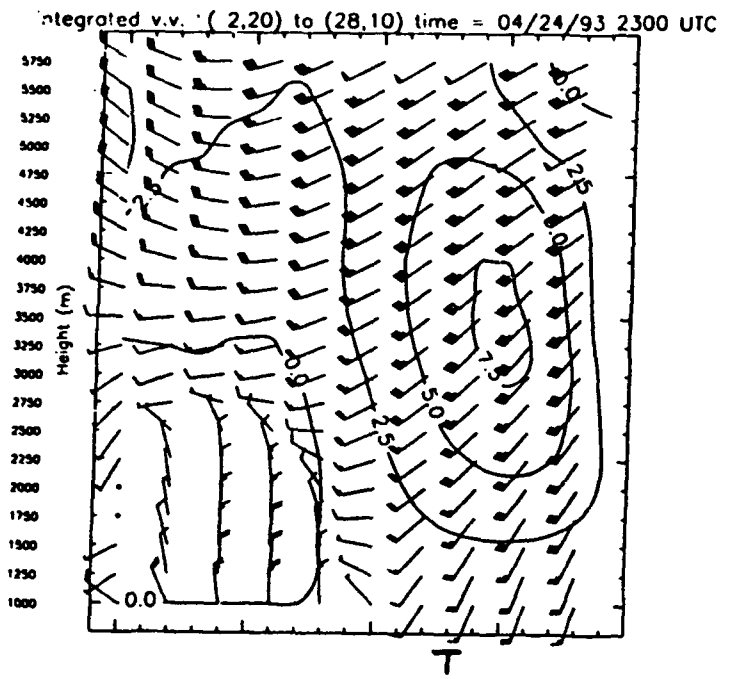

b)

Figure 152: Vertical cross section along line in Figure 151 of vertical velocities in cm s^{-1} calculated from integrating the divergence equation. (a) 2100 UTC 24 April 1993; (b) 2300 UTC 24 April 1993.

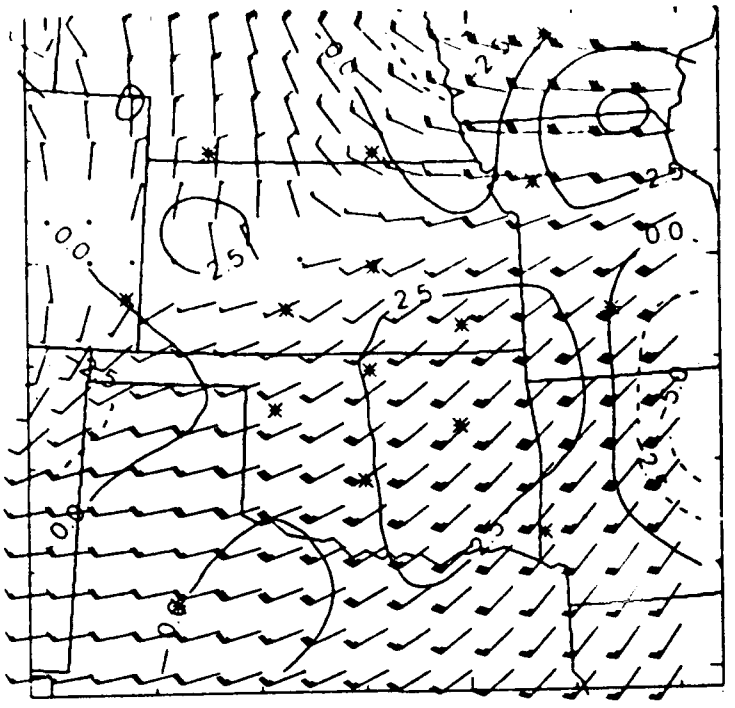

a)

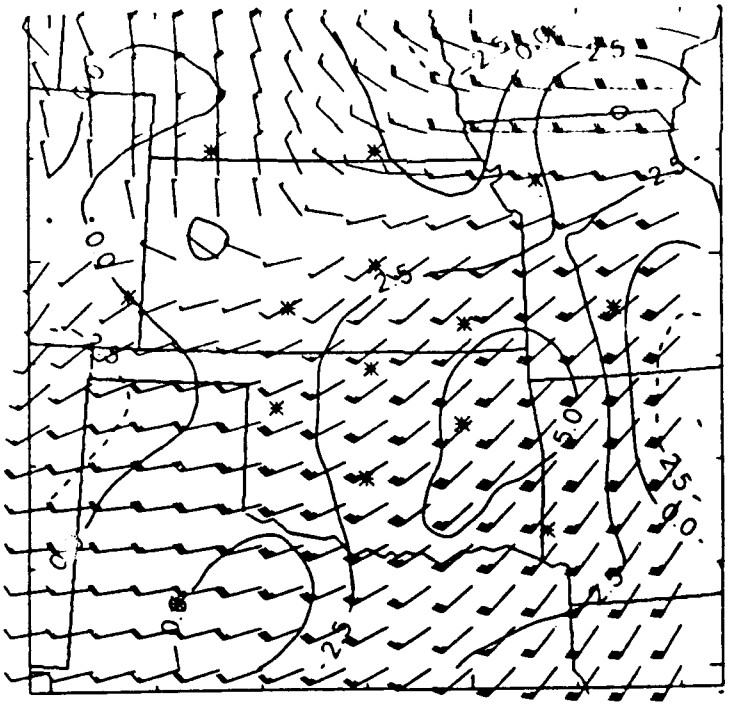

b)

Figure 153: Profiler network analysis horizontal plot of vertical velocity data at 3000 m for (a) 2000 UTC 24 April 1993; (b) 2100 UTC; (c) 2200 UTC; (d) 2300 UTC.

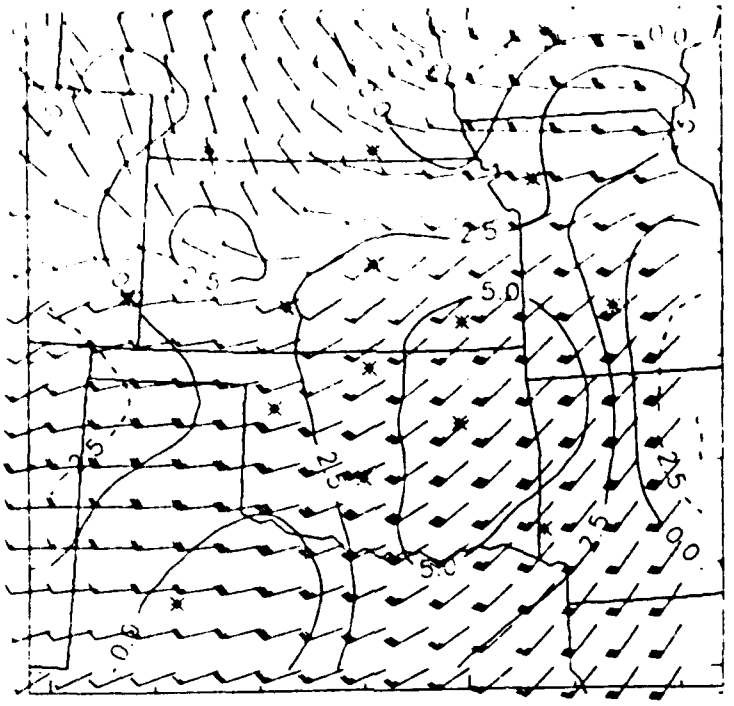

c)

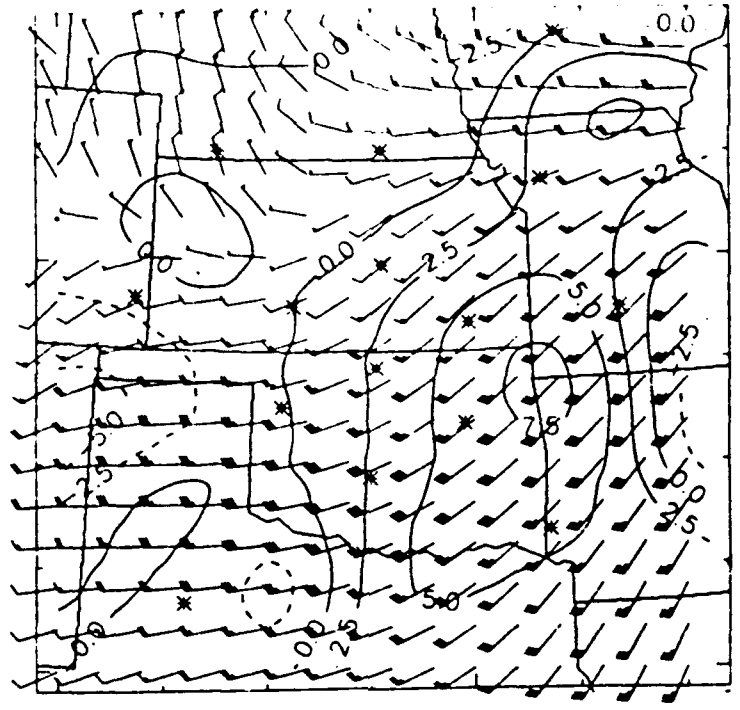

d)

Figure 153 (continued): Profiler network analysis horizontal plot of vertical velocity data at 3000 m for (a) 2000 UTC 24 April 1993; (b) 2100 UTC; (c) 2200 UTC; (d) 2300 UTC.

4. Summary and Conclusions

Software was developed to produce hourly analyses of the horizontal and directly measured vertical wind fields at several levels in the atmosphere, using data from the wind profiler demonstration network in the central US. A standard Barnes analysis was used to produce gridded wind fields from the profiler data. A first guess field was used in the analysis, consisting of the horizontal mean wind (for the first analysis in a cycle), or the previous hour's analysis (for subsequent analysis times); input data were subjected to a quality control step (beyond the quality control performed by the profiler data producers), consisting of a gross error and buddy check. Analysis parameters were chosen based on estimates of the statistics of the analysis increments. The analyzed wind field could be displayed along with kinematic quantities (vorticity, horizontal divergence, integrated vertical velocity, thermal wind, horizontal advection of various quantities) derived from the analyses. Display software allowed for looping of horizontal or vertical cross-sections, and display of time-height cross sections at any analysis grid point. Additional display software also allowed examination of the raw profiler data used in the analyses.

The utility of the profiler data, and profiler derived analyses, for short-term forecasting has been demonstrated in the case studies presented in the previous section. A total of eight case studies have been performed, covering a wide range of atmospheric conditions: two MCCs (26 July and 4 August 1992); several cases with convective and stratiform rain associated with upper level troughs (26 July 1992), dry lines (9 March 1992), cold fronts (26 July, 4 August, and 7 October 1992), and occluded fronts (9 December 1992); one case of an isolated, tornado-producing thunderstorm (24 April 1993); and two snowstorm cases (24 and 25 November 1992). The dynamic forcing ranged from weak flow to strong, deepening baroclinic systems.

In 6 of the 8 case studies, profiler data were useful in identifying forecast errors of the NGM guidance after 6 hours into the forecast, when conventional radiosonde data were not available. In two of those cases (9 March and 25 November 1992), the developing forecast errors could be identified after only 3 hours into the forecast, and in two others (7 October and 24 November 1992) this might have been possible if 3-hour forecast fields had been available. In one case

(24 April 1993), profiler data helped narrow down a broad area of upward motion where convection was most likely to occur. In only one case (9 December 1992), errors in the NGM precipitation forecasts could not be identified in the comparison of forecasted and profiler analyzed wind fields.

The analyzed fields of the horizontal profiler winds were found to be in general agreement with radiosonde observations (when available). The directly measured vertical velocity was strongly influenced by the fall velocity of precipitation, and is thus somewhat hard to interpret. Among the derived quantities, the low-level (e.g., 700 mb) vertical velocity derived from the horizontal convergence fields was found to be particularly useful in identifying areas of large scale forcing for stratiform precipitation, and areas of destabilization and enhanced convection. A direct correspondence between precipitation intensity and diagnosed ascent could be established in a number of cases, although there were also some cases in which this relationship did not hold because of other factors. The quasi-geostrophic forcing could be identified in a number of cases in displays of the mid-tropospheric wind and vorticity fields, and low-level geostrophic temperature advection. Areas of differential temperature advection, and corresponding stabilization or destabilization, could be identified, although vertical profiles of the geostrophic temperature advection were found to be somewhat noisy. Another limitation of the analysis technique was found in cases of sparse data coverage (at the edge of the network, or in cases of missing data), where small scale features of the analysis are suspect; we also identified one instance where analyzed fields departed from the input data due to erroneous rejection of good data. Thus, it is important to examine not only the analyses, but also the raw data used in the analyses.

The selection of cases for this study was hampered by several factors that would not be applicable to operational forecast offices. For several potential cases, sufficient conventional data were not available to us because of logistical problems. In addition, profiler data from the demonstration network during 1992, and the early part of 1993, suffered from several hardware problems that caused large data gaps, and resulted in only partial coverage of the network. As discussed in the previous section, the data gaps led to unreliable analyses over parts of the domain in some of the cases. The operational reliability of the wind

profilers has much improved since then (van de Kamp, 1993), thus alleviating many of the problems we encountered in our study.

There is an important caveat that applies to the results of our study in the context of a real-time forecasting environment: all our analyses had the benefit of hindsight - no attempt was made to simulate the situation in a forecast office. A rigorous proof of the utility of profiler data for forecasting, and a quantification of its effect on forecast skill, would require a comparison of forecasts issued with and without profiler data under otherwise identical conditions. Since there are a number of factors that influence the forecast quality (details of the data display, time pressures, experience of the individual forecasters, and effects of "information overload"), design and evaluation of such a forecast experiment is not an easy task (Heideman et al., 1991). However, we feel that even the qualitative conclusions reached from our case studies make a strong enough case for including profiler data i. the data stream of any forecast office.

Because of the potentially large amount of data available from individual profiler sites, the software we developed for producing and displaying gridded analyses should prove useful. For implementation in an operational environment, some enhancements would be advisable: the user interface should be integrated into whatever user interface is used for other display and analysis products; displays of the input data should be directly superimposed on the analyses, to allow examination of (and possibly interactive changes to) the quality control procedure; for direct comparisons with forecast guidance, display and manipulation on the same grid would be desirable; availability of gridded forecast guidance at more frequent intervals (at least every 3 hours) would be useful for early identification of forecast errors.

5. References

Barnes, S. L., 1964: A technique for maximizing details in numerical weather map analysis. *J. Appl. Meteor.*, **3**, 396-409.

Barnes, S. L., 1973: Mesoscale objective analysis using weighted time series observations. Tech. Memo. No. ERL NSSL-62. NOAA, Norman, OK. 60 pp. [NTIS COM-73-10781]

Bartello, P. and H. L. Mitchell, 1992: A continuous three-dimensional model of short-range forecast error covariances. *Tellus.*, **44A**, 217-235.

Benjamin, S. G., 1989: An isentropic meso α-scale system and its sensitivity to aircraft and surface observations. *Mon. Wea. Rev.*, **117**, 1586-1603.

Benjamin, S. G., K. A. Brewster, R. Brummer, B. J. Jewett, T. W. Schlatter, T. L. Smith and P. R. Stamus, 1991: An isentropic three-hourly data assimilation system using ACARS aircraft observations. *Mon. Wea. Rev.*, **119**, 888-906.

Brady, R. H. and K. A. Brewster, 1989: Profiler training manual #3 - subjective uses of wind profiler data in warm season analysis and forecasting. NOAA/ERL/FSL, Boulder, CO. 103 pp.

Brewster, K. A., 1989: Profiler training manual #2 - quality control of wind profiler data. NOAA/ERL/FSL, Boulder, CO. 39 pp.

Buell, C. E., 1972: Correlation functions for wind and geopotential on isobaric surfaces. *J. Appl. Met.*, **11**, 51-59.

Carlson, C. A., 1987: Kinematic quantities derived from a triangle of VHF doppler wind profilers. M. S. Thesis, Pennsylvania State University, University Park, PA, 136 pp.

Chadwick, R. B., 1988: The wind profiler demonstration network. Preprints, Lower Tropospheric Profiling: Needs and Technologies., Boulder, CO, Amer. Meteor. Soc., pp. 109-110.

Cram, J. M., M. L. Kaplan, C. A. Mattocks and J. W. Zack, 1991: The use and analysis of profiler winds to derive mesoscale height and temperature fields: simulation and real-data experiments. *Mon. Wea. Rev.*, **119**, 1040-1056.

Gustafson, G. B., J.-L. Moncet, C. F. Ivaldi, H.-C. Huang and J. M. Sparrow, 1991: Mesoscale prediction and satellite cloud analysis for advanced meteorological processing systems. PL-TR-91-2008. Phillips Laboratory, Geophysics Directorate, Hanscom AFB, MA. 112 pp. **ADA240510**

Gustafson, G. B., D. K. Roberts, C. F. Ivaldi, R. Schecter, T. J. Kleespies, K. R. Hardy, R. P. d'Entremont, G. W. Felde and R. Lynch, 1987: The AFGL Interactive Meteorological System. Preprints, Third Conference on Interactive Information Processing Systems, New Orleans, LA, Amer. Meteor. Soc.,

Hamill, T. M. and T. Nehrkorn, 1993a: A short-term cloud forecast scheme using cross correlations. *Wea. Forecasting.*, **8**, 401-411.

Hamill, T. M. and T. Nehrkorn, 1993b: A short-term cloud forecast scheme using cross correlations. 9th conference on Interactive Information Processing Systems, Anaheim, CA, Amer. Met. Soc.,

Heideman, K. F., T. R. Stewart, W. R. Moninger and P. Reagan-Cirincione, 1991: The weather information and skill epxeriment (WISE): the effect of varying levels of information on forecast skill. *Wea. Forecast.*, **8**, 25-36.

Hollett, S. R., 1975: Three-dimensional spatial correlation of PE forecast errors. M.S. Thesis, McGill University, 73 pp.

Hollingsworth, A. and P. Lönnberg, 1986: The statistical structure of short-range forecast errors as determined from radiosonde data. Part I: The wind field. *Tellus.*, **38A**, 111-136.

Jewett, B. F. and R. H. Brady, 1989: Profiler training manual #4 - subjective uses of wind profiler data in cool season analysis and forecasting. . NOAA/ERL/FSL, Boulder, CO. 92 pp.

Klein, W. H. and H. R. Glahn, 1974: Forecasting local weather by means of model output statistics. *Bull. Amer. Meteor. Soc.*, **55**, 1217-1227.

Koch, S. E., M. DesJardins and P. J. Kocin, 1983: An interactive Barnes objective map analysis scheme for use with satellite and conventional data. *J. Climate Appl. Meteor.*, **22**, 1487-1503.

Kuo, Y.-H., D. O. Gill and L. Cheng, 1987: Retrieving temperature and geopotential fields from a network of wind profiler observations. *Mon. Wea. Rev.*, **115**, 3146-3165.

Mitchell, H. L., C. Charette, C. Chouinard, and B. Brasnett, 1990: Revised interpolation statistics for the Canadian assimilation procedure: their derivation and application. *Mon. Wea. Rev.*, **118**, 1615-1627.

Naistat, R. J., 1993: An example of wind profiler depicted differential thermal advection and its impact on nowcasting convection. Preprints, 26th International Conference on Radar Meteorology, Norman, OK, Amer. Met. Soc., pp. 549-551.

Nehrkorn, T., T. M. Hamill and L. W. Knowlton, 1993: Nowcasting methods for satellite imagery. PL-TR-93-2021. Phillips Laboratory,Hanscom Air Force Base, MA. 113 pp. **ADA267294**

Neiman, P. J. and M. A. Shapiro, 1989: Retrieving horizontal temperature gradients and advections from single station wind profiler observations. *Wea. Forecasting.*, **4**, 222-233.

Ralph, F. M. and P. J. Neiman, 1993: Wind profiler observations of a mesoscale convective system. Preprints, 26th International Conference on Radar Meteorology, Norman, OK, Amer. Met. Soc., pp. 567-569.

Seaman, R. S., 1989: Tuning the Barnes objective analysis parameters by statistical interpolation theory. *J. Atmos. Ocean. Technol.*, **6**, 993-1000.

Smalley, D. J. and J. F. Morrisey, 1993: Observed differences of winds measured by a wind profiler and Loransondes. Preprints, 26th International Conference on Radar Meteorology, Norman, OK, Amer. Meteor. Soc., Boston, MA, pp. 617-619.

Smith, T. L. and S. G. Benjamin, 1993: Impact of network wind profiler data on a 3-h data assimilation system. *Bull. Amer. Meteor. Soc.*, **74**, 801-807.

Thiebaux, H. J., L. L. Morone and R. L. Wobus, 1990: Global forecast error correlation. Part 1: Isobaric wind and geopotential. *Mon Wea Rev.*, **118**, 2117-2137.

van de Kamp, D. W., 1993: Current status and recent improvements to the wind profiler demonstration network. Preprints, 26th International Conference on Radar Meteorology, Norman, OK, Amer. Met. Soc., pp. 552-554.

van de Kamp, D. W., 1988: Profiler training manual #1 - principles of wind profiler operation. . NOAA/ERL/FSL, Boulder, CO. 49 pp.

Walawender, B. P., 1993: Using wind profiler data as an aid in forecasting winter precipitation. Preprints, 26th International Conference on Radar Meteorology, Norman, OK, Amer. Met. Soc., pp. 546-548.

Weber, B. L. and D. B. Wuertz, 1990: Comparison of rawinsonde and wind profiler radar measurements. *J. Atmos. Ocean. Technol.*, **7**, 157-173.

Weber, B. L., D. B. Wuertz, R. G. Strauch, D. A. Merritt, K. P. Moran, D. C. Law, D. W. van de Kamp, R. B. Chadwick, M. H. Ackley, M. F. Barth, N. L. Abshire, P. A. Miller and T. W. Schlatter, 1990: Preliminary evaluation of the first NOAA demonstration network wind profiler. *J. Atmos. Ocean. Technol.*, **7**, 909-918.

Zamora, R. J., M. A. Shapiro and C. A. Doswell, 1987: The diagnosis of upper tropospheric divergence and ageostrophic wind using profiler wind observations. *Mon. Wea. Rev.*, **115**, 871-884.